Technische Universität München

Max-Planck-Institutit für Quantenoptik

Controlling the motion of an atom in an optical cavity

Thomas Fischer

Vollständiger Abdruck der von der Fakultät für Physik
der Technischen Universität München
zur Erlangung des akademischen Grades eines

Doktors der Naturwissenschaften (Dr. rer. nat.)

genehmigten Dissertation.

Vorsitzender :	Univ.-Prof. Dr. M. Kleber
Prüfer der Dissertation :	1. Hon.-Prof. Dr. G. Rempe
	2. Univ.-Prof. Dr. Dr. h. c. A. Laubereau

Die Dissertation wurde am 27. 6. 2002
bei der Technischen Universität München eingereicht
und durch die Fakultät für Physik am 18. 12. 2002 angenommen.

Abstract

An experiment is described where slow laser-cooled atoms are injected into a high-finesse optical cavity. Single atoms are trapped in the cavity light field and observed by measuring the light intensity transmitted through the cavity. Feedback-based methods are realized to extend the time the atom stays in the cavity. The influence of atoms on the cavity transmission and the light force on atoms in a cavity are also analyzed theoretically. This allows to study the motion of an atom in the cavity and to interpret the experimental transmission signals. The current limitations for the storage time are identified and a strategy to overcome them is suggested. Apart from that, a method is proposed which allows a two-dimensional position measurement of atoms in the cavity.

Zusammenfassung

Es wird über ein Experiment berichtet, in dem langsame laser-gekühlte Atome in einen Resonator hoher Finesse eingebracht werden. In dem Lichtfeld des Resonators werden einzelne Atome gefangen und beobachtet, indem die durch den Resonator transmittierte Lichtleistung gemessen wird. Um die Zeit, die ein Atom im Resonator verbleibt, zu verlängern, werden Verfahren, die auf Rückkopplung basieren, realisiert. Der Einfluß von Atomen auf die Transmission des Resonators und die Lichtkraft, die auf Atome in einem Resonator wirkt, werden auch theoretisch analysiert. Dies erlaubt es, die Bewegung eines Atoms im Resonator zu untersuchen und die experimentellen Transmissionssignale zu interpretieren. Die Faktoren, die die Speicherzeit zur Zeit begrenzen, werden identifiziert und eine Strategie zu derer Beseitigung wird vorgeschlagen. Außerdem wird eine Methode vorgeschlagen, die eine zweidimensionale Positionsmessung von Atomen in dem Resonator erlaubt.

Contents

Chapter 1

Introduction

In the field of quantum electrodynamics (QED), the quantum properties of light and its quantized interaction with matter are investigated. This theory is widely used, and has been thoroughly tested. Some of its early successes are the explanation of spontaneous emission (Dir27), the calculation of the Lamb shift in atomic hydrogen (Bet47) and of the magnetic moment of the electron (Rev48), and the prediction of inhibition and enhancement of spontaneous emission of an atom (Pur46). While the first three examples involve the radiation field of free space, the last effect is due to a change of the mode structure of the electromagnetic field by imposing new boundary conditions. This can, for example, be achieved by placing mirrors near to the atom. The interaction of the changed electromagnetic modes with the atom is, in general, different from the interaction with the modes in free space. This is, in a wide sense, the subject of a subdomain of QED, the so-called cavity QED.

Over the years, the manipulation of the interaction between an atom and the electromagnetic field has been employed in many experiments. As examples may serve the micromaser (MWM85; BNB$^+$92), the single-atom laser (ACDF94), and the generation of nonclassical states of the light field by its interaction with atoms in a cavity (RTB$^+$91). All these cavity QED experiments rely on a strong interaction between atoms and modes of the light field. Strong interaction means that the interaction between an atom and one mode of the electromagnetic field is stronger than the interaction between the atom or mode and all the other modes of the radiation field which are responsible for the irreversible decay of excitation in the atom or mode. This can be understood as follows: The interaction between an atom and a mode of the electromagnetic field is strongest when a transition frequency of the atom is close to the frequency of the mode. In free space, there is a continuum of modes, and there are many modes near-resonant to the transition frequency of the atom. The interaction between atom and a mode is proportional to the amplitude of the mode at the position of the atom. As the modes in free space are not localized, this amplitude is small. Thus, the atom interacts with many modes, and the interaction with a single mode is small as compared to the interaction with all the other

modes.

In a cavity, the situation is different: The frequencies of the modes supported by the cavity are discrete. In a suitable setup, only a single cavity mode has a frequency which is near-resonant to an atomic transition. The cavity modes are localized, leading to a large amplitude of the mode inside the cavity. In some experiments, especially in the optical domain, the cavity does not cover the full solid angle, and the atom is still coupled to the free-space mode. By a very strong localization of the cavity mode, i.e. by using a very small cavity, the interaction between the atom and the cavity mode can be so strong that it dominates the interaction of the atom with the other modes of the electromagnetic field. Because of this dominance, it is very likely that an excited atom emits a photon into the cavity mode and not into the other modes of the electromagnetic field.

The cavity mode itself is not totally isolated from the environment. In an experiment, the cavity mirrors have losses. Thus, light cannot be stored in the cavity mode forever, but will eventually leak out. This can be described as an interaction between the cavity mode and the modes of the environment (Car93, section 1.3). If the mirror losses are small, the interaction between the cavity mode and the environment can be made smaller than the interaction between cavity mode and atom. Then, a photon which is stored in the mode is absorbed by the atom with a high probability instead of leaking out at the mirrors.

If the interaction between atom and cavity field is stronger than both the interaction between atom and environment and the interaction between mode and environment, the atom-cavity system is said to be strongly coupled. The interaction between mode and environment can be quantified by the decay rate of the electromagnetic field in the cavity, κ. The decay rate of the atomic dipole moment, γ, is a measure for the interaction strength between atom and environment. The atom-mode coupling rate, g, quantifies the interaction between atom and mode, and is given by the interaction energy between a photon in the mode and an atom divided by $\hbar$. As the amplitude of the cavity mode changes with position, g depends also on the position of the atom. For strong coupling, $g > \kappa, \gamma$. In this case, atom and cavity mode cannot be regarded as separate systems any more, but should be considered one new entity, the atom-cavity system.

In a strongly coupled system, a photon is exchanged many times coherently between atom and mode before it is lost to the environment. This allows, for example, efficient transfer of a photon from an atom to a mode and vice versa. This is interesting for quantum information processing (BEZ00), where one would like to have an interface between a photon to transport information coherently and an atom to store the information. Another consequence of strong coupling is that not only a photon, but also quantum noise can be transferred between the atom and the mode, see section 3.5 of this work. This influences, e.g., the motion of the atom.

Experimentally, a strongly coupled system has been realized in two regimes: the microwave regime and the optical regime. The first cavity QED experiments have been performed using highly excited (Rydberg) atoms in an atomic beam interacting with

microwave photons. In the microwave regime, photons can be stored for a very long time in centimeter-sized superconducting cavities, which can have field decay rates as low as (BVW01a) $\kappa = 1.7\,\mathrm{Hz}$. As the cavity covers nearly the full solid angle and the decay rates of Rydberg states are small, the atoms couple to the modes of the environment only very weakly, i.e. $\gamma \approx 0$. The maximum atom-field coupling is larger than both atomic and field decay times, and usually is on the order of (RGO$^+$99; BVW01a) $2\pi \times 10\,\mathrm{kHz}$. Thus, the requirements of strong coupling are fulfilled. The interaction time between atom and mode usually is much shorter than both the cavity decay time and the decay time of the atomic state.

The amplitude of the microwave mode in the cavity changes on the length scale of λ, which is on the order of a centimeter. As the diameter of the atomic beam through the cavity is much smaller and the velocity of the atoms can be controlled accurately, the coupling constant as a function of time can also be controlled within some limits. This allows to manipulate the quantum state of the system deterministically by tuning the interaction time between atom and cavity mode (RWK87).

In the microwave experiments, the system is observed by measuring the state of the atoms which leave the cavity. It is not possible to detect single photons which are deposited by the atoms in the microwave cavity, as the transmission of the mirrors and the detection efficiency for microwave photons is very small. Current experiments in the microwave regime include the entanglement of several atoms (RGO$^+$00) and the generation of Fock states in the cavity (BVW01b).

In the optical regime, the cavity can consist of dielectric mirrors. A weak laser beam is either coupled to the cavity mode or to the atoms. In contrast to the microwave experiments, the light leaking out of the cavity can be observed with high efficiency. The interaction time usually is much larger than the polarization and field decay times (RTB$^+$91; MTCK96; MFPR99), which are typically some 10 ns. In most experiments, the coupling constant cannot be controlled accurately because it varies on the length scale of the optical wavelength. It is technically very demanding to position an atom with an accuracy smaller than the wavelength in a cavity. Very recently, a big step forward in this direction has been made by combining cavities with ion traps (GKH$^+$01). This offers the perspective of coupling a very well localized ion strongly to a cavity mode.

In the optical regime, the strong influence of an atom on the intracavity light field results in a large influence of the atom on the transmitted light field. This has been used, for example, to detect a single atom in the cavity (MTCK96; MFPR99). The quantum state of the cavity light field can also be changed by the atom. Unlike the cavity mode, where many photons can be stored in the mode, only one excitation can be stored in the atom. Once the atom is in the excited state, it can not absorb another photon. Thus, a single atom is a highly nonlinear medium for a light field on the single-photon level. This leads, for example, to the aforementioned generation of nonclassical light inside the cavity. The light leaks out at the mirrors and can be studied, e.g., by measuring photon autocorrelation functions (HBT56; RTB$^+$91) or other sophisticated methods (CCBFO00).

In this thesis, an experiment is described where laser-cooled atoms interact strongly with an optical high-finesse cavity. The small velocity of laser-cooled atoms in the cavity has two important consequences which are both connected to the dependence of the coupling constant on the position of the atom. First, the kinetic energy of the atom is on the order of the interaction energy between atom and mode. As the interaction depends on the atomic position, it results in a force acting on the atom (HCLK98; MFM$^+$99). The effect of this light force on the kinetic energy of the atom is on the order of the interaction energy between atom and mode, thus the light force becomes important for slow atoms with a kinetic energy on the order of $\hbar g$. Second, the slower the atoms are, the slower is the change in the coupling strength, and the better is the signal-to-noise ratio for the observation of single atoms in the cavity.

In one experiment (MFPR99), it was investigated whether the interaction time between atoms and mode can be controlled by adjusting the velocity of the atoms which are injected into the cavity. For atoms with a velocity above 0.5 m/s, it was observed that the interaction time is proportional to the inverse velocity of the atom. For slower atoms, the interaction time increases slower with decreasing velocity than $1/v$. It was suspected that this is due to the light force acting on the atom. To increase the interaction time further, this behaviour has to be understood, and new methods have to be found to avoid it.

The light force was investigated in detail for single atoms (MFM$^+$99) and for more than one atom at a time in the cavity (MFM$^+$00). The light force acting on single atoms interacting with a single mode of the cavity are described very well by a theory developed by Ritsch and co-workers (HGHR98; HHG$^+$97). The force can be divided into a conservative part which corresponds to the dipole force in free space, a part which heats the atom incoherently, and a velocity-dependent part which cools or heats the atoms, depending on the parameters. All these parts were needed to explain the measurements in (MFM$^+$99). The heating part of the light force is also the main reason why very slow atoms stay shorter in the cavity than expected.

The light force in the cavity differs from its free-space counterpart in two main aspects: First, a single photon in the cavity exerts a significant force on the atom. Thus, the quantum character of the light field becomes important. This influences the heating of the atom by the light field, see section 3.5. Second, unlike in free space, the photons in the cavity field are stored in the mode. In other words, the light field has a memory. If some change in the atom-cavity system occurs, e.g. if the atom moves and changes the coupling constant, the light field cannot adjust itself immediately to the new situation. This delay causes a non-conservative contribution to the light force, which can cool the atomic motion. The cooling mechanism does not rely on the spontaneous emission of photons by the atom as it is the case e.g. in Doppler-cooling in free space (MvdS99, section 6.1). Thus, cavity cooling may be a method to cool particles without a closed transition, like atoms with a complicated level structure or molecules (GR99; VC00).

In this thesis, the successful model for the light force on an atom in a single-mode

cavity is extended to describe an arbitrary number of atoms interacting with an arbitrary number of modes. The theory predicts, for example, a long-range light force between atoms in a cavity (FMP$^+$01). Also, using its framework, a novel method to measure the 2-dimensional position of an atom in the cavity with a high spatial and temporal resolution is proposed in this thesis (HRF$^+$02). This method depends on the interaction of the atom with several degenerate transversal modes of the cavity. The theory was successfully tested for more than one atom interacting with a single mode of the cavity in (MFM$^+$00).

Now that the light forces are understood, the question is whether they can be used to control the motion of an atom in the cavity. It was proposed that atoms might be trapped or reflected by the light force caused by a single photon in a cavity (HBR91; ESBS91). The experimental proof of trapping was given in the group of Jeff Kimble at Caltech (HLD$^+$00), and independently in an experiment described in this thesis (PFMR00). In these experiments, the trap is a light field which contains only few photons on average at one time. As the atom approaches from outside the trap, it gains kinetic energy while moving towards the trap centre. To prevent the atom from escaping the trap on the other side, the ratio of trap potential depth to kinetic energy has to be increased while the atom is in the cavity. This can either be done by external laser cooling of the atom in the cavity (YVK99), or by increasing the depth of the dipole potential while the atom is in the cavity (PFMR00; HLD$^+$00). The storage time of the trapped atoms is a factor on the order of 5 longer than the interaction time of atoms which are not trapped (PFMR00; DLHK00), and is currently limited by the heating part of the cavity light force.

In these trapping experiments, the same light field is used to trap the atoms and to observe them. As an alternative, different laser fields can be used for trapping and observing the atoms (YVK99). This approach has the advantage that the fields can be optimized for their function. A disadvantage might be that the trapping laser also changes the cavity transmission because it induces a position-dependent shift of the atomic levels. This alters the effect of the atom on the cavity transmission and makes the interpretation of experimental signals more difficult.

A further step towards the control of the motion of an atom in the cavity is the implementation of feedback concepts to diminish or even cancel the heating in the trap. Feedback on the motion of particles is used in particle accelerators (vdM85). There, information about the transversal velocity of the particles is gained, and a force is applied in the opposite direction. This reduces the transversal velocity spread of the particles. In other words, the particles are cooled. In an atom-cavity system, real-time information about the atomic position can be obtained from the transmission of the cavity. This information can be used to influence the light force on the atom via the pump laser. In the experiment presented here, the storage time of trapped atoms in the cavity was increased significantly by the feedback methods. To my knowledge, this is the first time that feedback methods were applied to the motion of a single neutral atom.

This thesis is organized as follows: In chapter 2, the atom-cavity system is analysed in

a model where the light field is treated as a classical electro-magnetic field. To illustrate the results, experiments are discussed where single atoms are observed traversing the cavity. However, the classical model has its limitations. For instance, it cannot be used to calculate the intracavity light force on an atom. Therefore, in the following chapter, the light field inside the cavity is treated quantum-mechanically. A model describing the interaction of an arbitrary number of atoms with an arbitrary number of modes is presented, and the light force acting on the atoms is calculated. A novel method to measure the position of atoms in the cavity using several degenerate cavity modes is presented in chapter 4. The setup for the experiments described in this thesis is discussed in chapter 5. In chapter 6, the motion of an atom in a cavity is analysed in detail. Experiments demonstrating the trapping of single atoms in a cavity and feedback on trapped atoms are presented. A strategy to improve on the current results is discussed. Finally, a conclusion and an outlook is given in section 7.

Chapter 2

Classical description

An atom strongly coupled to a light field in a cavity containing less than one photon on average is a system that calls for a quantum-mechanical theory. The word "photon" alone is a term which is very difficult to understand classically. Yet, many results of classical electrodynamics also hold for the atom-cavity system. The classical considerations rely on well-known concepts like scattering and index of refraction. As they provide an intuitive picture for the interaction between the light field and the atom, they will be discussed in this chapter.

In section 2.1, the transmission spectrum of the atom-cavity system is derived in a qualitative way. For interested readers, the spectrum is calculated in section 2.2. The main result of this part is given in Eq. (2.30). In section 2.3, the results are used to explain experimental transit signals of single atoms through the high-finesse cavity.

2.1 Qualitative discussion

The system under consideration is a Fabry-Perot type cavity consisting of highly reflective mirrors with one or more atoms inside, see Fig. 2.1. Monochromatic light is coupled into the cavity at one mirror, building up an electromagnetic field in the cavity, see Fig. 2.2. The light which leaks out of the cavity at the other mirror, the transmitted intensity, is measured.

As starting point for a qualitative discussion, a cavity without atoms is considered. If the frequency of the incoupled light is scanned, the transmitted intensity exhibits a sharp maximum whenever the light which has made one round trip in the cavity has the same phase as the light leaking through the incouple mirror (ST91, chapter 9). This leads to constructive interference between the two light fields. For a one-dimensional Fabry-Perot type cavity, for example, this is the case if twice the distance between the mirrors is an integer times the wavelength of the incoming light. The constructive interference builds up a large standing-wave field inside the resonator, a part of which leaks out through the

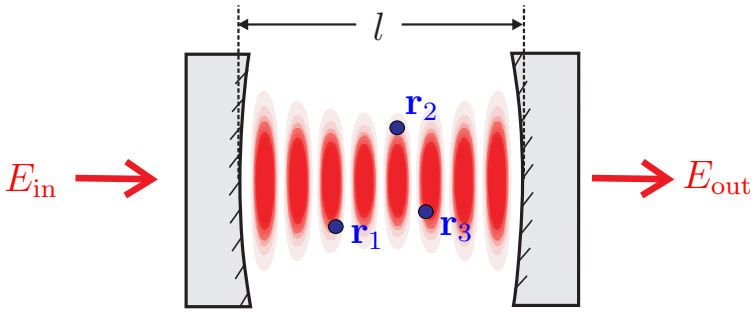

Figure 2.1: Sketch of the atoms-cavity system under consideration. The position of the atom j is $\mathbf{r}_j$, the incoming electric field is E_{in}, and the transmitted electric field is E_{out}. The length of the cavity is denoted by l. The red shading inside the cavity represents the standing wave of the light field inside the cavity.

outcoupling mirror. If the mirror losses are negligible as compared to the transmission of the mirrors, all incoming light can be transmitted.

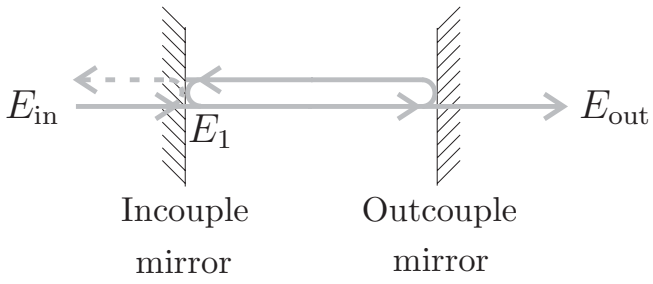

Figure 2.2: Paths of the light in a Fabry-Perot type cavity. A part of the incident electric field, E_{in}, leaks through the incouple mirror. The intracavity electric field, E_1, is the sum of this field and the part of the intracavity field which has done one round trip in the cavity. A part of the intracavity field leaks out at the outcouple mirror to give the transmitted electric field, E_{out}. The dashed line indicates the field which is reflected by the cavity.

If the light field which has made one round trip has a different phase from the incoupled light, the transmission of the cavity drops as compared to the case of equal phase, because the constructive interference is less efficient. It will now be investigated how much the phases must differ in order to get a significant drop in transmission. This can be answered by thinking of the incoupled light as composed of many short pulses. Each of these pulses circles round in the cavity. On every round trip, the pulse is attenuated, and it experiences

a phase shift with respect to the newly incoupled light. If the accumulated phase shift is on the order of 2π before the light pulse is significantly attenuated, the constructive interference of the light pulse and the newly incoupled light is destroyed, and the cavity has a small transmission. If, on the other hand, the phase shift per round trip is so small that the pulse is heavily attenuated before its phase difference to the newly incoupled light is 2π, this phase shift is of no consequence. Then, the interference is already limited by the damping of the intra-cavity light field by the mirrors, which also exists for a cavity exactly on resonance. Therefore, the transmission drops significantly if the phase shift per round trip times the average number of round trips of the light is on the order of 2π. If the reflectance of the mirrors is very high, the light in the cavity can circle round many times before it is significantly damped. Then, the transmitted intensity is sensitive to tiny phase shifts of the intra-cavity light field.

Atoms in the cavity can change the phase and the amplitude of the light inside the cavity. The phase shift of atoms and cavity per round trip of the light is considered as indicated in Fig. 2.3. The phase shift induced by detuning from the cavity resonance is linear in the detuning, while the phase shift induced by the atoms has a dispersion-like behaviour. The magnitude of the phase shift by the atoms depends on the number of atoms in the cavity and their position: The more atoms are in the cavity, and the better they are localised at positions where the light intensity is high, the larger is the phaseshift induced by the atoms. The total phase shift per round trip is the sum of the phase shifts by the cavity and by the atoms.

If both cavity and atom have the same resonance frequency, there are three frequencies where the phase shifts induced by atoms and cavity cancel. For these frequencies, the phase relation between incoupled light and light stored in the cavity is optimal for constructive interference, thus one would expect three peaks at these positions in the transmission spectrum. On the middle peak, however, the atom scatters much light out of the cavity mode, because the light field is on resonance with the atomic transition. This destroys the constructive interference inside the cavity. A calculation yields that the middle peak disappears totally. The outer peaks do not disappear, but atomic absorption diminishes their height as compared to the empty cavity, and it shifts the peaks further apart from each other, because atomic absorption is stronger on the side of the peak which is closer to the atomic resonance.

If cavity and atom are not exactly in resonance, there are still three positions where the phase shifts of atom and cavity cancel. Again, the middle peak is totally suppressed by atomic absorption. The two outer peaks do not disappear. The one which is closer to the atomic resonance suffers more from atomic absorption and is weaker than the peaks for exact resonance; the other peak is stronger. For a large atom-cavity detuning, this peak can be as high as the empty cavity peak. This can be seen as tuning the cavity resonance by introducing a medium which changes the optical path length inside the cavity by its refractive index, but has no significant absorption.

The calculation in the next chapter mainly follows the ideas which have been outlined

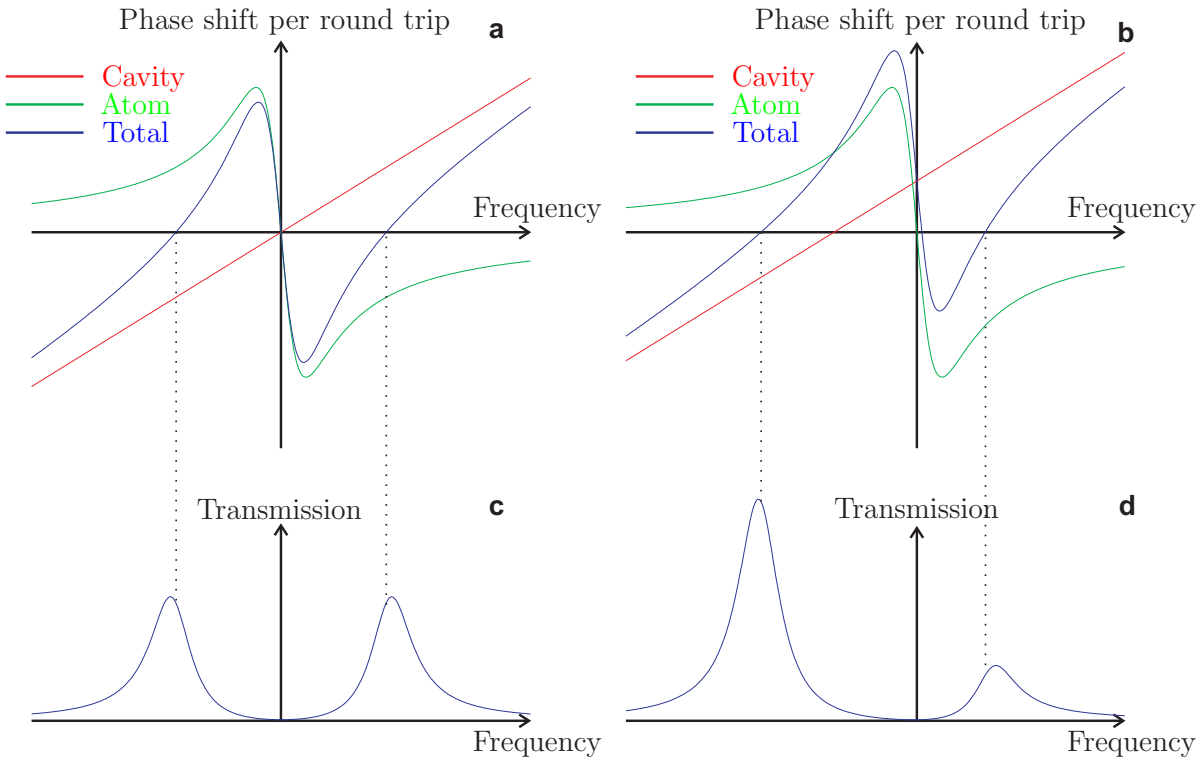

Figure 2.3: **a)**, **b)** Phase shift per round trip of a light field in an empty cavity, phase shift induced by an atom, and resulting phase shift for the cavity with an atom inside as a function of the light frequency. **c)**, **d)** The transmission of the cavity with an atom drawn against the light frequency. In a) and c), the resonance frequencies of atom and cavity are the same, whereas in b) and d), the resonance frequency of the atom is larger than that of the cavity. The peaks of the transmission are near to laser detunings where the total phase shift per round trip is zero, as indicated by the dotted black lines.

here.

2.2 Classical calculation

In this section, a Fabry-Perot type cavity is considered. It consists of two identical mirrors which are separated by a distance l, see Fig. 2.1. The mirrors have a power reflectance $\mathcal{R}$, a transmittance $\mathcal{T}$, and losses $\mathcal{L}$, with $\mathcal{R}+\mathcal{T}+\mathcal{L}=1$. It is assumed that the mirror reflectance is close to one, and the cavity geometry is such that it sustains a stable mode (Sie86, chapter 19, Eq. (8)). On one side, the cavity is illuminated with monochromatic light characterized by the electric field amplitude E_{in} and wavelength λ,

corresponding to the angular frequency ω_l. There are atoms at positions $\mathbf{r}_j$ inside the cavity, which together cause a small attenuation α_{atom} and a phase shift δ_{atom} per round trip of the light.

For a simple notation, the electric field, E, is written as a complex field here. The actual electric field is given by the real part of E times a polarisation vector.

As a first step, the attenuation and the phase shift induced by the atoms is assumed to be known, and their effect on the cavity transmission will be determined. In a second step, the phase shift and attenuation caused by the atoms will be calculated.

In steady state, the electric field behind the first mirror, E_1, is the sum of the transmitted part of the incident light field, $\sqrt{\mathcal{T}}E_{\mathrm{in}}$, and the intracavity field after one round trip. In this round trip, the light is reflected at two mirrors and interacts with the atoms twice. Hence, the amplitude is modified by the factor $\left(\sqrt{\mathcal{R}}\right)^2(1-\alpha_{\mathrm{atom}})$, and the phase by the total phase shift, $\delta_{\mathrm{tot}} = \delta_{\mathrm{cav}} + \delta_{\mathrm{atom}}$, which is the sum of the phase shifts in one round trip caused by detuning from the cavity resonance and the phaseshift caused by the atoms. Thus,

$$E_1 = \sqrt{\mathcal{T}}E_{\mathrm{in}} + \mathcal{R}\,(1-\alpha_{\mathrm{atom}})\,e^{-i\delta_{\mathrm{tot}}}E_1. \tag{2.1}$$

Now, the limit of small losses and phase shifts is applied, i.e it is assumed that $1-\mathcal{R}$, α_{atom} and δ_{tot} are small as compared to one. This is the case if the atoms have only a small influence on the light field per round trip, and if the frequency of the incident light field is close to a resonance of the empty cavity. Both conditions are well satisfied in the experiment. In this limit, the exponential function in Eq. (2.1) can be expanded linearly:

$$e^{-i\delta_{\mathrm{tot}}} = 1 - i\,\delta_{\mathrm{tot}}. \tag{2.2}$$

Inserting this into Eq. (2.1) yields

$$E_1\left\{1-\left[1-(1-\mathcal{R})\right](1-\alpha_{\mathrm{atom}})\,(1-i\delta_{\mathrm{tot}})\right\} = \sqrt{\mathcal{T}}E_{\mathrm{in}}. \tag{2.3}$$

Omitting products of the small quantities $1-\mathcal{R}$, α_{atom} and δ_{tot}, E_1 is calculated to be

$$E_1 = \frac{\sqrt{\mathcal{T}}}{(1-\mathcal{R}) + \alpha_{\mathrm{atom}} + i\,\delta_{\mathrm{tot}}}E_{\mathrm{in}}. \tag{2.4}$$

Neglecting the small attenuation and phase shift in half a round trip, the electrical field E_{out} which is transmitted through the cavity is given by $\sqrt{\mathcal{T}}E_1$, thus

$$E_{\mathrm{out}} = \frac{\mathcal{T}}{1-\mathcal{R}}\;\frac{1}{1+\frac{\alpha_{\mathrm{atom}}}{1-\mathcal{R}} + i\frac{\delta_{\mathrm{tot}}}{1-\mathcal{R}}}E_{\mathrm{in}}. \tag{2.5}$$

The first factor is a constant that depends only on mirror properties and gives the maximum transmittance for the electric field through the cavity. For $\mathcal{L} = 0$, this factor equals unity, and all incoupled light can be transmitted. The second factor describes the influence of the atoms on the cavity transmission. The magnitude of this influence is given by

the attenuation and/or phase shift per round trip induced by the atoms, multiplied with the mean number of round trips in the empty cavity, $1/\left[2\left(1-\mathcal{R}\right)\right]$. If the atoms should have a significant effect, this quantity should be on the order of one or larger.

To evaluate the above equation, the attenuation per round trip caused by the atom and the total phase shift per round trip have to be determined. The attenuation by the non-perfectly reflecting mirrors is already included in Eq. (2.5). Because this effect must not be included twice, it is assumed that the mirrors are perfectly reflecting in the following. This will not change the results for the phase shift per round trip and the attenuation by the atoms, as the attenuation of the mirrors per round trip is small and therefore has a negligible influence on the attenuation caused by the atoms and the total phase shift.

In the classical bistability literature (BCH$^+$81; Lug84), the absorption by the atom and the phase shift is usually determined using the slowly-varying amplitude and phase approximation. In this approximation, the electromagnetic field is written as a plane wave times a complex amplitude depending on position and time (MS99, section 1.1). It is assumed that the second spatial derivative of the amplitude in the propagation direction can be neglected. In my opinion, this approximation is not well justified for near-resonant atoms: The atom can be described as an oscillating dipole, which has a strong near-field which rapidly drops with the distance from the atom. This field cannot be described within such an approximation. Therefore, another approach will be used here. In the end, the results with the slowly-varying amplitude and phase approximation and the results derived here are the same, but I know no reason why this is clear in the beginning.

As a starting point, the wave equation for the electric field inside the cavity, $E\left(\mathbf{r},t\right)$, is used:

$$\triangle E\left(\mathbf{r},t\right)-\frac{1}{c^2}\frac{\partial^2 E\left(\mathbf{r},t\right)}{\partial t^2}=\frac{1}{\epsilon_0 c^2}\frac{\partial^2 P\left(\mathbf{r},t\right)}{\partial t^2}, \tag{2.6}$$

Now, $E\left(\mathbf{r},t\right)$ is written as a superposition of eigenfunctions of the Laplace operator, $\triangle$. For physical fields, this decomposition into eigenfunctions is always possible and a common tool in electrodynamics, see e.g. (Jac75, section 8.12). The decomposition is

$$E\left(\mathbf{r},t\right)=\sum_n \alpha_n\left(t\right)\psi_n\left(\mathbf{r}\right), \tag{2.7}$$

where the $\psi_n\left(\mathbf{r}\right)$ obey the eigenvalue equation

$$\triangle\psi_n\left(\mathbf{r}\right)=-\frac{\omega_n^2}{c^2}\psi_n\left(\mathbf{r}\right). \tag{2.8}$$

The $\psi_n\left(\mathbf{r}\right)$ are called mode functions. They are stationary solutions of the wave equation, their amplitude gives the distribution of the electric field of the light in the modes. As an example, the red shading in Fig. 2.1 indicates the modulus sqare of the mode function of a single mode supported by the cavity.

The $\psi_n(\mathbf{r})$ can be chosen such that they form an orthonormal basis, i.e.

$$\frac{1}{V}\int \mathrm{d}^3 r\, \psi_n^*(\mathbf{r})\, \psi_m(\mathbf{r}) = \delta_{nm}. \tag{2.9}$$

This is possible because the left hand side of Eq. (2.9) defines a scalar product between two functions. The Laplace operator is a hermitian operator with respect to that scalar product, thus the eigenfunctions for different eigenvalues are orthogonal (Lan72, chapter XI, §3, theorem 6). For eigenfunctions with the same eigenvalue, one can use a basis transformation to get an orthonormal basis. The volume V is the normalisation volume, which can be chosen arbitrarily and determines the amplitude of the $\psi_n(\mathbf{r})$.

For a given electric field, $E(\mathbf{r},t)$, the mode amplitudes, $\alpha_n(t)$, can be calculated by

$$\alpha_n(t) = \frac{1}{V}\int \mathrm{d}^3 r\, \psi_n^*(\mathbf{r})\, E(\mathbf{r},t)\,. \tag{2.10}$$

To use this equation, the electric field has to be known. In cases where the time dependence of the electric field should be calculated, another procedure is necessary. For example, a differential equation for the mode amplitudes can be used. To derive the differential equation, the operator $(1/V)\int \mathrm{d}^3 r\, \psi_n^*(\mathbf{r})$ can be applied to the wave equation, Eq. (2.6). Using Eqs (2.7) and (2.9), one gets

$$\frac{\mathrm{d}^2\alpha_n(t)}{\mathrm{d}t^2} = -\omega_n^2\,\alpha_n(t) - \frac{1}{\epsilon_0 V}\int \mathrm{d}^3 r\, \psi_n^*(\mathbf{r})\,\frac{\partial^2 P(\mathbf{r},t)}{\partial t^2}. \tag{2.11}$$

This equation shows that the time evolution of one mode amplitude, $\alpha_n(t)$, can be calculated separately from the time evolution of the other mode amplitudes, provided that the polarization, $P(\mathbf{r},t)$, is known. Note also that the polarization does not change the mode functions, but only the time dependence of the amplitudes of the modes.

Equation (2.11) will now be adapted to the situation of atoms interacting with a single mode of the cavity. Some assumptions will now be made, which can all be fullfilled in the experiment: The cavity is illuminated by light with a frequency ω_l close to the resonance frequency ω_c of one mode which is supported by the cavity. It is assumed that the other modes supported by the cavity are far detuned from the frequency of the laser light. In particular, the difference between the resonance frequency of the other modes and the laser frequency should be much larger than the linewidth of the other modes, and it should be so large that the phase shift induced by the atoms cannot shift the other modes near resonance. If this is the case and the mode matching is sufficient, i.e. if there is a significant overlap between pump mode and cavity mode, the mode which is nearly in resonance with the laser will have a far larger amplitude than the other modes supported by the cavity. Furthermore, it is assumed that the distance between the atoms and the distance between the atoms and the mirrors is large as compared to the wavelength of the light. Then, the light scattered by an atom has only a negligible effect on the other

atoms. Also, because the mirrors have a large reflectance, the field distribution of the near-resonant mode will in a very good approximation be given by the mode supported by a cavity which is made of perfectly reflecting mirrors with the same geometry. Under these circumstances, the electric field distribution inside the cavity which polarizes the atoms can be approximated by the mode of a cavity made of perfectly reflective mirrors. As a last assumption, the frequency of the light field should be far larger than the round trip frequency of the light inside the mode, which in turn should be much larger than the frequencies attributed to other mechanisms influencing the light field, e.g. the motion of the atoms or the decay rate of the atomic dipole moment. Then,

$$E(\mathbf{r},t) = A(t)\, e^{-i\omega_l t}\psi(\mathbf{r}) + E_{\text{scat}}(\mathbf{r},t)\,, \tag{2.12}$$

where $\psi(\mathbf{r})$ is the mode out of the $\psi_n(\mathbf{r})$ in Eq. (2.7) which is close to resonance, and $E_{\text{scat}}(\mathbf{r},t)$ is the part of the electric field scattered by the atoms which is orthogonal to the mode. The amplitude $A(t)$ is under the above assumptions slowly varying in time, i.e.

$$\left|\frac{\mathrm{d}^2 A(t)}{\mathrm{d}t^2}\right| \ll \omega_l \left|\frac{\mathrm{d}A(t)}{\mathrm{d}t}\right| \ll \omega_l^2 |A(t)|. \tag{2.13}$$

As the polarization of the atoms is also induced by the light field, it can be written as

$$P(\mathbf{r},t) = P_0(\mathbf{r},t)\, e^{-i\omega_l t} \tag{2.14}$$

with

$$\left|\frac{\mathrm{d}^2 P_0(\mathbf{r},t)}{\mathrm{d}t^2}\right| \ll \omega_l \left|\frac{\mathrm{d}P_0(\mathbf{r},t)}{\mathrm{d}t}\right| \ll \omega_l^2 |P_0(\mathbf{r},t)|. \tag{2.15}$$

Using this, time derivatives of $P_0(\mathbf{r},t)$ and the second time derivative of $A(t)$ can be neglected, and Eq. (2.11) can be recast as

$$\begin{aligned}\frac{\mathrm{d}A(t)}{\mathrm{d}t} &= i\frac{\omega_l^2-\omega_c^2}{2\omega_l} A(t) + i\frac{\omega_l}{2\epsilon_0 V}\int \mathrm{d}^3 r\, \psi^*(\mathbf{r})\, P_0(\mathbf{r},t) \\ &= i\Delta_c\, A(t) + i\frac{\omega_l}{2\epsilon_0 V}\int \mathrm{d}^3 r\, \psi^*(\mathbf{r})\, P_0(\mathbf{r},t)\,,\end{aligned} \tag{2.16}$$

where $\Delta_c = \omega_l - \omega_c$ is the detuning of the laser from the cavity resonance, and $\Delta_c \ll \omega_l$ was used to get to the second equation.

Now, the polarization, P_0, is left to be calculated. As was explained above, P_0 is induced by the electric field $E(\mathbf{r},t)$, which can be approximated by the electric field in the mode, $E(\mathbf{r},t) - E_{\text{scat}}(\mathbf{r},t)$, at the position of the other atoms. For two-level atoms which are exposed to monochromatic light with an intensity well below the saturation intensity at the position of the atoms, the polarization is given by (MS99, Eq. (5.26))

$$P_0(\mathbf{r},t) = iA(t)\,\frac{\mu^2}{\hbar}\frac{1}{\gamma - i\Delta_a}\sum_j \delta(\mathbf{r}-\mathbf{r}_j)\,\psi(\mathbf{r_j})\,. \tag{2.17}$$

Here, μ is the dipole matrix element of the atomic transition, $\Delta_a = \omega_l - \omega_a$ is the detuning of the laser from the atomic resonance, and $\delta(\mathbf{r})$ is the Dirac delta function.

If the intensity at the position of the atom is of the order of the saturation intensity, the classical theory predicts a phenomenon called "optical bistability" (Lug84), meaning that for one and the same input intensity, the intensity inside the cavity can have two stable values. However, for the cavity used in the experiments which are described in this thesis, an intracavity light field which is close to the atomic resonance and is strong enough to saturate an atom corresponds to an average number of photons in the mode which is much less than one. In this regime, the optical bistability is destroyed by the quantum "noise" of the electromagnetic field (SC88), therefore the discussion of this effect is omitted here.

The change of $A(t)$ can be reinterpreted as a phase shift and absorption per round trip by multiplying it with the round-trip time, $2l/c$, dividing through the mode amplitude and taking the real and imaginary part, respectively. Combining Eqs. (2.16) and (2.17), this yields

$$\begin{aligned} \alpha_{\text{atom}} &= -\frac{2l}{c}\,\mathrm{Re}\left(\frac{1}{A(t)}\frac{\mathrm{d}A(t)}{\mathrm{d}t}\right) \\ &= 2\,C_0 N_{\text{eff}}\,(1-\mathcal{R})\,\frac{1}{1+\Delta_a^2/\gamma^2} \qquad (2.18) \\ \delta_{\text{tot}} &= -\frac{2l}{c}\,\mathrm{Im}\left(\frac{1}{A(t)}\frac{\mathrm{d}A(t)}{\mathrm{d}t}\right) \\ &= (1-\mathcal{R})\left[2\,C_0 N_{\text{eff}}\frac{\Delta_a}{\gamma}\,\frac{1}{1+\Delta_a^2/\gamma^2} - \frac{\Delta_c}{\kappa}\right], \qquad (2.19) \end{aligned}$$

where

$$\kappa = \frac{c}{2\,l}\,(1-\mathcal{R}) \qquad (2.20)$$

is the decay rate of the electric field in the cavity, and

$$C_0 = \frac{\mu^2 l \omega_l}{2\hbar\epsilon_0 c\gamma V\,(1-\mathcal{R})}. \qquad (2.21)$$

C_0 is a measure for the influence which a single atom can have on the mode amplitude in the cavity. In the definition of C_0, the normalisation volume V is often chosen such that the maximum value of $|\psi_n(\mathbf{r})|^2$ is one. Then, V is the mode volume of the mode ψ_n which can be calculated by

$$V = \int \mathrm{d}^3\mathbf{r}\,|\psi(\mathbf{r})|^2, \qquad (2.22)$$

and C_0 is the maximum single-atom cooperativity. N_{eff} is the effective atom number, given by

$$N_{\text{eff}} = \sum_i |\psi(\mathbf{r_i})|^2. \qquad (2.23)$$

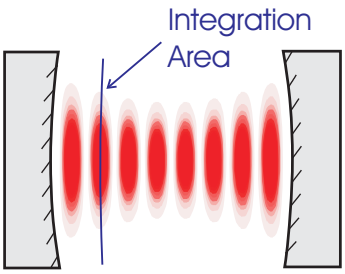

Figure 2.4: Sketch to illustrate the definition of the cross-section of the mode, a_0. Shown is a cut through the cavity mode. The blue line indicates the cut through the integration area for the integral in Eq. (2.24) if the second antinode from the left is chosen for integration. Of course, the integral can also be taken through another antinode.

It is rewarding to examine the formula for C_0 a bit closer. In a Fabry-Perot type cavity, the mode function is a standing wave in the direction of the cavity axis. The power which is circulating in the cavity is the same everywhere. It is proportional to the cross-section of the mode,

$$a_0 = \int_{\text{antinode}} \mathrm{d}^2 r \, |\psi(\mathbf{r})|^2, \tag{2.24}$$

see also Fig 2.4 For a TEM-00 mode, this is given by

$$a_0 = \pi w_0^2/2, \tag{2.25}$$

where w_0 is the $1/e$ radius of the field of the mode. From this, it can be concluded that the integral over the area of any antinode in the cavity must be the same. The mode volume, V, is then given by integrating over the standing wave along the cavity axis:

$$V = \frac{a_0 l}{2}. \tag{2.26}$$

Also, if the atomic transition is an electric dipole transition, if it is only radiatively broadened, and if its radiative broadening is the same as in free space, the dipole matrix element is related to the decay rate of the atomic polarization, γ, and the transition frequency, ω_a, by the Weisskopf-Wigner formula (MS99)

$$\mu^2 = \frac{6\pi\epsilon_0\hbar c^3\gamma}{\omega_a^3}. \tag{2.27}$$

Using furthermore that $c/\omega_a = \lambda/(2\pi)$, and that $\omega_c \approx \omega_a$, Eq. (2.21) can be rewritten as

$$C_0 = \frac{3}{2\pi}\frac{\lambda^2}{a_0}\frac{1}{1-\mathcal{R}}. \tag{2.28}$$

This shows that in order to be able to observe a single atom, one should have a cavity with a small cross-section, and the cavity should be built of mirrors with a large reflectance.

Now, the final result can be stated. Substituting Eqs. (2.18) and (2.19) into Eq. (2.5), one finds that

$$E_{\mathrm{out}} = \frac{\mathcal{T}}{1-\mathcal{R}} \, \frac{1}{1 + 2C_0 N_{\mathrm{eff}} \frac{1}{1+\Delta_a^2/\gamma^2} \left(1 + i\frac{\Delta_a}{\gamma}\right) - i\frac{\Delta_c}{\kappa}} E_{\mathrm{in}}. \tag{2.29}$$

The transmittance of the cavity, i.e. the ratio between transmitted power, P_{out}, and incoming power, P_{in}, is given by the modulus square of the ratio of incoming and transmitted electric fields:

$$\begin{aligned} \frac{P_{\mathrm{out}}}{P_{\mathrm{in}}} &= \left|\frac{E_{\mathrm{out}}}{E_{\mathrm{in}}}\right|^2 \\ &= \frac{\mathcal{T}^2}{(1-\mathcal{R})^2} \frac{1}{\left(1 + 2C_0 N_{\mathrm{eff}} \, \frac{1}{1+\Delta_a^2/\gamma^2}\right)^2 + \left(\frac{\Delta_c}{\kappa} - 2C_0 N_{\mathrm{eff}} \frac{\Delta_a}{\gamma} \, \frac{1}{1+\Delta_a^2/\gamma^2}\right)^2}. \end{aligned} \tag{2.30}$$

The maximum transmittance of the cavity is given by $\mathcal{T}^2/(1-\mathcal{R})^2$. The denominator of the second fraction consists of two terms in brackets: The first term describes the absorption of the atom, and the second the phase shift of the light. The regime where only the first term is important is called the absorptive regime. As an example, this is the case if the laser is both in resonance with the atom and the cavity ($\Delta_a = \Delta_c = 0$). Then, the transmittance drops by a factor of $1/(1 + 2C_0 N_{\mathrm{eff}})^2$ as compared to that of an empty resonator. In the experiment described in this thesis, $C_0 = 30$ for the TEM-00 mode of the cavity, so that even for a single atom in the antinode of the mode, i.e. $N_{\mathrm{eff}} = 1$, the transmittance drops by several orders of magnitude.

If the laser-atom detuning Δ_a is large, the first term in the denominator of the second fraction in Eq. (2.30) is on the order of one. This is called the dispersive regime. Now the phase shifts induced by the atom and the detuning from the empty cavity are important. For very large Δ_a, the effect of the atom is negligible. In this case, the behaviour of the empty cavity is regained, and the transmittance is a Lorentzian of the argument Δ_c/κ. For smaller Δ_a, an atom can still have negligible absorption, but its phase shift can shift the resonance frequency of the cavity. In particular, if the cavity without an atom is detuned from the pump laser, i.e. $\Delta_c \neq 0$, the parameters can be chosen such that the atoms shift the cavity closer to resonance. In this case, the transmittance can be increased by the presence of atoms.

In the next section, some experimental results will be presented, which can be explained using the theory described above, in particular Eq. (2.30).

2.3 Experimental transit signals of single atoms

In the last section, it was shown theoretically that a single atom in a high-finesse cavity can have a large influence on the transmission of the cavity. This is investigated experimentally by sending slow atoms through the high-finesse cavity described in section 5.3 and measuring the transmission of the cavity. The density of the atomic cloud was chosen so low that the mean number of atoms in the cavity is much less than one, so that only once every while, a single atom is strongly coupled to the cavity mode. As the atoms move independently from each other (MFPR99), the probability of finding two atoms at the same time in the cavity is much smaller than the probability of finding a single atom.

If the probe laser is in resonance with both the atom and the empty cavity, i.e. $\Delta_a = \Delta_c = 0$, a drop in the transmission of the cavity is expected if an atom enters the cavity. An experimental example is shown in Fig. 2.5. Most of the time, the transmission of the cavity is high, but sometimes, there are sudden drops in the transmission, which are caused by single atoms in the cavity. The noise in the transmission signal is mostly due to shot noise. Remarkable is the high time resolution of 200 kHz, i.e. only 5 μs are needed to detect a strongly coupled atom in the cavity.

In the next measurement, the probe laser was detuned from the empty cavity resonance. In this case, the atom can shift the cavity into resonance, increasing the cavity transmission. An example is shown in Fig. 2.6.

The comparison with the experiment shows that the classical theory can be used to calculate the transmission of the cavity if the atoms are not saturated. However, the motion of the atoms in the cavity is also important for the transmission signals: In Fig. 2.5, a fast motion of the atoms across the antinodes over the standing wave had to be assumed in order to explain the experimental signal, i.e. the transmission of the cavity was averaged over the standing wave. This fast motion is due to heating of the atoms by the light force in the cavity. The heating cannot be calculated correctly if the light field in the cavity is assumed to be classical. Therefore, a quantum model for the light field is considered in the next chapter. Quantum models are also needed to describe saturation effects in a strongly coupled atoms-cavity system.

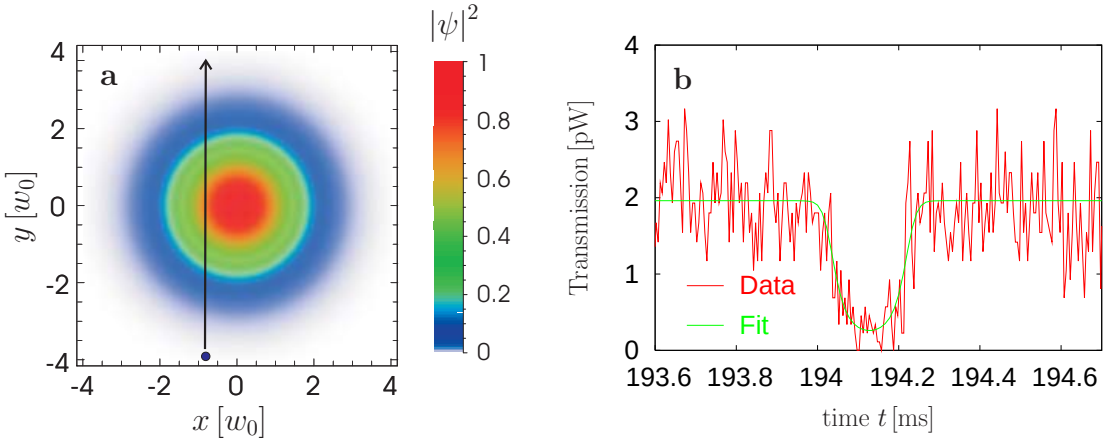

Figure 2.5: **a)** A cut through the TEM-00 mode of the high-finesse cavity perpendicular to the cavity axis. The x and y coordinates are given in units of the cavity waist, w_0. A possible path of the atom causing the signal in b) is indicated by the arrow. **b)** The transmission of the cavity versus time. A cloud of atoms was launched at $t = 0$. A single atoms crosses the TEM-00 mode and causes the sudden drop in the transmission at t=194.1 ms. The detunings are $\Delta_a = \Delta_c = 0$. The transmission of the resonant cavity without atoms is 2.0 pW. The velocity of the atom is 0.40 m/s. The red line is the experimental signal. The green line is the theoretical transmission, Eq. (2.30), for an atom flying straight through the cavity in the transversal direction. The minimum distance from the cavity axis was taken to be $0.8\,w_0$. In the axial direction, the transmission is averaged over the standing wave because for the detunings used here, the atom is heated in the axial direction by the cavity light forces and crosses nodes and antinodes of the standing wave. This modulates the transmission, but this structure is too fast to be resolved.

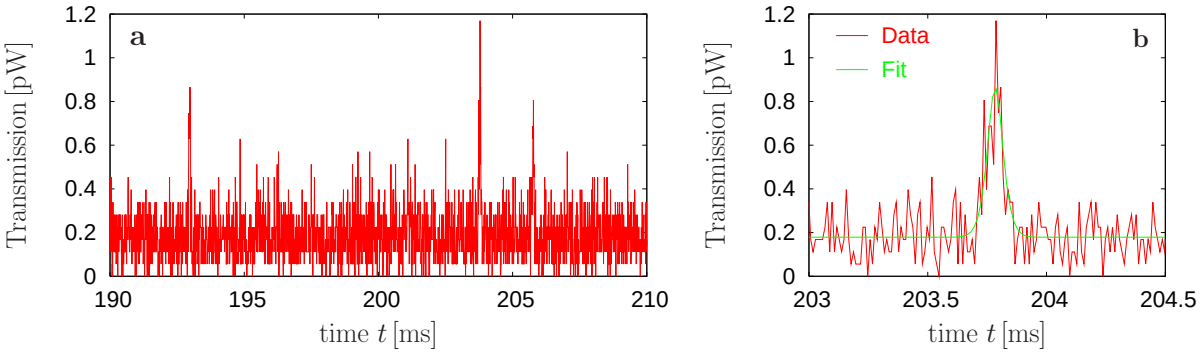

Figure 2.6: **a)** The cavity transmission as a function of time. The strong peaks are caused by single atoms from the atomic fountain. The detunings are $\Delta_a/(2\pi) = -45\,\mathrm{MHz}$ and $\Delta_c/(2\pi) = -5\,\mathrm{MHz}$. The transmission of the empty resonant cavity is 2.1 pW. The transmission is calculated from the number of measured photons per 10 μs-bin, i.e. the time resolution is 100 kHz. The noise of the base line is shot noise, caused by the average number of photons per bin which is as low as 3.8 for a cavity without atoms. This number includes 1.3 dark counts on average per bin, mostly caused by the repumping beam which is hitting the cavity from the side. **b)** Zoom of the peak at t=203.8 ms in a). The red line is the experimental signal, the green line is calculated from Eq. (2.30) for an atom flying straight through an antinode of the cavity. The minimal distance from the cavity axis was taken to be $0.5\,w_0$. For the detunings used here, no averaging over the standing wave as in Fig. 2.5 is necessary because the atoms are channeling through antinodes of the standing wave (MFM$^+$99). This can be seen in an analysis of the light forces derived in the next chapter.

Chapter 3

Quantum description

In the previous chapter, a classical description of the interaction of atoms with the light field inside a high-finesse cavity was given. However, this description has severe limitations. First, it is only valid if the saturation of the atoms is low. This is not only due to the fact that the saturation behaviour of the atom was neglected, it is because in the regime where the saturation of the atom is significant and a single photon more or less in the cavity makes the difference between a saturated and an unsaturated atom, a quantum description of the light field is indispensable to get correct results.

There is a second reason to describe the cavity mode quantum-mechanically: It is very difficult, if not impossible, to obtain a correct description of the light force acting on the atoms in a high-finesse cavity within the framework of classical electrodynamics. For example, the momentum diffusion (i.e. heating) of an atom inside the cavity is very different compared to an atom in free space (HGHR98; HHG$^+$97), which is not easily seen from a classical point of view. As momentum diffusion is important for the experiments described in this thesis, the concepts of quantum electrodynamics will be used to develop a model describing atoms interacting with a quantized light field in the cavity. For low saturation of the atom, the resulting equations can be solved analytically. Although the experiments described later on in this thesis are performed in a regime where the typical excitation of the atom was not negligible, the analytic formulas provide insight into the mechanisms which govern the behaviour of the atom-cavity system. Also, they can be used for orders-of-magnitude estimates even for higher atomic saturation, and can be extended to situations where other treatments are very difficult, e.g. if several atoms are interacting with several modes of the cavity.

In section 3.1, the ansatz for the analytical model is presented. Some of the basic ideas are taken from (HGHR98; HHG$^+$97). The calculations are similar to those in (FMP$^+$01). However, the derivations presented here are more general and more elegant. Basic properties of the analytical model which ease calculations are investigated in section 3.2. The connections between the quantum mechanical operators and measurable quantities are discussed in section 3.3. The formulas derived there are also valid for higher saturation

of the atoms where the analytic model fails. Section 3.4 presents the steady state solution for the analytical model. The general solution for an arbitrary number of atoms and modes is considered as well as special cases where just one atom interacts with degenerate modes or a single mode interact with atoms which have the same transition frequency and decay rate. The motion of atoms in the cavity light field is the topic of the next two sections. In section 3.5, the momentum diffusion (heating) of atoms in the cavity light field is calculated, and in section 3.6, the velocity-dependent part of the light force is derived. Both sections rely on the low saturation approximation, and treat the general case as well as the case of a single mode interacting with the atoms. In section 3.7, the limit of large atom-laser detuning is considered for a low atomic saturation. This limit is interesting for trapping single atoms, and for laser-cooling particles which have no closed transitions, like molecules. In section 3.8, numerical methods are described which can be used for saturated atoms or for other situations where the analytical model fails.

3.1 Model

As a starting point, N_a two-level atoms in an optical cavity supporting N_c modes of the electromagnetic field are considered, see Fig. 3.1. The light field inside the cavity and the internal states of the atoms are treated quantum mechanically, while the atomic motion is treated classically. This is usually a good approximation if the atom's temperature is well above the recoil limit and if the cavity linewidth and the atomic linewidth are large as compared to the recoil frequency of the atom (DLHK00). The cavity mode i is described by a quantum field with annihilation and creation operators a_i and $a_i^\dagger$, respectively. The ith mode's resonance angular frequency is denoted by $\omega_{\mathrm{c},i}$. The field of the mode i decays with the rate κ_i, which is assumed to be much smaller than the inverse round trip time of the light in the cavity. The mode i is pumped by an external field with strength η_i. The jth atom's raising and lowering operators are σ_j^+ and σ_j^-, respectively. Its transition angular frequency is $\omega_{\mathrm{a},j}$. The atomic dipole moments decay with a rate γ_j. The ith mode is coupled to atom j with the coupling constant g_{ij}, which depends on the position $\mathbf{r}_j$ of the jth atom and may be a complex number. For an electric dipole transition and if the relative difference between the $\omega_{\mathrm{c},i}$ is small, the coupling constant is given by (MS99, Eq. (14.3))

$$g_{ij} = g_0 \psi_i \left(\mathbf{r}_j\right), \tag{3.1}$$

where ψ_i is the mode function of the ith mode, see Eq. (2.7), and

$$g_0 = \mu \sqrt{\omega_{\mathrm{c}} / \left(2\hbar\epsilon_0 V\right)}. \tag{3.2}$$

Here, μ is the dipole matrix element of the transition, V is the normalization volume, see Eq. (2.9), and ω_{c} is any of the $\omega_{\mathrm{c},i}$. It is assumed that the mode functions are orthonormal, see the discussion at Eq. (2.9). An orthonormal basis can usually be found, except for exotic cases such as unstable cavities (vdLvEvDW01).

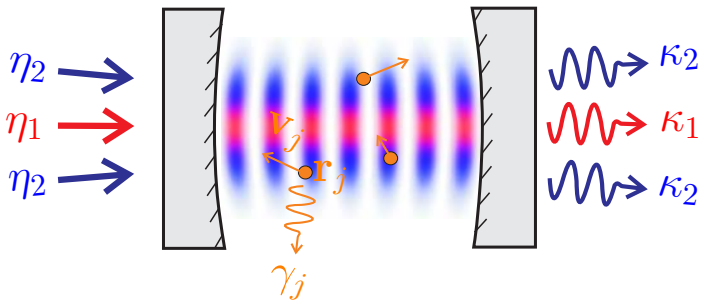

Figure 3.1: $N_a = 3$ atoms (orange) moving in a cavity supporting $N_c = 2$ modes (red,blue) with field decay rates κ_i, which are pumped by an external laser with the strengths η_i. The atom j at position $\mathbf{r}_j$ moves with a velocity $\mathbf{v}_j$, and couples to mode i with the position-dependent coupling constant $g_{ij}(\mathbf{r}_j)$

As the starting point of the calculation, quantum Langevin equations will be used. They describe the interaction of a system with a large reservoir. The reservoir is the continuum of the electromagnetic modes which are not supported by the cavity. Examples of these modes are the modes which enter the cavity from the side or the modes which hit the outside of the mirrors. Both the atoms and the cavity modes couple to this continuum, the former by their dipole moment, the latter through the lossy mirrors. This coupling gives rise to an irreversible decay of the cavity light field and the atomic dipole moments, which is described by the decay rates κ_i and γ_j. A simple derivation of the quantum Langevin equations used here can be found in (MS99), whereas the description in (GZ00) is broader.

After applying rotating wave and Markov approximations, the quantum Langevin equations for the operators a_i and σ_j^- read

$$\dot{a}_i = i\Delta_{\mathrm{c},i} a_i - \sum_{j=1}^{N_a} i g_{ij} \sigma_j^- - \kappa_i\, a_i + \eta_i + F_{\mathrm{mode},i}, \tag{3.3}$$

$$\dot{\sigma}_j^- = i\Delta_{\mathrm{a},j} \sigma_j^- + i \sum_{i=1}^{N_c} {g_{ij}}^* \sigma_{z,j} a_i - \gamma_j\, \sigma_j^- - \sigma_{z,j} F_{\mathrm{atom},j}. \tag{3.4}$$

Here, $\Delta_{\mathrm{c},i} = \omega_l - \omega_{\mathrm{c},i}$ is the detuning between laser and the resonance of cavity mode i, and $\Delta_{\mathrm{a},j} = \omega_l - \omega_{\mathrm{a},j}$ is the detuning between laser and the transition of atom j. $\sigma_{z,j} = \left[\sigma_j^+, \sigma_j^-\right]$ is the pseudo-spin operator of the jth atom. The raised asterisk * denotes the complex conjugate of a number. The operators $F_{\mathrm{atom},j}$ and $F_{\mathrm{mode},i}$ are called noise operators and are time-dependent. They describe the quantum noise which stems from the coupling between system and reservoir. They yield zero if applied to a state describing an environment with zero temperature, i.e. all expectation values of normally ordered products of the noise

operators vanish. This can be seen as follows: The reservoir consists of modes which can be described by a harmonical oscillator model. In the rotating wave approximation, the noise operators are a linear combination of annihilation operators of the reservoir's field modes (MS99). At room temperature, the modes associated with visible frequencies are in their ground state. As the annihilation operators yield zero when they are applied to a ground state, the noise operators also yield zero. The temperature of the reservoir is assumed to be zero throughout this thesis, which is a very good approximation in the optical regime.

Finding an exact solution of these equations is by no means easy. Therefore, as an approximation, the Hilbert space of each two-level atom is replaced by the Hilbert space of a harmonic oscillator. In the following, it will be investigated in which cases this approximation yields correct results.

First, the approximation will certainly fail if the population of the higher excited states of the atomic harmonic oscillator is not small. In this case, as those states do not exist in reality, there would be a large difference between the quantum state of the approximate system and the one of the real system. For a small enough pump parameter η, however, this will not be the case. Therefore, the approximation is valid only for small saturation of the atoms, which can be achieved by a small enough pump strength η.

Second, even for weak excitation, where only leading order terms in η are important, the coupled-oscillator model can introduce significant errors when calculating higher-order expectation values. For example, it is clear from our ansatz that the exact result $\sigma_j^- \sigma_j^- = 0$ will not be reproduced in the simplified theory. Also, one cannot hope to find correct solutions for the second-order photon correlation function, which involves the operator product $a^\dagger a^\dagger a a$. The reason is that here the leading order in η comes from the population of the second excited state of the cavity field. In the harmonic oscillator model, this two-photon state couples indirectly to the second excited state of the atomic harmonic oscillator, see Fig. 3.2. The strength of this coupling is given by the g_{ij} and thus does not vanish with vanishing pump strength η. As the second excited state of the atom does not exist in the exact theory, the amplitude of the two-photon state will also deviate from the correct result, even in the limit of small saturation. However, only expectation values where the leading-order term in η depends on the amplitudes of the first excited states of the atomic and cavity harmonic oscillators, respectively, will be calculated in this chapter. These expectation values will be correct in leading order of η. Therefore, the exact equation of motion (3.4) can be approximated by

$$\dot{\sigma}_j^- = i\Delta_{\mathrm{a},j}\sigma_j^- - i\sum_{i=1}^{N_\mathrm{c}} {g_{ij}}^* a_i - \gamma_j\,\sigma_j^- + F_{\mathrm{atom},j}. \tag{3.5}$$

To check in which regime this approximation is good, the steady state of the system was calculated numerically for a single atom inside the cavity, including the saturation effects. These calculations indicate that the harmonic-oscillator approximation leads to results

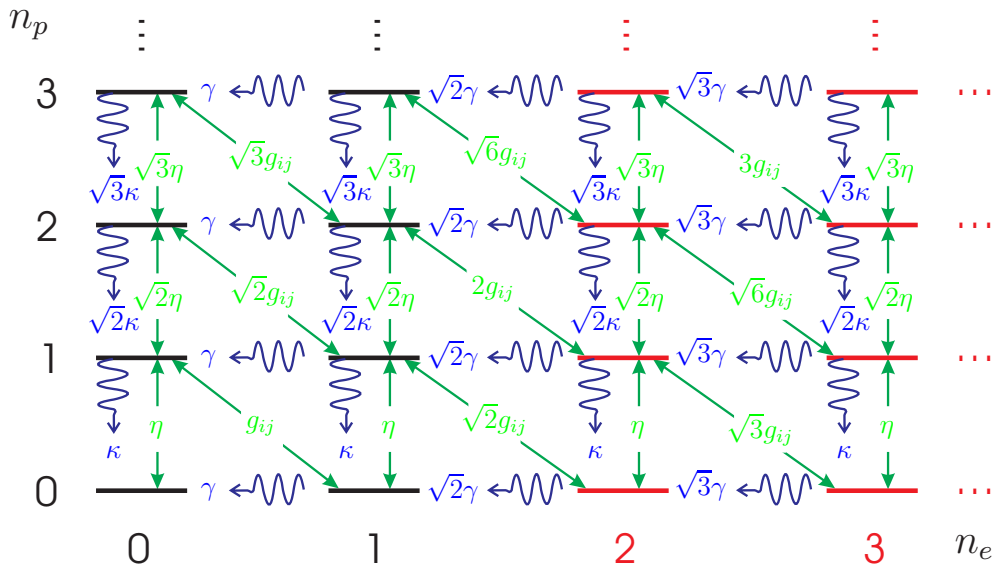

Figure 3.2: The coupling between different states in the bare-state basis for a single atom interacting with a single cavity mode. The states are characterized by the number of photons in the mode, n_p, and the number of excitations in the atom, n_e. Green straight arrows between the states denote a coherent interaction, blue curved arrays indicate a incoherent decay. The numbers beneath the arrow give the amplitude of the interaction. This figure illustrates the difference between the harmonic oscillator model and an exact model: The states in black ($n_e \leq 1$) exist in both models, the states in red ($n_e > 1$) exist only in the harmonic oscillator model.

for the mean intracavity photon number and the force acting on the atom which deviate from the correct result by only a few percent, as long as $\left\langle \sigma_j^+ \sigma_j^- \right\rangle$ does not exceed a value of 0.1, which is equivalent to $\langle \sigma_{z,j} \rangle < -0.8$. This is expected to hold also in the case of more than one intra-cavity atom and more than one mode.

3.2 Properties of the low-saturation model

With Eqs. (3.3) and (3.5), the time evolution of the operators a_i and σ_j^- is described by a set of coupled inhomogeneous linear equations. Because the inhomogeneities $F_{\text{mode},i}$ and $F_{\text{atom},j}$ are time-dependent and operator-valued, they are not easy to handle. To ease the calculations, the noise-operator part of the equations will be separated from the rest, by writing the operators as a sum of the operator's expectation value and an additional

operator with expectation value zero. It is convenient to define a vector $\mathbf{Y}$ which consists of the a_i and σ_j^-:

$$\mathbf{Y} = \begin{pmatrix} a_1 \\ a_2 \\ \vdots \\ a_{N_c} \\ \sigma_1^- \\ \sigma_2^- \\ \vdots \\ \sigma_{N_a}^- \end{pmatrix}. \tag{3.6}$$

This vector can be split into its expectation value, $\langle \mathbf{Y} \rangle$ and the remainder, $\tilde{\mathbf{Y}}$:

$$\mathbf{Y} = \langle \mathbf{Y} \rangle + \tilde{\mathbf{Y}}. \tag{3.7}$$

The equation of motion for the two terms on the right hand side of this equation can be obtained from Eqs. (3.3) and (3.5):

$$\langle \dot{\mathbf{Y}} \rangle = \mathbf{Z} \langle \mathbf{Y} \rangle + \mathbf{I}_{\text{pump}}, \tag{3.8}$$

$$\dot{\tilde{\mathbf{Y}}} = \mathbf{Z} \tilde{\mathbf{Y}} + \mathbf{I}_{\text{noise}}, \tag{3.9}$$

where

$$\mathbf{Z} = \begin{pmatrix} -\kappa + i\Delta_{\text{c},1} & 0 & \cdots & 0 & -ig_{11} & -ig_{12} & \cdots & -ig_{1N_a} \\ 0 & -\kappa + i\Delta_{\text{c},2} & \cdots & 0 & -ig_{21} & -ig_{22} & \cdots & -ig_{2N_a} \\ \vdots & \vdots & \ddots & \vdots & \vdots & \vdots & & \vdots \\ 0 & 0 & \cdots & -\kappa + i\Delta_{\text{c},N_c} & -ig_{N_c1} & -ig_{N_c2} & \cdots & -ig_{N_cN_a} \\ -ig_{11}^* & -ig_{21}^* & \cdots & -ig_{N_c1}^* & -\gamma + i\Delta_a & 0 & \cdots & 0 \\ -ig_{12}^* & -ig_{22}^* & \cdots & -ig_{N_c2}^* & 0 & -\gamma + i\Delta_a & \cdots & 0 \\ \vdots & \vdots & & \vdots & \vdots & \vdots & \ddots & \vdots \\ -ig_{1N_a}^* & -ig_{2N_a}^* & \cdots & -ig_{N_cN_a}^* & 0 & 0 & \cdots & -\gamma + i\Delta_a \end{pmatrix}, \tag{3.10}$$

$$\mathbf{I}_{\text{pump}} = \begin{pmatrix} \eta_1 \\ \eta_2 \\ \vdots \\ \eta_{N_c} \\ 0 \\ 0 \\ \vdots \\ 0 \end{pmatrix}, \tag{3.11}$$

and

$$\mathbf{I}_{\text{noise}} = \begin{pmatrix} F_{\text{mode},1} \\ F_{\text{mode},2} \\ \vdots \\ F_{\text{mode},N_c} \\ F_{\text{atom},1} \\ F_{\text{atom},2} \\ \vdots \\ F_{\text{atom},N_a} \end{pmatrix}. \tag{3.12}$$

Note that the equation for the expectation value $\langle \mathbf{Y} \rangle$ does not contain the vector $\tilde{\mathbf{Y}}$ and vice versa, i.e. the equations decouple from each other. Also, the equation for the expectation values does not contain the noise operators $F_{\text{mode},i}$ and $F_{\text{atom},j}$ any more, because the expectation values of the noise operators vanish. Therefore, the equation for the expectation values $\langle a_i \rangle$ and $\left\langle \sigma_j^- \right\rangle$ have become quite simple.

As a next step, products of raising and lowering operators will be considered. The goal is to calculate the expectation value of the product from the expectation values of the single operators alone. This will be discussed using the product $\left\langle a^\dagger \sigma_j^- \right\rangle$ as an example. Using Eq. (3.7), one may write

$$\begin{aligned} \left\langle a_i^\dagger \sigma_j^- \right\rangle &= \left\langle \left(\left\langle a_i^\dagger \right\rangle + \tilde{a}_i^\dagger \right) \left(\left\langle \sigma_j^- \right\rangle + \tilde{\sigma}_j^- \right) \right\rangle \\ &= \langle a_i \rangle^* \left\langle \sigma_j^- \right\rangle + \langle a_i \rangle^* \left\langle \tilde{\sigma}_j^- \right\rangle + \langle \tilde{a}_i \rangle^* \left\langle \sigma_j^- \right\rangle + \left\langle \tilde{a}_i{}^\dagger \tilde{\sigma}_j^- \right\rangle. \end{aligned} \tag{3.13}$$

The unknowns on the right hand side of this equation are the expectation values $\left\langle \tilde{\sigma}_j^- \right\rangle$, $\langle \tilde{a}_i \rangle$ and $\left\langle \tilde{a}_i^\dagger \tilde{\sigma}_j^- \right\rangle$. To calculate them, the quantities $\tilde{\sigma}_j^- |\Psi\rangle$ and $\tilde{a}_i |\Psi\rangle$ are considered, where $|\Psi\rangle$ is the state of the atom-cavity system combined with a zero-temperature reservoir. Those quantities are known if $\tilde{\mathbf{Y}} |\Psi\rangle$ is known. The equation of motion for this expression is

$$\begin{aligned} \frac{\mathrm{d}}{\mathrm{d}t} \tilde{\mathbf{Y}} |\Psi\rangle &= \mathbf{Z} \tilde{\mathbf{Y}} |\Psi\rangle + \mathbf{I}_{\text{noise}} |\Psi\rangle \\ &= \mathbf{Z} \tilde{\mathbf{Y}} |\Psi\rangle . \end{aligned} \tag{3.14}$$

The second term of the right hand side in the first line is zero because the noise operators yield zero when applied to a state with zero-temperature reservoir, as explained above.

Eq. (3.14) is the equation of motion for a set of coupled damped harmonic oscillators with no external excitation. Because of the damping, the solution for $t \to \infty$ is $\tilde{\mathbf{Y}} |\Psi\rangle = 0$. Even if $\tilde{\mathbf{Y}} |\Psi\rangle$ was not zero at the start of the calculation, this quantity would be very close to zero after several typical damping times of the system. Thus, one can conclude that

$$\tilde{\mathbf{Y}} |\Psi\rangle = \mathbf{0}, \tag{3.15}$$

and

$$\tilde{\sigma}_j^- |\Psi\rangle = \tilde{a}_i |\Psi\rangle = 0. \tag{3.16}$$

Inserting this into Eq. (3.13) yields

$$\left\langle a_i^\dagger \sigma_j^- \right\rangle = \langle a_i \rangle^* \left\langle \sigma_j^- \right\rangle. \tag{3.17}$$

The same proof can be used for any normally ordered operator product of atomic and cavity raising and lowering operators. Thus, in the harmonic-oscillator model, the expectation value of such a product is the product of expectation values of the single raising and lowering operators.

For products which are not normally ordered, the operator commutator relations can be used to order the product normally. In the harmonic-oscillator model, the commutators at equal time are

$$\left[Y_i, Y_j^\dagger\right] = \delta_{ij}, \quad [Y_i, Y_j] = \left[Y_i^\dagger, Y_j^\dagger\right] = 0. \tag{3.18}$$

Thus, the steady state of any combination of raising and lowering operators can be calculated, with the restrictions mentioned when introducing the harmonic-oscillator model before Eq. (3.5).

3.3 Connection to measurable quantities

In this section, the relation between some quantities which can be measured experimentally and the parameters and operators in the quantum mechanical model are investigated. The equations in this section are also valid outside the model of coupled harmonic oscillators.

The power transmitted through the cavity can be deduced from the expectation values of the photon number operators for the modes, $a_i^\dagger a_i$. The flux of energy out of all cavity modes which is caused by the non-perfectly reflecting mirrors is given by

$$P_{\text{tot}} = 2\hbar\omega_l \sum_{i=1}^{N_c} \kappa_i \left\langle a_i^\dagger a_i \right\rangle. \tag{3.19}$$

For a Fabry-Perot type cavity consisting of two identical mirrors, the energy flux through the back mirror is half of P_{tot}. Of the photons associated with this flux, only $\mathcal{T}/(\mathcal{T}+\mathcal{L})$ are transmitted through the mirror, where $\mathcal{T}$ is the power transmittance of the mirrors, and $\mathcal{L}$ are the losses. The other photons are lost. Thus, the transmitted power is

$$P_{\text{trans}} = \hbar\omega_l \frac{\mathcal{T}}{\mathcal{T}+\mathcal{L}} \sum_{i=1}^{N_c} \kappa_i \left\langle a_i^\dagger a_i \right\rangle. \tag{3.20}$$

The power of the incident pump light for mode i, $P_{\text{in},i}$, is related to the pump parameter of mode i, η_i, by

$$P_{\text{in},i} = \hbar\omega_l \frac{\mathcal{T}+\mathcal{L}}{\mathcal{T}} \frac{|\eta_i|^2}{\kappa_i}. \tag{3.21}$$

Here, perfect mode matching between the pump beam and the mode is assumed. For non-perfect mode matching, the left hand side of the equation has to be multiplied by the fraction of the pump light which has perfect overlap with the mode, see also the discussion near Eq. (4.2). Equation (3.21) can be deduced by comparing the steady state transmission of an empty cavity in the classical model, see Eq. (2.30) for $N_{\text{eff}} = 0$, and in the quantum model, see Eq. (3.38) for $g_{\text{eff}} = 0$ and Eq. (3.20).

In some cases, especially if more than one mode is interacting with the atom, it is interesting to know the intensity in the cavity as a function of position. For example, the intensity and the relative phases of the light field in the different modes can be measured by observing the interference pattern of the modes. This is nothing else but the spatial dependence of the intensity of the total light field. Also, the intensity distribution of the transmitted light is closely connected to the intensity distribution in the cavity: If the transmittance of the outcoupling mirror is uniform over the mirror, the intensity pattern just after the mirror is the same as the intensity pattern in the cavity just before the outcoupling mirror.

The electric field operator for the cavity light field is given by (MS99, chapter 13)

$$E(\mathbf{r},t) = E^{+}(\mathbf{r},t) + E^{-}(\mathbf{r},t), \tag{3.22}$$

where

$$E^{+}(\mathbf{r},t) = \sqrt{\frac{\hbar\omega_l}{2\epsilon_0 V}} \sum_{i=1}^{N_c} a_i(t)\,\psi_i(r)\,e^{-i\omega t}, \tag{3.23}$$

$$E^{-} = \left(E^{+}\right)^{*}, \tag{3.24}$$

and V is the mode volume, see Eq. (2.22). The intensity operator of the light field inside the cavity, $I(\mathbf{r})$, is given by (Car93, Eq. (5.37)) :

$$I(\mathbf{r},t) = \hbar\frac{\omega_l c}{V} \sum_{i,j=1}^{N_c} \psi_i^{*}(\mathbf{r})\,\psi_j(\mathbf{r})\,a_i^{\dagger}(t)\,a_j(t), \tag{3.25}$$

As was mentioned in the introduction, the atoms are subject to light forces. The position of the atoms determines the coupling constants, which in turn determine the steady state of the system. Thus, the light forces can have a large influence on the time evolution of the system. The operator describing the cavity light force acting on atom j is given by (HGHR98, Eq. (30))

$$\mathbf{F}_{\text{cav},j} = -\hbar \sum_{i=1}^{N_c} \left[\left(\boldsymbol{\nabla}_j g_{ij}\right) a_i^{\dagger}\sigma_j^{-} + \left(\boldsymbol{\nabla}_j g_{ij}^{*}\right)\sigma_j^{+} a_i \right]. \tag{3.26}$$

Here, $\boldsymbol{\nabla}_j$ denotes the gradient with respect to the position of the jth atom, $\mathbf{r}_j$. Note that $\mathbf{F}_{\text{cav},j}$ contains both radiation pressure and dipole force.

3.4 Steady-state expectation values

In this section, the steady-state solutions of Eq. (3.8) are calculated. It is assumed that the atoms do not move, i.e. all expectation values will be calculated in zeroth order in the velocities of the atom, which will be denoted by a subscript $_0$.

The steady state of Eq. (3.8) is obtained by setting the time derivative of $\langle \mathbf{Y} \rangle$ equal to zero. This results in the steady-state solution

$$\langle \mathbf{Y} \rangle_0 = -\mathbf{Z}^{-1} \mathbf{I}_{\text{pump}}. \tag{3.27}$$

This solution gives the steady-state expectation values of all single lowering operators. The expectation values of raising operators are the complex conjugate of the lowering operators. The expectation values of products of operators can easily be calculated as explained in the previous section, see the discussion of Eq. (3.17). As an example, the expectation value of the total number of photons in the cavity for one atom and three modes is drawn in Fig. 3.3.

In the following, some expectation values are explicitly calculated for two special cases: First, for N_a atoms with the same decay rates and resonance frequencies interacting with a single mode of the cavity, i.e. $\Delta_{\mathrm{a},j} = \Delta_a$, $\gamma_j = \gamma$, and $N_c = 1$. As second case, a single atom in a cavity with N_c degenerate modes of the cavity which have the same field decay rate, i.e. $\Delta_{\mathrm{c},i} = \Delta_c$, $\kappa_i = \kappa$, and $N_a = 1$, is considered. Mathematically, these two special cases are nearly equivalent, if one exchanges the atoms and cavity modes. The only exception is the pump vector, $\mathbf{I}_{\text{pump}}$, as only the cavity modes are pumped. The very special case of a single atom interacting with a single mode of the cavity is contained in both cases. The results of section 3.4.1 can conveniently be specialized for this case.

3.4.1 Atoms interacting with a single mode

In this section, it is assumed that the atoms interact with a single mode of the cavity, and that all atoms have the same decay rate and the same transition frequency, i.e. $\gamma_j = \gamma$ and $\Delta_{a,j} = \Delta_a$. The detuning and the decay rate of the single mode are called Δ_c and κ, respectively. In this case, the inverse of the matrix $\mathbf{Z}$ is given by

$$\mathbf{Z}^{-1} = \frac{1}{A} \begin{pmatrix} -\gamma + i\Delta_{\mathrm{a}} & ig_{11} & ig_{12} & ig_{13} & \cdot & ig_{1N_a} \\ ig_{11}^* & \frac{A-|g_{11}|^2}{-\gamma+i\Delta_{\mathrm{a}}} & \frac{-g_{11}^* g_{12}}{-\gamma+i\Delta_{\mathrm{a}}} & \frac{-g_{11}^* g_{13}}{-\gamma+i\Delta_{\mathrm{a}}} & \cdots & \frac{-g_{11}^* g_{1N_a}}{-\gamma+i\Delta_{\mathrm{a}}} \\ ig_{12}^* & \frac{-g_{12}^* g_{11}}{-\gamma+i\Delta_{\mathrm{a}}} & \frac{A-|g_{12}|^2}{-\gamma+i\Delta_{\mathrm{a}}} & \frac{-g_{12}^* g_{13}}{-\gamma+i\Delta_{\mathrm{a}}} & \cdots & \frac{-g_{12}^* g_{1N_a}}{-\gamma+i\Delta_{\mathrm{a}}} \\ ig_{13}^* & \frac{-g_{13}^* g_{11}}{-\gamma+i\Delta_{\mathrm{a}}} & \frac{-g_{13}^* g_{12}}{-\gamma+i\Delta_{\mathrm{a}}} & \frac{A-|g_{13}|^2}{-\gamma+i\Delta_{\mathrm{a}}} & \cdots & \frac{-g_{13}^* g_{1N_a}}{-\gamma+i\Delta_{\mathrm{a}}} \\ \vdots & \vdots & \vdots & \vdots & \ddots & \vdots \\ ig_{1N_a}^* & \frac{-g_{1N_a}^* g_{11}}{-\gamma+i\Delta_{\mathrm{a}}} & \frac{-g_{1N_a}^* g_{12}}{-\gamma+i\Delta_{\mathrm{a}}} & \frac{-g_{1N_a}^* g_{13}}{-\gamma+i\Delta_{\mathrm{a}}} & \cdots & \frac{A-|g_{1N_a}|^2}{-\gamma+i\Delta_{\mathrm{a}}} \end{pmatrix}, \tag{3.28}$$

where

$$A = (\Delta_{\mathrm{c}}\gamma + \Delta_{\mathrm{a}}\kappa)(S - i), \tag{3.29}$$

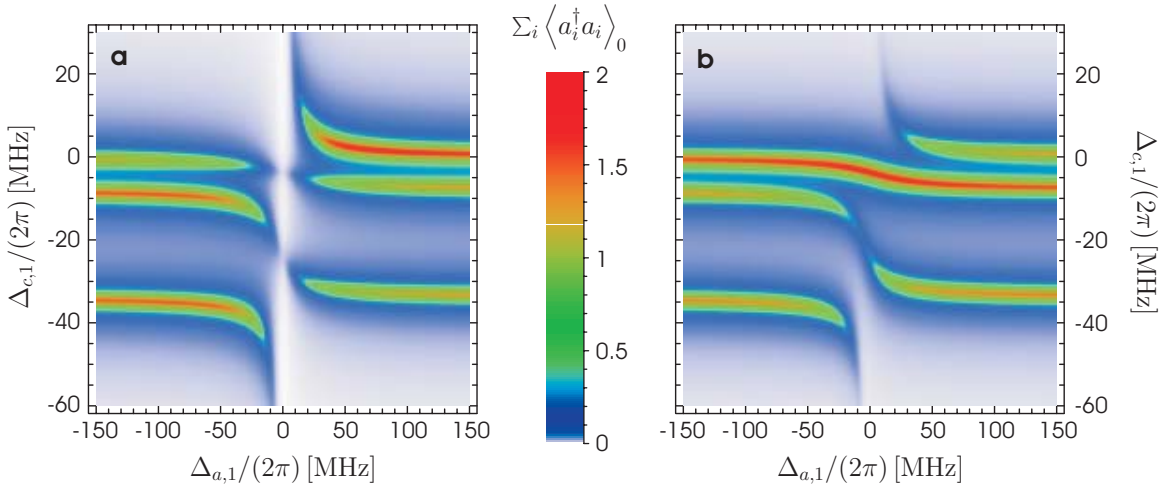

Figure 3.3: The expectation value of the total photon number inside the cavity, $\sum_i \left\langle a_i^\dagger a_i \right\rangle_0$, for one atom and three cavity modes. The horizontal and vertical axes are the laser-atom detuning $\Delta_{a,1}$ and the detuning between laser and the cavity mode with the highest resonance frequency, $\Delta_{c,1}$, respectively. The other modes are resonant at $\Delta_{c,2}/(2\pi) = -8\,\mathrm{MHz}$ and $\Delta_{c,3}/(2\pi) = -34\,\mathrm{MHz}$, the field decay rates are $\kappa_i/(2\pi) = 1.4\,\mathrm{MHz}$. The atomic dipole decay rate is $\gamma/(2\pi) = 3\,\mathrm{MHz}$. The pump is $\eta_i = \kappa_i$ in a) and $\eta_1 = \eta_3 = \kappa_i$, $\eta_2 = -\kappa_i$ in b). The coupling constants between atom and modes are $g_{i1}/(2\pi) = 10\,\mathrm{MHz}$. For large laser-atom detuning, the refractive index of the atom shifts the cavity resonances only by a small amount, whereas close to the atomic resonance, new eigenstates are visible. The decay rates and distances between the modes are taken from the experiment for the modes of order 2, which are a linear combination of the TEM-20, TEM-11 and TEM-02 modes. See also Fig. 5.8

$$S = \frac{g_{\mathrm{eff}}^2 - \Delta_\mathrm{a}\Delta_\mathrm{c} + \gamma\kappa}{\Delta_\mathrm{c}\gamma + \Delta_\mathrm{a}\kappa}, \tag{3.30}$$

and

$$g_{\mathrm{eff}} = \sqrt{\sum_{j=1}^{N_a} |g_{1j}|^2}. \tag{3.31}$$

The quantity g_{eff} is called effective coupling constant, because the system behaves in some aspects as if the cavity mode was interacting with only one "effective" atom which is coupled to the cavity mode with the effective coupling constant. This can be seen by multiplying the differential equations (3.5) with g_{1j}/g_{eff}, and then summing over all these

equations. For atoms at rest, i.e. $\mathrm{d}g_{1j}/\mathrm{d}t = 0$ for all j, the resulting equations are

$$\dot{\langle a\rangle}_0 = i\Delta_\mathrm{c}\langle a\rangle_0 - ig_\mathrm{eff}\left\langle\sigma_\mathrm{eff}^-\right\rangle_0 - \kappa\langle a\rangle_0 + \eta, \tag{3.32}$$

$$\dot{\left\langle\sigma_\mathrm{eff}^-\right\rangle}_0 = i\Delta_\mathrm{a}\left\langle\sigma_\mathrm{eff}^-\right\rangle_0 - ig_\mathrm{eff}\langle a\rangle_0 - \gamma\left\langle\sigma_\mathrm{eff}^-\right\rangle_0, \tag{3.33}$$

where

$$\sigma_\mathrm{eff}^- = \sum_{j=1}^{N_a}\frac{g_{1j}}{g_\mathrm{eff}}\sigma_j^- \tag{3.34}$$

is the lowering operator for the effective atom. Eqs. (3.32) and (3.33) are the set of differential equations describing the interaction of one atom with a single mode of the cavity. One can also use this idea to calculate all quantities of interest, see (FMP$^+$01). However, the treatment presented in this thesis is more general and more elegant.

By multiplying the inverse matrix with the pump vector and using the rule for multiplying operators, Eq. (3.17), the expectation values of the atomic lowering operators, the excitation of the atoms, the lowering operator of the mode, the photon number, and the force are obtained as

$$\langle\sigma_j\rangle_0 = \eta\frac{-ig_{1j}^*}{\Delta_\mathrm{c}\gamma + \Delta_\mathrm{a}\kappa}\,\frac{1}{S-i}, \tag{3.35}$$

$$\begin{aligned}\left\langle\sigma_j^+\sigma_j^-\right\rangle_0 &= \left\langle\sigma_j^-\right\rangle_0^*\left\langle\sigma_j^-\right\rangle_0 \\ &= |\eta|^2\frac{|g_{1j}|^2}{\left(\Delta_\mathrm{c}\gamma + \Delta_\mathrm{a}\kappa\right)^2}\,\frac{1}{1+S^2},\end{aligned} \tag{3.36}$$

$$\langle a\rangle_0 = \eta\frac{\gamma - i\Delta_\mathrm{a}}{\Delta_\mathrm{c}\gamma + \Delta_\mathrm{a}\kappa}\,\frac{1}{S-i}, \tag{3.37}$$

$$\left\langle a^\dagger a\right\rangle_0 = |\eta|^2\frac{\gamma^2 + {\Delta_\mathrm{a}}^2}{\left(\Delta_\mathrm{c}\gamma + \Delta_\mathrm{a}\kappa\right)^2}\,\frac{1}{1+S^2}, \tag{3.38}$$

$$\langle\mathbf{F}_{\mathrm{cav},j}\rangle_0 = -2\hbar|\eta|^2\Delta_\mathrm{a}\frac{g_{1j}^*\boldsymbol{\nabla}_j g_{1j}}{\left(\Delta_\mathrm{c}\gamma + \Delta_\mathrm{a}\kappa\right)^2}\,\frac{1}{1+S^2}. \tag{3.39}$$

As an example, the expectation value of the photon number and the expectation value of the atomic excitation are drawn in Fig. 3.4. These expectation values divided by $|\eta|^2$ are large if S is small as compared to one. The detunings where S equals zero are the positions of the normal modes of the coupled harmonic-oscillator system. Thus, S can be considered as dimensionless distance from a normal mode of the system.

For the calculation of the expectation value of the cavity light force, it was assumed that

$$g_{ij}\left(\mathbf{r}_j\right) = e^{i\phi}\,\tilde{g}_{ij}\left(\mathbf{r}_j\right), \tag{3.40}$$

where $\tilde{g}_{ij}\left(\mathbf{r}_j\right)$ is a real-valued function, and ϕ does not depend on position. This is the case because $g_{ij} = g_0\,\psi_i\left(\mathbf{r}_j\right)$, where g_0 is constant. The mode function $\psi_i\left(\mathbf{r}_j\right)$ is a solution

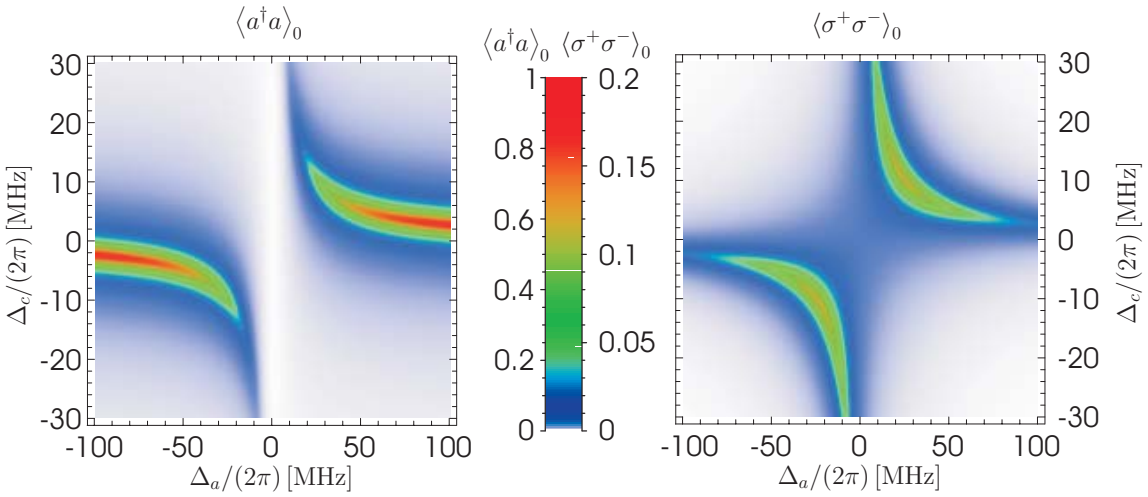

Figure 3.4: The expectation value of the photon number, $\left\langle a^\dagger a\right\rangle_0$, and the excitation of an atom, $\left\langle \sigma_j^+\sigma_j^-\right\rangle_0$, drawn against the laser-atom detuning Δ_a and the laser-cavity detuning Δ_c. The other parameters are $\kappa/(2\pi) = 1.4\,\mathrm{MHz}$, $\gamma/(2\pi) = 3\,\mathrm{MHz}$, $\eta = \kappa$, and $g_{\mathrm{eff}}/(2\pi) = 16\,\mathrm{MHz}$. As compared to Fig. 3.3, the pattern looks simpler, because of the correspondence with the single-atom system. The excitation of the atom and the photon number are both large near to the normal modes of the system.

of the Laplace equation, $\triangle\psi_i - \omega_c^2/c^2\psi_i = 0$. As ω_c^2/c^2 is a real number, also the real and the imaginary part of $\psi_i(\mathbf{r}_j)$ are a solution of the Laplace equation. Because it was assumed that only one mode interacts with the atoms, the imaginary part and the real part of the mode function must be linearly dependent. This means that the real part is a constant times the imaginary part or vice versa. Therefore, the whole mode function is proportional to its real part or its imaginary part, which is expressed in Eq. (3.40).

The expectation value of the cavity light force, $\langle \mathbf{F}_{\mathrm{cav},j}\rangle$, can be integrated to give a N-particle potential

$$V_{\mathrm{cav}} = \hbar|\eta|^2 \frac{\Delta_a}{\Delta_{\mathrm{c}}\gamma + \Delta_{\mathrm{a}}\kappa} \arctan(S)\,, \tag{3.41}$$

which depends via S and g_{eff} on the positions of all particles. Fig. 3.5 gives an example of the dipole potential of one atom in presence of other atoms. For each atom, the dipole potential strongly depends on the coupling of the other atoms, which shows that one atom influences the light force on the other atoms via the common cavity light field. For a further discussion of this point and sample movies showing the interaction between two atoms via the cavity light field, see (FMP$^+$01).

For a single atom interacting with a single mode, one can replace the effective coupling

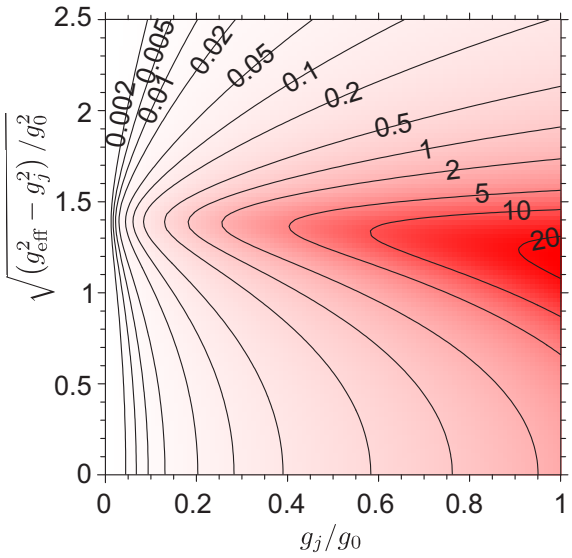

Figure 3.5: The potential energy for the atom j as a function of its coupling constant, g_{1j}, and the effective coupling constant of all the other atoms, $\sqrt{g_{\rm eff}^2 - g_{1j}^2}$. The other parameters are $\Delta_a/(2\pi) = -50\,\mathrm{MHz}$, $\Delta_c/(2\pi) = -10\,\mathrm{MHz}$; κ and γ are the same as in Fig. 3.4. Dark red shading denotes regions of large negative potential. The numbers on the contour lines indicate the values of the quasi-single-atom potential $-\left[V_{\rm cav}\left(g_{\rm eff}\right) - V_{\rm cav}\left(\sqrt{g_{\rm eff}^2 - g_{1j}^2}\right)\right]/(10^6\hbar)$ in units of 1/s. The effective coupling constant of the other atoms has a strong influence on the dipole potential and thus on the dipole force acting on atom j.

constant $g_{\rm eff}$ with the single-atom coupling constant g_{11}, and the results stay correct.

The intensity transmitted through the cavity, calculated in the quantum-mechanical model by the expectation value $\left\langle a^\dagger a \right\rangle_0$ and Eq. (3.20), yields the same result as the transmitted intensity which was calculated for a classical electromagnetic field, Eq. (2.30). For the comparison, one needs the relations

$$2C_0 N_{\rm eff} = g_{\rm eff}^2/\left(\kappa\gamma\right), \tag{3.42}$$

which can be deduced using the definitions for C_0, $N_{\rm eff}$, g_0, g_{ij}, and $g_{\rm eff}$, Eqs. (2.21), (2.23), (3.2), (3.1) and (3.31), and the relation between η and the incident intensity, Eq. (3.21). Thus, the classical model can also be used for a correct calculation of the steady state of the light field and the atoms for low saturation of the atoms. This may be somewhat surprising, as for less than one photons in the cavity, the quantum fluctuations of the field are comparable to or larger than its mean value. In the classical model, these fluctuations are neglected. Yet, the linearity of the system "rescues" the classical behaviour. For a

non-linear system, e.g. if the atom is saturated, the classical calculation fails.

In the quantum model, the minimum number of photons n_p needed to saturate an atom can be calculated as

$$n_p = \left.\frac{\left\langle a^\dagger a\right\rangle_0}{2\left\langle \sigma_j^+\sigma_j^-\right\rangle_0}\right|_{\Delta_a=0,g_{ij}=g_0} = \frac{\gamma^2}{2g_0^2}. \tag{3.43}$$

This definition is the same as the definition of the saturation intensity of a classical light field(MS99, Eqs. (5.19), (5.21) and (5.23)) in the limit of small saturation. A value of n_p smaller than one indicates that a single intracavity photon can have a large effect on the internal state of an atom in the cavity.

3.4.2 Single atom interacting with degenerate modes

In this section, the case where a single atom interacts with N_c degenerate cavity modes which have the same field decay rates is investigated. Then, $\Delta_{c,i} = \Delta_c$, and $\kappa_i = \kappa$. The laser-atom detuning and the decay rate for the single atom are Δ_a and γ, respectively. The inverse of the matrix $\mathbf{Z}$ is similar to the single-mode case. It is given by

$$\mathbf{Z}^{-1} = \frac{1}{A}\begin{pmatrix} \frac{A-|g_{11}|^2}{-\kappa+i\Delta_c} & \frac{-g_{11}g_{21}^*}{-\kappa+i\Delta_c} & \frac{-g_{11}g_{31}^*}{-\kappa+i\Delta_c} & \cdots & \frac{-g_{11}g_{N_c1}^*}{-\kappa+i\Delta_c} & ig_{11} \\ \frac{-g_{21}g_{11}^*}{-\kappa+i\Delta_c} & \frac{A-|g_{21}|^2}{-\kappa+i\Delta_c} & \frac{-g_{21}g_{31}^*}{-\kappa+i\Delta_c} & \cdots & \frac{-g_{21}g_{N_c1}^*}{-\kappa+i\Delta_c} & ig_{21} \\ \frac{-g_{31}g_{11}^*}{-\kappa+i\Delta_c} & \frac{-g_{31}g_{21}^*}{-\kappa+i\Delta_c} & \frac{A-|g_{31}|^2}{-\kappa+i\Delta_c} & \cdots & \frac{-g_{31}g_{N_c1}^*}{-\kappa+i\Delta_c} & ig_{31} \\ \vdots & \vdots & \vdots & \vdots & \ddots & \vdots \\ \frac{-g_{N_c1}g_{11}^*}{-\kappa+i\Delta_c} & \frac{-g_{N_c1}g_{21}^*}{-\kappa+i\Delta_c} & \frac{-g_{N_c1}g_{31}^*}{-\kappa+i\Delta_c} & \cdots & \frac{A-|g_{N_c1}|^2}{-\kappa+i\Delta_c} & ig_{N_c1} \\ ig_{11}^* & ig_{21}^* & ig_{31}^* & \cdots & ig_{N_c1}^* & -\kappa+i\Delta_c \end{pmatrix}. \tag{3.44}$$

In this context, A is defined as in Eqs. (3.29) and (3.30), but the effective coupling is now

$$g_{\text{eff}} = \sqrt{\sum_{i=1}^{N_c}|g_{i1}|^2} \tag{3.45}$$

The steady-state solutions are

$$\left\langle \sigma^-\right\rangle_0 = \eta_{\text{eff}}\frac{-ig_{\text{eff}}}{\Delta_c\gamma+\Delta_a\kappa}\frac{1}{S-i} \tag{3.46}$$

$$\left\langle \sigma^+\sigma^-\right\rangle_0 = |\eta_{\text{eff}}|^2\frac{g_{\text{eff}}^2}{(\Delta_c\gamma+\Delta_a\kappa)^2}\frac{1}{1+S^2} \tag{3.47}$$

$$\langle a_i\rangle_0 = \frac{\eta_i}{\kappa-i\Delta_c} - \frac{g_{\text{eff}}\,\eta_{\text{eff}}\,g_{i1}}{(\kappa-i\Delta_c)(\Delta_c\gamma+\Delta_a\kappa)}\frac{1}{S-i} \tag{3.48}$$

$$\left\langle a_i^\dagger a_i\right\rangle_0 = \langle a_i\rangle_0^*\langle a_i\rangle_0 \tag{3.49}$$

$$\left\langle \mathbf{F}_{\text{cav},1}\right\rangle_0 = \hbar\left[\frac{g_{\text{eff}}^2\eta_{\text{eff}}\left(\boldsymbol{\nabla}\eta_{\text{eff}}^*\right)(S+i)}{(\Delta_c-i\kappa)(\Delta_c\gamma+\Delta_a\kappa)} + c.c. - |\eta_{\text{eff}}|^2\frac{\Delta_a\left[\boldsymbol{\nabla}\left(g_{\text{eff}}^2\right)\right]}{(\Delta_c\gamma+\Delta_a\kappa)^2}\right]\frac{1}{1+S^2}, \tag{3.50}$$

where

$$\eta_{\text{eff}} = \sum_{i=1}^{N_c} \frac{g_{i1}^*}{g_{\text{eff}}} \eta_i. \tag{3.51}$$

In some cases, the calculations are significantly simplified if the basis consists of real-valued modefunctions. For every subspace of interacting modes where the modes have the same κ and Δ_c, such a basis can be found. This may be seen as follows: The mode functions are solutions of the Laplace equation, $\triangle\psi_i - (\omega_c^2/c^2)\psi_i = 0$. As ω_c^2/c^2 is a real number, the real part and the imaginary part of each mode function is also a solution of this equation. Thus, the subspace of interacting modes is generated by the set of real parts and imaginary parts of the mode functions. This means that every interacting mode can be obtained as a linear superposition of the real parts and the imaginary parts of the original mode functions. Note that the $2N_c$ real and imaginary parts do not form a basis, as they are linearly dependent, but they are already real-valued. From this set of functions, one can choose N_c linearly independent functions, which then form a basis. This basis can be ortho-normalized by Gram-Schmidt orthonormalization (Lan72, chapter IV, §2, theorem 5), in which the mode functions stay real-valued.

Similar to the effective-atom approach in section 3.4.1, the system can be described as an atom interacting with one effective mode only. The reason is that the modes form the basis of a Hilbert space. Because every mode, i.e every basis vector, has the same resonance frequency and the same decay rate, any superposition of the modes also has the same properties. Thus, any orthonormal basis of the space of interacting modes can be used to describe the system. In particular, a orthonormal basis can be chosen where only one mode couples to the atom. This mode is called the 'effective mode'. All the other modes do not sense the presence of an atom and thus behave as if there was no atom present. This condition determines the effective mode except for a constant phase factor, as it has to be orthogonal to a $(N_c - 1)$-dimensional subspace of the N_c-dimensional vector space. The mode function of the effective mode is given by

$$\psi_{\text{eff}}(\mathbf{r}) = \sum_{i=1}^{N_c} \frac{g_{i1}^*}{g_{\text{eff}}} \psi_i(\mathbf{r}). \tag{3.52}$$

This can be seen as follows: For a fixed $\mathbf{r}$, the value of $|\psi_i|^2(\mathbf{r})$ does not depend on the choice of the basis, if the basis is orthonormal. This can be proved by showing that $g_{\text{eff}}^2(\mathbf{r})$ is constant under basis transformations with an unitary matrix U_{ki}:

$$\begin{aligned}
\sum_{k=1}^{N_c} \left| \sum_{i=1}^{N_c} U_{ki}\, \psi_i(\mathbf{r}) \right|^2 &= \sum_{k=1}^{N_c} \sum_{i=1}^{N_c} \sum_{l=1}^{N_c} U_{ki}\, \psi_i(\mathbf{r})\, U_{kl}^*\, \psi_{l1}^*(\mathbf{r}) \\
&= \sum_{k=1}^{N_c} \sum_{i=1}^{N_c} \sum_{l=1}^{N_c} U_{ki}\, \psi_i(\mathbf{r})\, (\mathbf{U}^{-1})_{lk}\, \psi_l^*(\mathbf{r}) \\
&= \sum_{i=1}^{N_c} \sum_{l=1}^{N_c} \psi_i(\mathbf{r}) \psi_l^*(\mathbf{r})\, \delta_{il}
\end{aligned}$$

$$= \sum_{i=1}^{N_c} |\psi_i(\mathbf{r})|^2. \tag{3.53}$$

From the first line to the second line, the property of unitary matrices that $\mathbf{U}^\dagger = \mathbf{U}^{-1}$ was used. The matrix $\mathbf{U}^\dagger$ is the hermitian conjugate of $\mathbf{U}$, defined by $\left(\mathbf{U}^\dagger\right)_{mk} = (U_{km})^*$.

Having proved this, one can now choose an unitary basis transformation such that ψ_{eff} is one of the basis vectors, because ψ_{eff} is normalized. From the definition of $\psi_{\text{eff}}(\mathbf{r})$, it is easy to show that

$$|\psi_{\text{eff}}(\mathbf{r})|^2 = \sum_{i=1}^{N_c} |\psi_i(\mathbf{r})|^2. \tag{3.54}$$

From this and Eq. (3.53), it follows that the other basis vectors of the transformed basis containing ψ_{eff} are zero at the position $\mathbf{r}$, which is the condition for ψ_{eff} being the effective mode, qed.

From Eq. (3.52), the effective mode is real-valued if the mode functions are real-valued. As the effective mode does not depend on the choice of basis, except in that it may acquire a constant phase, one can conclude that the effective mode always can be made real-valued by multiplying it with a constant number with a modulus of one.

The pump of the effective mode is given by η_{eff}. Note that unlike g_{eff}, the effective pump η_{eff} may be a complex number. The lowering operator, a_{eff}, of the effective mode is

$$a_{\text{eff}} = \sum_{i=1}^{N_c} \frac{g_{i1}^*}{g_{\text{eff}}} a_i \tag{3.55}$$

The steady-state solution for the effective mode lowering operator is given by

$$\langle a_{\text{eff}} \rangle_0 = \eta_{\text{eff}} \frac{\gamma - i\Delta_a}{\Delta_{\text{c}}\gamma + \Delta_{\text{a}}\kappa} \frac{1}{S - i} \tag{3.56}$$

An application of an atom interacting with several degenerate modes is given in chapter 4.

3.5 The momentum diffusion constant

Until now, only the expectation value of the light force acting on an atom was calculated. However, the light force also increases the width of the momentum distribution of the atom. This can be described as a diffusion in momentum space, the so-called momentum diffusion. As the graph kinetic energy vs momentum has a constant positive second derivative everywhere, a broader momentum distribution leads to an increase of the expectation value of the kinetic energy of the atom, i.e. to heating. The rate of gain in kinetic energy for atom j is proportional to the trace of the momentum diffusion tensor, $\mathbf{D}_j$, which will be calculated in this section. It is assumed that all atoms are at rest, i.e. all quantities will be calculated in zeroth order in atomic velocity. For moving atoms,

the corrections will be small as long as the atoms move slowly $[v_j/\lambda \ll (\kappa_i, \gamma_j)]$ and can in most cases safely be omitted. Readers who are not interested in the details of the calculation can proceed from Eq. (3.57) to the results, Eqs. (3.78), (3.79) and (3.81).

With $\mathbf{P}_j$ denoting the momentum of the jth atom, the diffusion matrix is defined as

$$2\mathbf{D}_j = \frac{\mathrm{d}}{\mathrm{d}t}\left(\langle \mathbf{P}_j \otimes \mathbf{P}_j \rangle - \langle \mathbf{P}_j \rangle \otimes \langle \mathbf{P}_j \rangle\right), \tag{3.57}$$

where the symbol $\otimes$ denotes a tensor product of two vectors. The diagonal elements of the diffusion matrix describe the rate of change in the spread of the atomic wave packet, the off-diagonal elements describe correlations between different coodinates of the atomic motion.

The momentum operator can be related to the force operator acting on atom j via the equation of motion $\mathbf{F}_j = \dot{\mathbf{P}}_j$. Expressing Eq. (3.57) in terms of $\mathbf{F}_j$ yields

$$\mathbf{D}_j = Re \int_{-\infty}^{0} \mathrm{d}t \left[\langle \mathbf{F}_j(0) \otimes \mathbf{F}_j(t) \rangle_0 - \langle \mathbf{F}_j(0) \rangle_0 \otimes \langle \mathbf{F}_j(t) \rangle_0\right]. \tag{3.58}$$

Because the atoms do not move and the system is in equilibrium at $t = 0$, $\langle \mathbf{F}_j(t) \rangle_0$ does not depend on time. Thus, $\langle \mathbf{F}_j(t) \rangle_0$ and $\langle \mathbf{F}_j(0) \rangle_0$ can be replaced by $\langle \mathbf{F}_j \rangle_0$. Also, the integral from minus infinity to zero can be replaced by the integral from zero to infinity:

$$\mathbf{D}_j = Re \int_{0}^{\infty} \mathrm{d}t \left[\langle \mathbf{F}_j(0) \otimes \mathbf{F}_j(t) \rangle_0 - \langle \mathbf{F}_j \rangle_0 \otimes \langle \mathbf{F}_j \rangle_0\right]. \tag{3.59}$$

To carry the calculation further, an explicit expression for the force operator $\mathbf{F}_j$ is necessary. The force operator can be divided into two parts, namely the cavity light force operator, $\mathbf{F}_{\mathrm{cav},j}$, and the force operator, $\mathbf{F}_{\mathrm{se},j}$, which is due to the interaction of the atomic dipole with the modes of the light field which are not supported by the cavity. The latter operator has an expectation value of zero (HGHR98, appendix B), but its nonzero fluctuations contribute to the momentum diffusion. As the light modes which are supported by the cavity are not correlated to the modes which are not supported by the cavity, there is no cross-term, and the two contributions can be calculated separately.

The momentum diffusion matrix, $\mathbf{D}_{\mathrm{cav},j}$, which enters through the cavity light force, $\mathbf{F}_{\mathrm{cav},j}$, is calculated first. The definition of the cavity light force operator, Eq. (3.26), leads to

$$\begin{aligned}
\mathbf{D}_{\mathrm{cav},j} \;=\; & \hbar^2 \sum_{i,k=1}^{N_c} Re \int_0^\infty \mathrm{d}t \\
& \Big\{ \Big\langle \Big[\left(\boldsymbol{\nabla}_j g_{ij}^*\right) \sigma_j^+(0)\, a_i(0) + \left(\boldsymbol{\nabla}_j g_{ij}\right) a_i^\dagger(0)\, \sigma_j^-(0) \Big] \otimes \\
& \quad \Big[\left(\boldsymbol{\nabla}_j g_{kj}^*\right) \sigma_j^+(t)\, a_k(t) + \left(\boldsymbol{\nabla}_j g_{kj}\right) a_k^\dagger(t)\, \sigma_j^-(t) \Big] \Big\rangle_0 \\
& - \Big\langle \left(\boldsymbol{\nabla}_j g_{ij}^*\right) \sigma_j^+ a_i + \left(\boldsymbol{\nabla}_j g_{ij}\right) a_i^\dagger \sigma_j^- \Big\rangle_0 \otimes \\
& \quad \Big\langle \left(\boldsymbol{\nabla}_j g_{kj}^*\right) \sigma_j^+ a_k + \left(\boldsymbol{\nabla}_j g_{kj}\right) a_k^\dagger \sigma_j^- \Big\rangle_0 \Big\},
\end{aligned} \tag{3.60}$$

All the a_i and σ_j^- are contained in the vector $\mathbf{Y}$, see Eq. (3.6). Thus, the diffusion matrix $\mathbf{D}_{\mathrm{cav},j}$ is easily calculated if the correlation integrals α_{ijkl} are known, which are defined by

$$\alpha_{ijkl} = \int_0^\infty \mathrm{d}t \left\langle Y_i^\dagger(0)\, Y_j(0)\, Y_k^\dagger(t)\, Y_l(t)\right\rangle_0 - \left\langle Y_i^\dagger Y_j\right\rangle_0 \left\langle Y_k^\dagger Y_l\right\rangle_0. \tag{3.61}$$

As the operators in the second term under the integral in Eq. (3.61) are evaluated at the same time and they are in normal order, $\left\langle Y_i^\dagger Y_j\right\rangle_0 = \langle Y_i\rangle_0^* \langle Y_j\rangle_0$. Using this, Eq. (3.61) can be rearranged to

$$\begin{aligned}
\alpha_{ijkl} \;=\; & \int_0^\infty \mathrm{d}t \left\langle Y_i^\dagger(0)\, Y_j(0) \left(Y_k^\dagger(t) - \langle Y_k\rangle^*\right) \left(Y_l(t) - \langle Y_l\rangle\right)\right\rangle_0 \\
& + \langle Y_l\rangle_0 \int_0^\infty \mathrm{d}t \left\langle Y_i^\dagger(0)\, Y_j(0) \left(Y_k^\dagger(t) - \langle Y_k\rangle^*\right)\right\rangle_0 \\
& + \langle Y_k\rangle_0^* \int_0^\infty \mathrm{d}t \left\langle Y_i^\dagger(0)\, Y_j(0) \left(Y_l(t) - \langle Y_l\rangle\right)\right\rangle_0 .
\end{aligned} \tag{3.62}$$

The last term on the right hand side of this equation is evaluated most easily. According to the quantum regression theorem (see e.g. Car93, chapter 3.2), the equation of motion for an expectation value of a correlation function of a linear operator is the same as the equation of motion for an expectation value of an operator alone, if the equation of motion is linear in the operator. This is also true if a constant number is added to the linear operator, which can be proved along the same line as the proof starting with Eq. (3.35) in (Car93). In other words, because

$$\mathrm{d}/\mathrm{d}t \left\langle Y_l(t) - \langle Y_l\rangle\right\rangle = \sum_m Z_{lm} \langle Y_m(t) - \langle Y_m\rangle\rangle, \tag{3.63}$$

see Eqs. (3.8) and (3.27), it is also true that

$$\frac{\mathrm{d}}{\mathrm{d}t}\left\langle Y_i^\dagger(0)\, Y_j(0) \left(Y_l(t) - \langle Y_l\rangle\right)\right\rangle = \sum_m Z_{lm} \left\langle Y_i^\dagger(0)\, Y_j(0) \left(Y_m(t) - \langle Y_m\rangle\right)\right\rangle. \tag{3.64}$$

However, at $t = 0$, for atoms at rest and for all m, the expectation value on the right hand side is

$$\begin{aligned}
\left\langle Y_i^\dagger(0)\, Y_j(0) \left(Y_m(t) - \langle Y_m\rangle\right)\right\rangle_0\Big|_{t=0} \;&=\; \langle Y_i\rangle_0^* \langle Y_j\rangle_0 \left(\langle Y_m\rangle_0 - \langle Y_m\rangle_0\right) \\
&=\; 0
\end{aligned} \tag{3.65}$$

Thus, the solution of the differential equation (3.64) is

$$\left\langle Y_i^\dagger(0)\, Y_j(0) \left(Y_l(t) - \langle Y_l\rangle\right)\right\rangle_0 = 0, \tag{3.66}$$

and the third term of the right hand side of Eq. (3.62) is zero.

The first term of the right hand side of Eq. (3.62) can be calculated in a similar manner. The equation of motion for $\left(Y_k^\dagger(t) - \left\langle Y_k^\dagger \right\rangle\right)(Y_l(t) - \langle Y_l\rangle)$ is given by Eq. (3.63) as

$$\begin{aligned}
&\frac{\mathrm{d}}{\mathrm{d}t}\Big\langle \left(Y_k^\dagger(t) - \langle Y_k\rangle^*\right)(Y_l(t) - \langle Y_l\rangle)\Big\rangle \\
&\quad = \sum_m \Big\langle \left(Y_m^\dagger(t) - \left\langle Y_m^\dagger \right\rangle\right)(Y_l(t) - \langle Y_l\rangle)\Big\rangle Z_{mk}^\dagger \\
&\qquad + \sum_n Z_{ln}\Big\langle \left(Y_k^\dagger(t) - \left\langle Y_k^\dagger \right\rangle\right)(Y_n(t) - \langle Y_n\rangle)\Big\rangle,
\end{aligned} \tag{3.67}$$

therefore the quantum regression theorem states that

$$\begin{aligned}
&\frac{\mathrm{d}}{\mathrm{d}t}\left\langle Y_i^\dagger(0)\, Y_j(0)\left(Y_k^\dagger(t) - \left\langle Y_k^\dagger \right\rangle\right)(Y_l(t) - \langle Y_l\rangle)\right\rangle \\
&\quad = \sum_m \left\langle Y_i^\dagger(0)\, Y_j(0)\left(Y_m^\dagger(t) - \left\langle Y_m^\dagger \right\rangle\right)(Y_l(t) - \langle Y_l\rangle)\right\rangle Z_{mk}^\dagger \\
&\qquad + \sum_n Z_{ln}\left\langle Y_i^\dagger(0)\, Y_j(0)\left(Y_k^\dagger(t) - \left\langle Y_k^\dagger \right\rangle\right)(Y_n(t) - \langle Y_n\rangle)\right\rangle.
\end{aligned} \tag{3.68}$$

The expectation value at $t = 0$ can be calculated as

$$\begin{aligned}
&\left\langle Y_i^\dagger(0)\, Y_j(0)\left(Y_m^\dagger(t) - \left\langle Y_m^\dagger \right\rangle\right)(Y_n(t) - \langle Y_n\rangle)\right\rangle_0\Big|_{t=0} \\
&\quad = \left\langle Y_i^\dagger\left[Y_m^\dagger - \left\langle Y_m^\dagger \right\rangle, Y_j\right](Y_n - \langle Y_n\rangle)\right\rangle_0 \\
&\qquad + \langle Y_i\rangle_0^*\left(\langle Y_m\rangle_0^* - \langle Y_m\rangle_0^*\right)\langle Y_j\rangle_0\left(\langle Y_n\rangle_0 - \langle Y_n\rangle_0\right) \\
&\quad = \langle Y_i\rangle_0^*\delta_{mj}\left(\langle Y_n\rangle_0 - \langle Y_n\rangle_0\right) \\
&\quad = 0,
\end{aligned} \tag{3.69}$$

where the commutator relation, Eq. (3.18), was used. Again, this gives the trivial solution of Eq. (3.68), namely

$$\left\langle Y_i^\dagger(0)\, Y_j(0)\left(Y_k^\dagger(t) - \left\langle Y_k^\dagger \right\rangle\right)(Y_l(t) - \langle Y_l\rangle)\right\rangle_0 = 0. \tag{3.70}$$

Thus, also the first term of the right hand side of Eq. (3.62) is zero, and Eq. (3.62) is simplified to

$$\alpha_{ijkl} = \langle Y_l\rangle_0 \int_0^\infty \mathrm{d}t \left\langle Y_i^\dagger(0)\, Y_j(0)\left(Y_k^\dagger(t) - \left\langle Y_k^\dagger \right\rangle\right)\right\rangle_0 \tag{3.71}$$

The equation of motion for the expectation value under the integral is

$$\frac{\mathrm{d}}{\mathrm{d}t}\left\langle Y_i^\dagger(0)\, Y_j(0)\left(Y_k^\dagger(t) - \langle Y_k\rangle^*\right)\right\rangle_0 = \sum_m \left\langle Y_i^\dagger(0)\, Y_j(0)\left(Y_m^\dagger(t) - \langle Y_m\rangle^*\right)\right\rangle_0 \left(\mathbf{Z}^\dagger\right)_{mk}. \tag{3.72}$$

The solution is

$$\left\langle Y_i^\dagger(0)\, Y_j(0) \left(Y_k^\dagger(t) - \langle Y_k\rangle^*\right)\right\rangle_0 = \sum_m \left\langle Y_i^\dagger(0)\, Y_j(0) \left(Y_m^\dagger(t) - \langle Y_m\rangle^*\right)\right\rangle_0\Big|_{t=0} \left(e^{\mathbf{Z}^\dagger t}\right)_{mk}, \tag{3.73}$$

where the standard definition of the exponential of a matrix with a power series, (e.g. Wal91, §2.18, Beispiele 2.), is used. The value at $t = 0$ is given by

$$\begin{aligned}
\left\langle Y_i^\dagger(0)\, Y_j(0) \left(Y_m^\dagger(t) - \langle Y_m\rangle^*\right)\right\rangle_0\Big|_{t=0} &= \langle Y_i\rangle_0^* \left(\langle Y_m\rangle_0^* - \langle Y_m\rangle_0^*\right) \langle Y_j\rangle_0 \\
&\quad -\left\langle Y_i^\dagger \left[\left(Y_m^\dagger - \langle Y_m\rangle^*\right), Y_j\right]\right\rangle_0 \\
&= -\left\langle Y_i^\dagger \left[Y_m^\dagger, Y_j\right]\right\rangle_0 \qquad (3.74) \\
&= \langle Y_i\rangle^* \delta_{mj}, \qquad (3.75)
\end{aligned}$$

where again the commutator relation, Eq. (3.18), was used. Inserting Eqs. (3.73) and (3.75) in Eq. (3.71) yields

$$\begin{aligned}
\alpha_{ijkl} &= \sum_m \langle Y_i\rangle_0^* \langle Y_l\rangle_0\, \delta_{mj} \left(\int_0^\infty \mathrm{d}t\, e^{\mathbf{Z}^\dagger t}\right)_{mk} \\
&= \langle Y_i\rangle_0^* \langle Y_l\rangle_0 \left(\left[\mathbf{Z}^{\dagger -1} e^{\mathbf{Z}^\dagger t}\right]_{t=0}^\infty\right)_{jk} \qquad (3.76)
\end{aligned}$$

The value of $e^{\mathbf{Z}^\dagger t}$ for $t = \infty$ can be deduced as follows: The equation of motion for $\left\langle Y_i^\dagger(0)\, Y_j(0) \left(Y_k^\dagger(t) - \langle Y_k\rangle^*\right)\right\rangle$ is the equation of motion for $N_a + N_c$ damped coupled harmonic oscillators without external excitation. Because of the damping, the final state of such a system is $\left\langle Y_i^\dagger(0)\, Y_j(0) \left(Y_k^\dagger(\infty) - \langle Y_k\rangle^*\right)\right\rangle = 0$, and therefore $e^{\mathbf{Z}^\dagger t}$ must also be zero for $t = \infty$, see Eq. (3.73). The initial state of $e^{\mathbf{Z}^\dagger t}$ for $t = 0$ is $\mathbf{1}$. Inserting this into Eq. (3.76) yields the simple result

$$\begin{aligned}
\alpha_{ijkl} &= -\langle Y_i\rangle^* \langle Y_l\rangle \left(\mathbf{Z}^{\dagger -1}\right)_{jk} \\
&= -\langle Y_i\rangle^* \langle Y_l\rangle \left(\mathbf{Z}^{-1\dagger}\right)_{jk}. \qquad (3.77)
\end{aligned}$$

Collecting the results Eqs. (3.60) and (3.77), the final result for the momentum diffusion constant due to the cavity light force is

$$\begin{aligned}
\mathbf{D}_{\mathrm{cav},j} &= -\hbar^2 \sum_{i,k=1}^{N_c} Re \\
&\quad \Big[\left(\boldsymbol{\nabla}_j g_{ij}^*\right) \otimes \left(\boldsymbol{\nabla}_j g_{kj}^*\right) \left\langle \sigma_j^- \right\rangle_0^* \langle a_k\rangle_0 \left(\mathbf{Z}^{-1\dagger}\right)_{i\, N_c+j} \\
&\quad + \left(\boldsymbol{\nabla}_j g_{ij}^*\right) \otimes \left(\boldsymbol{\nabla}_j g_{kj}\right) \left\langle \sigma_j^- \right\rangle_0^* \left\langle \sigma_j^- \right\rangle_0 \left(\mathbf{Z}^{-1\dagger}\right)_{i\, k} \\
&\quad + \left(\boldsymbol{\nabla}_j g_{ij}\right) \otimes \left(\boldsymbol{\nabla}_j g_{kj}^*\right) \langle a_i\rangle_0^* \langle a_k\rangle_0 \left(\mathbf{Z}^{-1\dagger}\right)_{N_c+j\; N_c+j} \\
&\quad + \left(\boldsymbol{\nabla}_j g_{ij}\right) \otimes \left(\boldsymbol{\nabla}_j g_{kj}\right) \langle a_i\rangle_0^* \left\langle \sigma_j^- \right\rangle_0 \left(\mathbf{Z}^{-1\dagger}\right)_{N_c+j\; k}\Big]. \qquad (3.78)
\end{aligned}$$

Because a general expression for $\mathbf{Z}^{-1}$ is complicated, it is more appropriate to calculate $\mathbf{Z}^{-1}$ for a specific situation. A special case is investigated in section 3.5.1.

Now, consider the second part of the momentum diffusion matrix, $\mathbf{D}_{\mathrm{se},j}$, which is due to spontaneous emission of the atom. This part can be calculated by determining the correlations of the force operator $\mathbf{F}_{\mathrm{se},j}$, which describes the interaction of the atomic dipole with the modes of the light field which are not supported by the cavity. This part of momentum diffusion has been calculated in (HGHR98, appendix B). The result is

$$\mathbf{D}_{\mathrm{se},j} = \hbar^2 k^2 \gamma_j \left\langle \sigma_j^+ \sigma_j^- \right\rangle \mathbf{P}, \tag{3.79}$$

where $\mathbf{P}$ is a 3×3-matrix with a trace of 1, which depends on the polarization of the light field. For circularly polarized light propagating in the z-direction, $\mathbf{P}$ is given by

$$\mathbf{P} = \begin{pmatrix} \frac{3}{10} & 0 & 0 \\ 0 & \frac{3}{10} & 0 \\ 0 & 0 & \frac{2}{5}. \end{pmatrix} \tag{3.80}$$

The total diffusion matrix, $\mathbf{D}_j$, is the sum of the two contributions Eq. (3.78) and (3.79):

$$\mathbf{D}_j = \mathbf{D}_{\mathrm{cav},j} + \mathbf{D}_{\mathrm{se},j}. \tag{3.81}$$

In some contexts, only the total heating rate of the atom by momentum diffusion is important. In this case, a scalar diffusion coefficient, D_j, can be calculated as the trace of the diffusion matrix, $\mathbf{D}_j$. This scalar gives the total heating rate without specifying the 'direction' of the heating.

3.5.1 Single mode

As in section 3.4.1, it is assumed that the cavity supports only a single mode which has a resonance frequency close to the atomic resonance frequency, and that all atoms have the same decay rate γ and the same laser-atom detuning Δ_a. In this case, the inverse of the matrix $\mathbf{Z}$ is given in Eq. (3.28). The results for the expectation values needed in Eq. (3.77) are stated in Eqs. (3.35) and (3.37). After using Eq. (3.40) and a bit of algebra, one arrives at the result

$$\mathbf{D}_{\mathrm{cav},j} = \hbar^2 \gamma |\eta|^2 \frac{(\boldsymbol{\nabla}_j g_{1j}) \otimes \left(\boldsymbol{\nabla}_j g_{1j}^*\right)}{\left(\Delta_{\mathrm{c}}\gamma + \Delta_{\mathrm{a}}\kappa\right)^2} \frac{1}{1+S^2} \left(1 + \frac{4\Delta_a |g_{1j}|^2}{\gamma\left(\Delta_{\mathrm{c}}\gamma + \Delta_{\mathrm{a}}\kappa\right)} \frac{1}{1+S^2}\right). \tag{3.82}$$

In a coordinate system in which one axis points in the direction of $\boldsymbol{\nabla} g_{1j}$, this diffusion matrix is particularly simple: It is a diagonal matrix with only one non-zero element, $D_{\mathrm{cav},j}$, which can be calculated by taking the trace of $\mathbf{D}_{\mathrm{cav},j}$, i.e. by adding all diagonal

elements of the diffusion matrix:

$$D_{\mathrm{cav},j} = tr\, \mathbf{D}_{\mathrm{cav},j} \tag{3.83}$$

$$= \hbar^2 \gamma |\eta|^2 \frac{(\boldsymbol{\nabla}_j g_{1j}) \cdot \left(\boldsymbol{\nabla}_j g_{1j}^*\right)}{\left(\Delta_\mathrm{c}\gamma + \Delta_\mathrm{a}\kappa\right)^2} \frac{1}{1+S^2} \left(1 + \frac{4\Delta_a |g_{1j}|^2}{\gamma\left(\Delta_\mathrm{c}\gamma + \Delta_\mathrm{a}\kappa\right)} \frac{1}{1+S^2}\right). \tag{3.84}$$

In practice, this means that heating induced by this momentum diffusion affects only the coordinate parallel to $\boldsymbol{\nabla} g_{1j}$. A plot of the momentum diffusion due to the cavity light force is shown in Fig. 3.6.

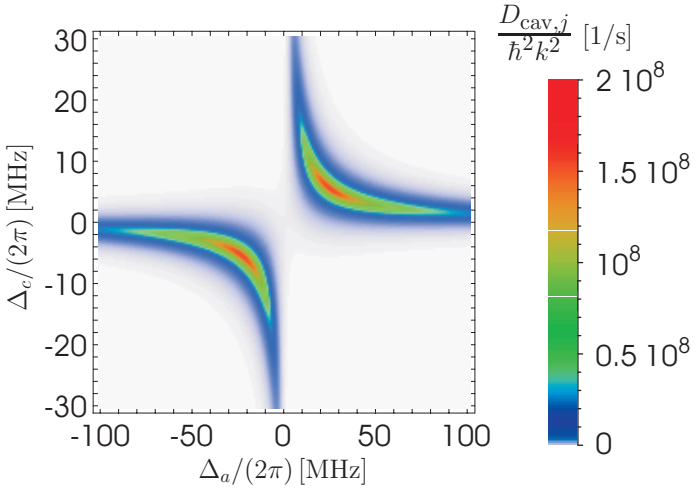

Figure 3.6: The momentum diffusion for an atom in the cavity due to the cavity light force as a function of the detunings Δ_a and Δ_c. The atom is located half way between node and antinode of a standing wave which has a maximum coupling constant of $g_0 = 2\pi \cdot 16\,\mathrm{MHz}$, i.e. $g_{1j} = g_{\mathrm{eff}} = 2\pi \cdot 16/\sqrt{2}\,\mathrm{Mhz}$, and $\boldsymbol{\nabla}_j g_{1j} = 2\pi k \cdot 16/\sqrt{2}\,\mathrm{Mhz}$. The wave number k is $2\,\pi/(780\,\mathrm{nm})$, the other parameters are the same as in Fig. 3.4.

3.5.2 Interpretation

The momentum diffusion due to the cavity light field, $\mathbf{D}_{\mathrm{cav},j}$, can be interpreted as follows: This momentum diffusion is the result of correlations between the operators $a_1^\dagger$, σ_j^+ and a_1, σ_j^-, see Eq. (3.60). In the following, the origin of these correlations will be investigated.

First, the correlations at equal times are considered. They are of special interest, as the correlations are damped exponentially, see Eq. (3.73). As an interpretation, one might say that the origin of nonzero correlations at different times is the existence of nonzero correlations at equal times. From Eq. (3.74), it is clear that the correlations at equal times

are zero if all commutators are zero. Therefore, one can conclude that the correlations are quantum correlations.

Second, the momentum diffusion in the cavity is different from the momentum diffusion in a free-space light field with the same intensity and shape as the intra-cavity light field. The free-space diffusion lacks the second term in the brackets in Eq. (3.82). The limit of a free light field can, for example, be obtained for $g_{1j} \to 0$ and $\eta \to \infty$.

To investigate this difference, it is instructive to consider the time dependence of the correlation function $\left\langle Y_i^\dagger(0)\, Y_j(0)\, Y_k^\dagger(t)\, Y_l(t)\right\rangle_0 - \left\langle Y_i^\dagger Y_j\right\rangle_0 \left\langle Y_k^\dagger Y_l\right\rangle_0$. One can follow the steps from Eq. (3.62) to Eq. (3.71) to see that not only the integral of the first and the third term in Eq. (3.62) are zero, also the correlation functions over which is integrated are zero. Therefore,

$$\begin{aligned}\left\langle Y_i^\dagger(0)\, Y_j(0)\, Y_k^\dagger(t)\, Y_l(t)\right\rangle_0 - \left\langle Y_i^\dagger Y_j\right\rangle_0 \left\langle Y_k^\dagger Y_l\right\rangle_0 \\ = \langle Y_l\rangle_0 \left\langle Y_i^\dagger(0)\, Y_j(0)\left(Y_k^\dagger(t) - \left\langle Y_k^\dagger\right\rangle\right)\right\rangle_0 \end{aligned} \tag{3.85}$$

From Eq. (3.75), only the correlation functions where $j = k$ are different from zero at $t = 0$. The time evolution of the correlation functions is given by the matrix $\mathbf{Z}^\dagger$, see Eq. (3.72). In the free-space limit, i.e. the limit of $g_{1j} \to 0$, this matrix is a diagonal matrix, see Eq. (3.10). Thus, only the correlation functions which have been different from zero at $t = 0$ can be different from zero at later times in this limit. Because of this, only the contributions from corresponding creation and annihilation operators are different from zero. Of those, only the commutators $\left[a^\dagger, a\right]$ and $\left[\sigma_j^+, \sigma_j^-\right]$ must be considered for atom j. If one evaluates the contribution from these commutators separately, one finds that in the limit of $g_{1j} \to 0$, the contribution from $\left[a^\dagger, a\right]$ vanishes. Only the contribution from the atomic dipole operator, $\left[\sigma_j^+, \sigma_j^-\right]$ remains. Therefore, in the free-space limit, momentum diffusion is caused by the quantum nature of the atomic dipole moment. This is the reason why momentum diffusion in free space is often said to be due to 'dipole fluctuations'.

In the strong coupling regime, $g_{1j} > (\kappa, \gamma)$, the picture looks completely different. The matrix $\mathbf{Z}^\dagger$, which describes the time evolution of the correlation function, has large off-diagonal elements. In other words, quantum correlations can be 'transferred' between the atomic dipoles and the field. As an example, consider the correlation function $\left\langle \sigma_j^+(0)\, a(0)\, \sigma_j^+(t)\, a(t)\right\rangle - \left\langle \sigma_j^+ a\right\rangle^2$. This correlation function is zero at $t = 0$, because the value at $t = 0$ is proportional to a commutator between non corresponding operators, $\left[a, \sigma_j^+\right]$. However, it will in general be different from zero at later times and also contribute to momentum diffusion.

Also, the quantum nature of the electromagnetic field makes an important contribution to the momentum diffusion. In fact, half of the 'cavity contribution' to momentum diffusion, i.e the second term within the round brackets in Eq. (3.82), is due to the commutator $\left[a^\dagger, a\right]$. This can be seen by formally setting the commutator $\left[a, a^\dagger\right]$ to zero. This can be achieved by changing the commutator $\left[Y_m^\dagger, Y_j\right]$ from δ_{mj} to $\delta_{mj} - \delta_{m1}\delta_{1j}$ in the step

between Eqs. (3.74) and (3.75).

To summarize, the difference between momentum diffusion in free space and in a strongly-coupled atom-cavity system are due to two reasons: The quantum nature of the light field becomes important in the strongly-coupled system, and quantum correlations can be 'transferred' between operators, which leads to additional operator correlations which do not exist in a weakly coupled system.

The 'cavity contribution' to momentum diffusion is no small effect. For the cavity used in the experiments in this thesis, the 'cavity contribution' can be a factor of 250 larger than the momentum diffusion in free space which is due to dipole fluctuations.

3.6 The velocity-dependent force

So far, only atoms at rest were considered in the calculations. If the atoms move, the system is not in equilibrium because of its finite response time determined by the κ_i and γ_j. This leads to a non-conservative contribution to the total force on each atom. If the velocities of the atoms are small, i.e. if $v/\lambda \ll (\kappa_i, \gamma_j)$, the system stays close to equilibrium, and the non-equilibrium contributions are small. In this case, the expectation value of each operator can be expanded in the velocities of all atoms, and only the linear terms are important.

Of special interest is the expansion of the expectation values $\langle a_i \rangle$ and $\left\langle \sigma_j^- \right\rangle$, because other expectation values can then be calculated using the factorization of expectation values. Their expansion in the atomic velocities is

$$\begin{aligned} \langle a_i \rangle &= \langle a_i \rangle_0 + \textstyle\sum_{k=1}^{N} \langle a_i \rangle_{1,k} + ..., \\ \left\langle \sigma_j^- \right\rangle &= \left\langle \sigma_j^- \right\rangle_0 + \textstyle\sum_{k=1}^{N} \left\langle \sigma_j^- \right\rangle_{1,k} + ..., \end{aligned} \tag{3.86}$$

where the subscripts 0 again denotes zeroth order in the velocity of all atoms, while the subscript $(1,k)$ indicates the expectation value of first order in the velocity $\mathbf{v}_k$ of the kth atom, and zeroth order in the velocities of the other atoms. The zeroth-order terms have already been calculated in Eq. (3.27). For the first-order terms of $\langle a_i \rangle$ and $\left\langle \sigma_j^- \right\rangle$, $\langle \mathbf{Y} \rangle_{1,k}$ has to be calculated. The total time derivative of $\langle \mathbf{Y} \rangle$ can be split into partial derivatives by

$$\langle \dot{\mathbf{Y}} \rangle = \left(\frac{\partial}{\partial t} + \sum_{k=1}^{N} \mathbf{v}_k \cdot \boldsymbol{\nabla}_k \right) \langle \mathbf{Y} \rangle, \tag{3.87}$$

Now, Eq. (3.8) is substituted for $\langle \dot{\mathbf{Y}} \rangle$, and only first order terms in the velocity $\mathbf{v}_k$ are considered. Also, it is assumed that there is no explicit time-dependence in the system therefore $\frac{\partial}{\partial t} \langle \mathbf{Y} \rangle = 0$. The resulting equation can be multiplied with $\mathbf{Z}^{-1}$ to yield

$$\langle \mathbf{Y} \rangle_{1,k} = \mathbf{Z}^{-1} \mathbf{v}_k \cdot \boldsymbol{\nabla}_k \langle \mathbf{Y} \rangle_0, \tag{3.88}$$

where $\langle \mathbf{Y} \rangle_0$ is given by Eq. (3.27). This result can be used to calculate the expectation value of the force operator, Eq. (3.26), in first order of the velocity $\mathbf{v}_k$,

$$\langle \mathbf{F}_{\mathrm{cav},j} \rangle_{1,k} = -\hbar \sum_{i=1}^{N_c} (\boldsymbol{\nabla}_j g_{ij}) \left(\langle a_i \rangle_0^* \left\langle \sigma_j^- \right\rangle_{1,k} + \langle a_i \rangle_{1,k}^* \left\langle \sigma_j^- \right\rangle_0 \right) + c.c. \tag{3.89}$$

In the following, the first order of $\langle a_i \rangle$, $\left\langle \sigma_j^- \right\rangle$ and $\langle \mathbf{F}_{\mathrm{cav},j} \rangle$ are evaluated for a special case.

3.6.1 Single mode

Again, it is assumed that only one mode interacts with the atoms in the cavity and that all atom have the same transition frequency ω_a and the same decay rate γ. In this case, Eq. (3.89) yields for the first-order expectation values $\langle a \rangle_{1,k}$ and $\left\langle \sigma_j^- \right\rangle_{1,k}$

$$\begin{aligned} \langle a \rangle_{1,k} &= -\eta\, g_{1k} \left(\mathbf{v}_k \cdot \boldsymbol{\nabla}_k g_{1k}^* \right) \\ &\quad \frac{A - 2\left(-\gamma + i\Delta_a\right)\left[-\gamma - \kappa + i\left(\Delta_a + \Delta_c\right)\right]}{A^3}, \end{aligned} \tag{3.90}$$

$$\begin{aligned} \left\langle \sigma_j^- \right\rangle_{1,k} &= i\eta \left(\mathbf{v}_k \cdot \boldsymbol{\nabla}_k g_{1k}^* \right) \\ &\quad \frac{-\delta_{jk} A^2 + g_{1j}^* g_{1k} \left\{ A + 2\left(-\gamma + i\Delta_a\right)\left[-\gamma - \kappa + i\left(\Delta_a + \Delta_c\right)\right] \right\}}{\left(-\gamma + i\Delta_a\right) A^3}, \end{aligned} \tag{3.91}$$

where Eq. (3.40) was used. Using this, the first order in atomic velocity of the cavity light force is

$$\langle \mathbf{F}_{\mathrm{cav}} \rangle_{1,k} = -4\hbar |\eta|^2 \left(\boldsymbol{\nabla}_j g_{1j} \right) \left(\mathbf{v}_k \cdot \boldsymbol{\nabla}_k g_{1k}^* \right) \left(\delta_{jk} F_{\mathrm{gj}} + g_{1j}^* g_{1k} F_{\mathrm{geff}} \right), \tag{3.92}$$

where

$$F_{\mathrm{gj}} = \frac{-\Delta_{\mathrm{a}} \gamma}{|A|^2 \left(\gamma^2 + {\Delta_{\mathrm{a}}}^2 \right)}, \tag{3.93}$$

and

$$\begin{aligned} F_{\mathrm{geff}} &= \Big(\Delta_{\mathrm{a}} \gamma g_{\mathrm{eff}}^6 + 2\gamma {\Delta_{\mathrm{a}}}^3 g_{\mathrm{eff}}^4 + \gamma^3 \Delta_{\mathrm{c}} g_{\mathrm{eff}}^4 + 2{\Delta_{\mathrm{a}}}^3 \kappa g_{\mathrm{eff}}^4 + 2\gamma^3 \Delta_{\mathrm{a}} g_{\mathrm{eff}}^4 \\ &\quad -3{\Delta_{\mathrm{a}}}^2 \Delta_{\mathrm{c}} \gamma g_{\mathrm{eff}}^4 + 6\Delta_{\mathrm{a}} \kappa \gamma^2 g_{\mathrm{eff}}^4 - 6\gamma^2 \Delta_{\mathrm{c}} {\Delta_{\mathrm{a}}}^2 \kappa g_{\mathrm{eff}}^2 + 3\gamma^3 {\Delta_{\mathrm{c}}}^2 \Delta_{\mathrm{a}} g_{\mathrm{eff}}^2 + 4{\Delta_{\mathrm{a}}}^5 \kappa g_{\mathrm{eff}}^2 \\ &\quad +8\gamma^2 {\Delta_{\mathrm{a}}}^3 \kappa g_{\mathrm{eff}}^2 + 4\gamma^4 \Delta_{\mathrm{a}} \kappa g_{\mathrm{eff}}^2 + 2\gamma^4 \Delta_{\mathrm{c}} \kappa g_{\mathrm{eff}}^2 + 9\gamma^3 \kappa^2 \Delta_{\mathrm{a}} g_{\mathrm{eff}}^2 + 7\gamma {\Delta_{\mathrm{c}}}^2 {\Delta_{\mathrm{a}}}^3 g_{\mathrm{eff}}^2 \\ &\quad +5\gamma \kappa^2 {\Delta_{\mathrm{a}}}^3 g_{\mathrm{eff}}^2 + 2\gamma^2 \kappa^3 {\Delta_{\mathrm{a}}}^3 + 2\gamma^2 {\Delta_{\mathrm{c}}}^2 {\Delta_{\mathrm{a}}}^3 \kappa + \gamma^5 \Delta_{\mathrm{c}} \kappa^2 - 5{\Delta_{\mathrm{a}}}^4 {\Delta_{\mathrm{c}}}^3 \gamma \\ &\quad -4\gamma^3 {\Delta_{\mathrm{c}}}^3 {\Delta_{\mathrm{a}}}^2 - 2{\Delta_{\mathrm{a}}}^5 {\Delta_{\mathrm{c}}}^2 \kappa + 4\gamma^4 \kappa^3 \Delta_{\mathrm{a}} + 4\gamma^4 {\Delta_{\mathrm{c}}}^2 \Delta_{\mathrm{a}} \kappa - 4\gamma^3 {\Delta_{\mathrm{a}}}^3 {\Delta_{\mathrm{c}}}^2 \\ &\quad -5{\Delta_{\mathrm{a}}}^4 \Delta_{\mathrm{c}} \kappa^2 \gamma - 4\gamma^3 \Delta_{\mathrm{c}} \kappa^2 {\Delta_{\mathrm{a}}}^2 - 2{\Delta_{\mathrm{a}}}^5 \kappa^3 - 4\Delta_{\mathrm{c}} {\Delta_{\mathrm{a}}}^6 \kappa + 4\gamma^3 \kappa^2 {\Delta_{\mathrm{a}}}^3 - 2\gamma {\Delta_{\mathrm{a}}}^5 {\Delta_{\mathrm{c}}}^2 \\ &\quad -2\gamma^5 \Delta_{\mathrm{a}} {\Delta_{\mathrm{c}}}^2 + 2\gamma {\Delta_{\mathrm{a}}}^5 \kappa^2 - 4\gamma^4 \kappa \Delta_{\mathrm{c}} {\Delta_{\mathrm{a}}}^2 - 8\gamma^2 \Delta_{\mathrm{c}} {\Delta_{\mathrm{a}}}^4 \kappa + \gamma^5 {\Delta_{\mathrm{c}}}^3 + 2\gamma^5 \Delta_{\mathrm{a}} \kappa^2 \Big) \\ &\quad / \left(|A|^6 \left(\gamma^2 + {\Delta_{\mathrm{a}}}^2 \right) \right). \end{aligned} \tag{3.94}$$

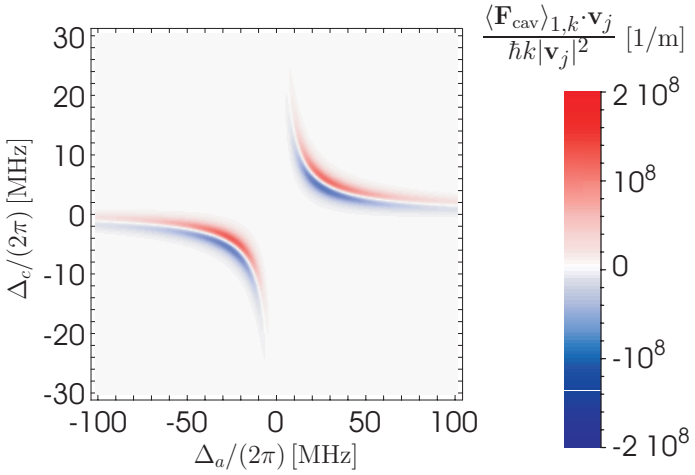

Figure 3.7: The friction force as a function of the detunings Δ_a and Δ_c. The other parameters are the same as in Fig. 3.6.

Note that $\langle \mathbf{F}_{\rm cav}\rangle_{1,k}$ always points in the direction of $\boldsymbol{\nabla}_j g_{1j}$. A plot of the velocity-dependent force is shown in Fig. 3.7.

In order to explain the physical origin of the different terms, Eqs. (3.93) and (3.94), the friction force on atom j if atom k moves is analyzed . Through its motion, atom k changes its own coupling g_{1k} as well as the effective coupling $g_{\rm eff}$. Hence, it is convenient to discuss the effects of the changes of those coupling coefficients separately by considering only the change of one coupling coefficient at a time, keeping the other formally constant.

The change in g_{1k} leads to a non-equilibrium state of the operator σ_k^-, which gives a friction force on atom k. As the friction force on atom j is considered, this is a force on atom j only if $j = k$. This part of the friction force is described by $F_{\rm gj}$, and gives the Doppler force on an atom moving in a time-independent light field with photon number $\left\langle a^\dagger a\right\rangle_0$. This force would also appear in free space.

On the other hand, the change in $g_{\rm eff}$ leads to a non-equilibrium value of the operator a. As the atomic operators adjust themselves to the light field, they are not in an equilibrium state, too. These non-equilibrium states give the second part of the friction force, $F_{\rm geff}$. This is a genuine cavity-effect, because in free space, the light field is not significantly affected by the atomic motion.

Note that the separation of the friction force, $\langle \mathbf{F}_{\rm cav}\rangle_{1,k}$, into the two contributions $F_{\rm gj}$ and $F_{\rm geff}$, is not the same as the separation in the work of Hechenblaikner et al. (HGHR98). For the single-atom case, they find that the friction force is the sum of two terms, F_{ca} and F_{at}, obtained by adiabatic elimination of the atomic operator, σ^-, and the cavity-field operator, a, respectively. At first sight, one might think that their F_{at} and the $F_{\rm gj}$ used here describe the same part of the friction force in the single-atom case, as they both give,

in some sense, the "atomic" part of the friction force. However, they are actually not the same, because the adiabatic elimination of the field operator, a, employed to derive F_{at} means that a adjusts itself immediately upon change of the coupling constant, g_{eff}, while F_{gj} describes the force on an atom in a constant light field. Of course, in the special case of one atom, i.e. $g_{1j} = g_{\text{eff}}$ and $j = k$, the *total* velocity-dependent force, Eq. (3.92), is exactly the velocity-dependent force calculated in Ref. (HGHR98).

3.7 Far-detuned limit for a single-mode cavity

For some experiments, e.g. trapping a single atom in the cavity, it has turned out that a good regime for trapping an atom in the cavity is the dispersive regime where $|\Delta_a|$ is large. Under this condition, the analytical expressions found in the sections 3.4.1, 3.5.1, and 3.6.1 can be simplified further. In these sections, it was assumed that the atoms which have the same resonance frequency ω_a and the same polarization decay rate γ, their saturation is small, and they interact with a single mode of a cavity. Throughout this section, the following additional assumptions will be made:

$$\kappa, \gamma, |\Delta_c| \ll |\Delta_a| \tag{3.95}$$

$$\frac{\gamma}{\kappa}|\Delta_c| \ll |\Delta_a| \tag{3.96}$$

It is easiest to start by approximating A, which is given by Eq. (3.29) as

$$A = g_{\text{eff}}^2 - \Delta_{\text{a}}\Delta_{\text{c}} + \gamma\kappa - i\left(\Delta_{\text{c}}\gamma + \Delta_{\text{a}}\kappa\right). \tag{3.97}$$

Because of Eq. (3.95), $\gamma\kappa$ may be neglected as compared to $\Delta_{\text{a}}\kappa$. Eq. (3.96) states that $\Delta_{\text{c}}\gamma$ can also be dropped as it is much smaller than $\Delta_{\text{a}}\kappa$. Thus,

$$A = g_{\text{eff}}^2 - \Delta_{\text{a}}\Delta_{\text{c}} - i\Delta_{\text{a}}\kappa. \tag{3.98}$$

The approximation of the dimensionless distance from a normal mode peak, S, is then

$$S = \frac{g_{\text{eff}}^2 - \Delta_{\text{a}}\Delta_{\text{c}}}{\Delta_{\text{a}}\kappa}. \tag{3.99}$$

Using this, Eq. (3.98) can be recast as

$$A = \Delta_{\text{a}}\kappa\left(S - i\right). \tag{3.100}$$

In a similar manner, the expectation values calculated in section 3.4.1 can be approximated as

$$\langle\sigma_j\rangle_0 = \frac{\eta}{\kappa}\frac{g_{1j}^*}{\Delta_{\text{a}}}\frac{-i}{S-i} \tag{3.101}$$

$$\left\langle \sigma_j^+ \sigma_j^- \right\rangle_0 = \frac{|\eta|^2}{\kappa^2} \frac{|g_{1j}|^2}{{\Delta_\mathrm{a}}^2} \frac{1}{S^2+1}, \tag{3.102}$$

$$\langle a \rangle_0 = \frac{\eta}{\kappa} \frac{-i}{S-i} \tag{3.103}$$

$$\left\langle a^\dagger a \right\rangle_0 = \frac{|\eta|^2}{\kappa^2} \frac{1}{S^2+1}, \tag{3.104}$$

$$\langle \mathbf{F}_{\mathrm{cav},j} \rangle_0 = -2\hbar \left(\boldsymbol{\nabla}_j g_{1j} \right) \frac{|\eta|^2}{\kappa^2} \frac{g_{1j}^*}{\Delta_\mathrm{a}} \frac{1}{S^2+1}. \tag{3.105}$$

The potential is given by

$$V_\mathrm{cav} = \hbar \frac{|\eta|^2}{\kappa} \arctan S, \tag{3.106}$$

The momentum diffusion matrix describing the momentum diffusion which is due to the cavity light force, Eq. (3.82), can be simplified to

$$\mathbf{D}_{\mathrm{cav},j} = \hbar^2 \gamma \frac{|\eta|^2}{\kappa^2} \frac{\left(\boldsymbol{\nabla}_j g_{1j} \right) \otimes \left(\boldsymbol{\nabla}_j g_{1j}^* \right)}{{\Delta_\mathrm{a}}^2} \frac{1}{S^2+1} \left(1 + 4 \frac{|g_{1j}|^2}{\kappa\gamma} \frac{1}{S^2+1} \right), \tag{3.107}$$

while momentum diffusion due to spontaneous emission is given by Eqs. (3.79) and (3.102).

The friction force in this approximation is easiest to find by calculating the approximation of $\langle a \rangle_{1,k}$ and $\langle \sigma \rangle_{1,k}^-$. They are given by

$$\langle a \rangle_{1,k} = -\frac{\eta}{\kappa} \frac{g_{1k} \left(\mathbf{v}_k \cdot \boldsymbol{\nabla}_k g_{1k}^* \right)}{\Delta_a^2} \frac{2\Delta_a + \kappa (S-i)}{\kappa^2 (S-i)^3}, \tag{3.108}$$

$$\left\langle \sigma_j^- \right\rangle_{1,k} = -\frac{\eta}{\kappa} \frac{\left(\mathbf{v}_k \cdot \boldsymbol{\nabla}_k g_{1k} \right)}{\Delta_a} \left[\frac{\delta_{jk}}{\Delta_\mathrm{a} (S-i)} + \frac{g_{1j}^* g_{1k}}{{\Delta_\mathrm{a}}^2} \frac{2\Delta_a - \kappa (S-i)}{\kappa^2 (S-i)^3} \right]. \tag{3.109}$$

Inserting these results in Eq. (3.89) yields a friction force of

$$\langle \mathbf{F}_\mathrm{cav} \rangle_{1,k} = -16\hbar \frac{|\eta|^2}{\kappa^2} \frac{\left(\boldsymbol{\nabla}_j g_{1j} \right) \left(\mathbf{v}_k \cdot \boldsymbol{\nabla}_k g_{1k}^* \right)}{\Delta_a^2} \frac{g_{1j}^* g_{1k}}{\kappa^2} \frac{S}{\left(S^2+1 \right)^3}. \tag{3.110}$$

3.8 Numerical methods for larger pump power

In this section, numerical methods are discussed which can be used where the analytical model fails. This is the case if the pump power is too large, or if expectation values should be calculated where the first excited levels of the system are not dominant, see the discussion when introducing Eq. (3.5).

In principle, these methods work for an arbitrary number of modes and atoms. However, computation times are rising dramatically with the number of atoms and modes, thus

only as single mode interacting with a single atom is discussed here. The generalization to more than one mode and more than one atom is straightforward.

The first possibility to deal with situations where the weak pump approximation fails is the direct integration of the Master equation, which is for a single atom and a single mode given by

$$\dot{\rho} = \frac{i}{\hbar}\left[H, \rho\right] - \gamma\left(\left\{\sigma^+\sigma^-, \rho\right\}_+ - 2\sigma^-\rho\,\sigma^+\right) - \kappa\left(\left\{a^\dagger a, \rho\right\}_+ - 2a\rho\,a^\dagger\right). \tag{3.111}$$

This equation describes the time evolution of the density operator ρ of the system. The Hamilton, H, is given by

$$H = -\hbar\Delta_a\,\sigma^+\sigma^- - \hbar\Delta_c\,a^\dagger a + \hbar\left(g\,a^\dagger\sigma^- + g^*\sigma^+ a\right) - i\hbar\eta\left(a + a^\dagger\right) \tag{3.112}$$

For a derivation and more background information, see (MS99; GZ00).

As the number of photons in each cavity mode is in principle unlimited, the density matrix is infinite-dimensional, which is inconvenient for numerical integration. The usual solution is to introduce a cutoff photon number, n_{cut}, and consider only states with at most n_{cut} photons in a mode. The cutoff can be chosen according to the pump strength.

Now, two different ansatzes can be made to calculate the trajectory of atoms through the cavity. The first possibility is to integrate the master equation and calculate the motion of the atom simultaneously, i.e. to use the expectation values of the force and the momentum diffusion coefficient to propagate the atoms through the cavity, and use the coupling constants from the position of the atom as input for the master equation. This algorithm has the advantage that the velocity-dependence of the expectation values is implicitly considered. The disadvantage of the approach is the long computation time. Also, the momentum diffusion which enters the cavity light force, $\mathbf{D}_{\mathrm{cav},j}$, must be calculated separately.

The other approach is to calculate the expectation values of the relevant operators for a discrete set of sampling points of the coupling. The expectation values for any position of the atom can be obtained by interpolating between the sampling points. Thus, the dipole force, the velocity-dependent force and momentum diffusion are known, and the equations of motion can be solved numerically.

The number of points which are needed for the interpolation depends on the system parameters. For the simulations in this thesis, the sampling points were $g = (0,\, 0.05,\, 0.1,\, \ldots\, 0.95,\, 1)g_0$. This method allows to calculate trajectories of atoms much faster than the direct integration of the master equation. Also, the momentum diffusion constants can be calculated for the sampling points, and be considered in the atomic motion. A more thorough discussion of this method can be found in (Mau99; Mau).

A method which is faster than the numerical integration of the Master equation, but has also the advantage of taking into account all orders in the velocity of atoms, is the method of quantum trajectories (Car93, chapters 7,8), (MCD93). In this approach, a state

vector is propagated in time. This vector has $2n_{\mathrm{cut}}$ elements, in contrast to the $4n_{\mathrm{cut}}^2$ of the density matrix in the Master equation approach. The time evolution of the vector is governed by a stochastic differential equation. The implementation of this method for the experiment described in this thesis is described in (Mau99; Mau). The computation time for calculating a single quantum trajectory of an atom through the cavity is typically 10 minutes on a Pentium-2 PC with 400 MHz CPU clock frequency.

To include also the momentum diffusion due to the dipole force directly into the simulation, the position space of the atom has to be quantized. As the momentum diffusion due to the dipole force is proportional to the gradient of the coupling constant squared, this momentum diffusion is only important in the direction of the standing wave, where gradients are large. Thus, only the coordinate of position space in direction of the standing wave would have to be quantized, the other coordinates could be still calculated classically.

For the numerical calculation of a quantized motion in a standing-wave light field, it is common to introduce a cutoff momentum, which is typically larger than $10\hbar k$. This increases the Hilbert space of the system by at least a factor of 10, which leads to an increase in computation time of a factor of 10 for the quantum trajectory method at least, and a factor of 10^2 for the direct solution of the Master equation. As the experimental results are described very well by numerical simulations without quantization of position space, this increase was not tolerable. However, if the effects of quantized motion would become important, it would still be possible to perform numerical simulations including quantized motion.

Chapter 4

Measurement of the atomic position

In the previous chapter, it was shown that an atom which is strongly coupled to one or several cavity modes has a large influence on the light field in the cavity and thus on the light transmitted through the cavity. This influence depends on the atomic position via the coupling constants between mode(s) and atom. In this chapter, it will be investigated how this effect can be used to determine the position of the atom from the light transmitted through the cavity. Section 4.1 deals with an atom interacting with a single mode of a cavity. As an example, experimental transits of atoms through the TEM-10 Hermite-Gaussian mode are discussed. The case of several degenerate cavity modes is considered in section 4.2. For this, the modes of order 10, i.e. superpositions of TEM-ij modes with $i + j = 10$, in a Fabry-Perot type cavity are taken as an example.

4.1 Single-mode cavity

In this section, it will be investigated to what extent the position of an atom can be measured by its interaction with a single mode of a high-finesse cavity. As was discussed in chapter 2, the presence of an atom in the cavity can be detected by measuring the total transmitted intensity. This can already be interpreted as a kind of position measurement: Given the knowledge that there is a single atom present, one can tell whether it is in the cavity or not. However, this is not everything which can be learned about the atomic position.

Consider the situation where the atom interacts with a single mode only, and stays at the position $\mathbf{r}_a$. For simplicity, it is assumed that the atom is weakly saturated. By measuring the transmission of the cavity and comparing it to Eqs. (3.20) and (3.38), the coupling constant, g_{eff}, can be determined. Because there is only a single atom present, $g_{\text{eff}} = g_0|\psi(\mathbf{r}_a)|$. Thus, the modulus of the modefunction at the position of the atom is known, and information about the atom's position is gained.

In general, if the atom moves in a three-dimensional space, the set of points $\mathbf{r}$ where

$|\psi(\mathbf{r})| = const.$ is a two-dimensional surface. As an example, the TEM-00 mode of a Fabry-Perot type cavity is considered. In this case, the mode function is given by

$$\psi_{00}(\mathbf{r}) = e^{-\rho^2/w_0^2} \cos(kz), \tag{4.1}$$

where $\rho = \sqrt{x^2+y^2}$, $\phi = (x/|x|) \arctan(y/x)$, and z form a cylindrical coordinate system. The coordinate system is oriented such that the cavity axis is the z-axis. By measuring the amplitude $|\psi 0\,0(\mathbf{r}_a)|$ of the mode function at the position of the atom, information about a product of functions of ρ and z is gained, see Eq. (4.1) and Fig. 4.1. From this, one can conclude e.g. that the maximum possible distance of the atom from the cavity axis is $\rho_{\max} = w_0\sqrt{-ln(|\psi(\mathbf{r}_a)|)}$. If one assumes that the atom is always close to an antinode in z-direction, which is ensured by the cavity light force for certain parameters, this is also the actual distance from the cavity axis, i.e. $\rho = \rho_{\max}$. The angle ϕ, can not be measured with this method, because the mode function is axially symmetric with respect to the z axis.

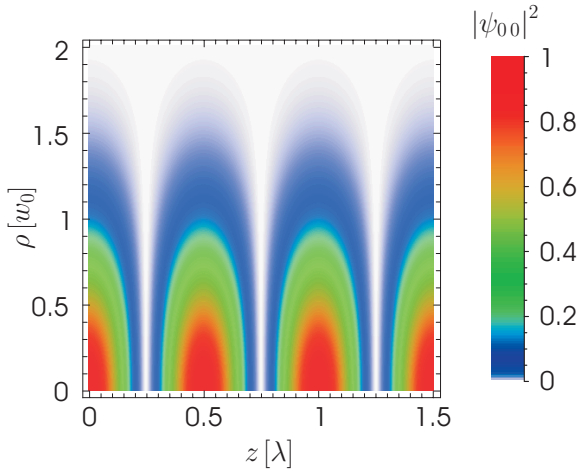

Figure 4.1: The modulus square of the mode function of the TEM-00 mode.

To demonstrate the potential of this method experimentally, atoms were observed passing through the TEM-10 mode in the cavity. This mode is oriented such that the atoms cross two maxima of the mudulus of the mode function, see Fig. 4.2. In the transversal direction, the atoms are expected to traverse the mode in a straight line, as the atoms are too fast for transversal light forces to be important. For the chosen detunings of $\Delta_a = \Delta_c = 0$, the cavity light force heats the atoms in the axial directions so that they pass over nodes and antinodes of the mode very quickly. This leads to a modulation of the transmitted intensity which is too fast to be observed directly. To calculate the transmission of the cavity for a given transversal position, this modulation has to be included

by averaging over the nodes and antinodes of the standing wave. From the mode function of the TEM-10 mode, two subsequent dips in the transmission of the cavity are expected. These dips are clearly resolved in the experimental signal. In turn, this indicates that information about the transversal position of the atom can be obtained by the transmission of the cavity.

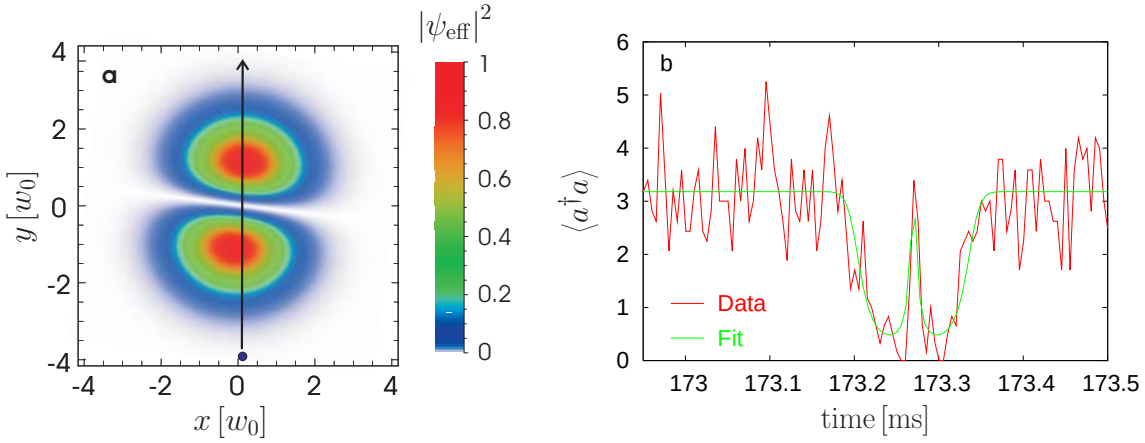

Figure 4.2: **a)** The TEM-10 mode of the cavity in the experiment. The shown cut is perpendicular to the cavity axis. The y direction corresponds to the vertical direction in the experiment. The arrow indicates a possible trajectory of the atom observed in b). **b)** The transmission of the cavity versus time. Because $|\psi(\mathbf{r})|^2$ has two maxima on the path of the atom, it causes two subsequent drops in the transmission. The red line is the experimental signal. The green line is the calculated transmission for an atom flying straight through the cavity, averaged over the standing wave in the z direction. The velocity of the atom was fitted to be 0.74 m/s. From the arrival time, a velocity of 0.67 m/s is expected. The slight difference between the two values can be easily explained by the velocity spread of the atoms due to the optical pumping and momentum diffusion and through the shot noise in the transmitted intensity.

The TEM-01 mode is degenerate with the TEM-10 mode for a cavity consisting of perfectly spherical mirrors. In the experiment, however, the TEM-01 mode has a resonance frequency which lies 25 MHz below the TEM-10 resonance. Therefore, the TEM-01 mode influences the transmission of the cavity only marginally for the chosen detunings. Its influence was neglected for the calculation of the transmitted intensity.

In Ref. (HLD$^+$00), $\rho(t)$ was observed for an atom trapped in the light field of a TEM-00 cavity mode. From this and the known equation of motion, the magnitude of the angular momentum and thus the change of the angle ϕ with time can be determined. This can be integrated to give $\phi(t)$, up to an offset ϕ_0 and the sign of ϕ. Although this is a very beautiful experiment, the angle ϕ is not *measured*, it is only *determined* via the

equation of motion: The method can not be used to gain knowledge about ϕ if it is not known at former times.

4.2 Cavity with degenerate modes

For an ideal position measurement, one would like to constrain the position of the atom, $\mathbf{r}_a = (x_a, y_a, z_a)$, to a single point by observing the light transmitted trough the cavity. To achieve this, at least three independent quantities at the output of the cavity have to be measured, as three independent variables, namely x_a, y_a and z_a, are unknown. One possibility to achieve this is to observe the transmission pattern of a cavity, where more than one mode interact with the atom (HRF$^+$02). From the distribution of the transmitted intensity, information about the amplitudes and the relative phase between the modes can be extracted, see Eq. (3.25). In the following, this will be discussed in detail.

4.2.1 Number of required modes

In the general case, it is difficult to say how many modes are needed as a minimum for a full three-dimensional (3-D) position measurement. One could suspect at first sight that one gets N_c independent equations from the mode amplitudes and $N_c - 1$ equations from the relative phases between the modes, thus only two modes are needed. This might be true in some cases. However, for the special case where all interacting modes have the same resonance frequency and the same decay rate, a more precise statement can be made, which shows that more modes are needed.

The situation is best discussed in the effective mode picture, using a basis of real-valued mode functions. In the following, the numbers of independent equations which can be used to determine the position of the atoms are counted. From the amplitude of the effective mode, the detunings and the known pump, the effective coupling constant, g_{eff}, can be determined, which gives one independent equation. As the phase of the effective mode light field also depends only on g_{eff}, the pump and the detunings, no new information is gained from it. Also, the mode function of the effective mode itself carries a lot of information. From Eqs. (3.52) and (3.1), all mode amplitudes of the original basis can be determined. Because all coupling constants are real, this gives $N_c - 1$ independent equations. The -1 is there because the effective coupling constant is already known, which determines the coupling constant of the last mode from the other coupling constants and g_{eff} via Eq. (3.45). The amplitudes and phases of the other modes of the effective-mode basis only depend on the detunings and the pump, thus they do not carry any information about the position of the atom.

In total, there are N_c independent equations for the position of the atom. Thus, to determine the three-dimensional position of an atom with degenerate modes, one needs

at least three modes. However, the results are easier to interpret if more modes are used. In the next section, an example is given where eleven degenerate modes interact with the atom.

4.2.2 Example: Transversal modes of order 10

As an example, the transversal modes of order 10, i.e. the TEM-ij modes (Sie86, chapter 16.4) with $i + j = 10$, in a Fabry-Perot type cavity are considered. The TEM-ij modes with $i + j = const.$ and with the same number of antinodes are degenerate in the paraxial approximation for a cavity with sperical mirrors, see Eq. (5.3), and form an orthonormal real-valued basis of the space of near-resonant modes. For the calculations presented here, the maximum effective coupling constant was $g_0 = 2\pi \times 16\,\mathrm{MHz}$, the field decay rates of the modes were $\kappa_i = 2\pi \times 1.4\,\mathrm{MHz}$, and the decay rate of the atomic polarisation was $\gamma = 2\pi \times 3\,\mathrm{MHz}$. It is assumed that the modes of order 10 are degenerate. The mode functions are given by Eq. (5.2).

Effective mode

Again, the situation can be described using an effective mode. The effective modes for several positions of the atom are depicted in Fig. 4.3. The effective mode has an intensity maximum close to the position of the atom. This is clear from the graph of the effective coupling against the radius, Fig. 4.4: From $0.2\,w_0 < \rho < 3.1\,w_0$, the effective coupling constant stays nearly constant. In the effective mode basis, all modes except the effective mode are zero at the position of the atom. Therefore, the whole effective coupling at this position is due to the effective mode. At positions where the atom does not reside, the other modes are not zero in general, and the effective coupling is "shared" between the effective mode and the other modes, see Eq. (3.45). Thus, the effective mode will in general have a smaller amplitude elsewhere.

Also, the effective mode has an even symmetry with respect to the cavity axis. This is because all the basis mode functions have an even symmetry. The reason for this is that the Hermite polynomials of even order have an even symmetry with respect to zero and the odd ones have a odd symmetry. For a reconstruction of the position of the atom, this implies that it is not possible to distuinguish between an atom at two positions where the one position is the other position mirrored at the cavity axis.

Detunings

Now, the parameters which are suitable for a position measurement will be determined. The detunings and the pump vector have to be chosen. For the detunings, there are two issues to consider: First, the detunings should be chosen such that it is easy to determine the effective mode, i.e. the influence of the atom on the photon number should be large.

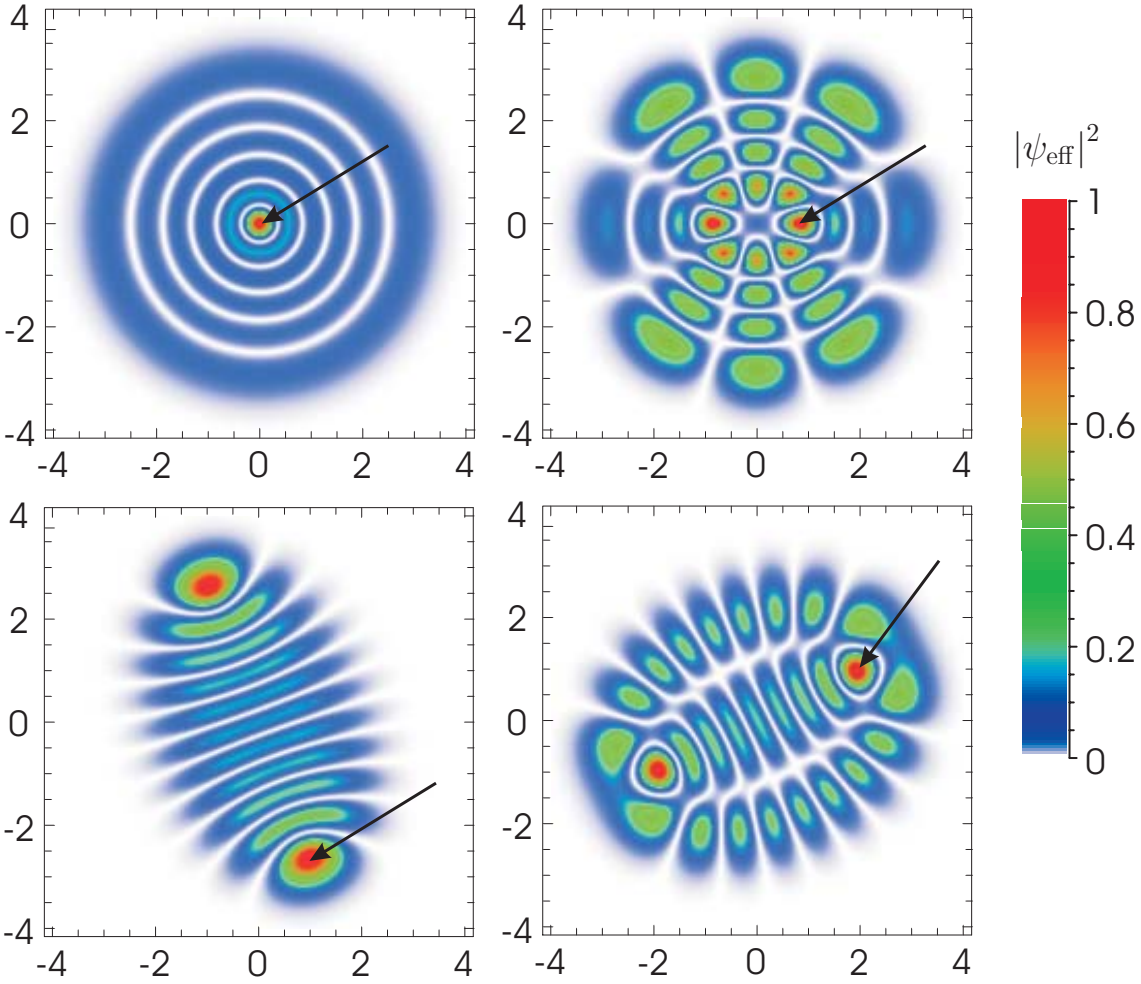

Figure 4.3: Effective modes for several atomic positions for the TEM-ij modes of order 10. The modulus square of the effective mode's mode function is color-coded and normalised such that its maximum is 1. The atom resides at the tip of the arrow. The numbers at the axes give the x- and y-coordinates in units of w_0.

Second, in cases where the effective coupling constant, g_{eff}, has to be determined, the dependence of the photon number in the effective mode on the effective coupling should have a considerable slope everywhere, for a reason which is best discussed in an example:

Consider the extreme parameters where the atom has the maximum influence on the light field. This is the case at resonance, i.e. $\Delta_a = 0$ and $\Delta_c = 0$. However, the slope of the photon number in the effective mode for large coupling constants is negligible, see Fig. 4.5. Therefore, it is virtually impossible to measure the precise effective coupling constant if

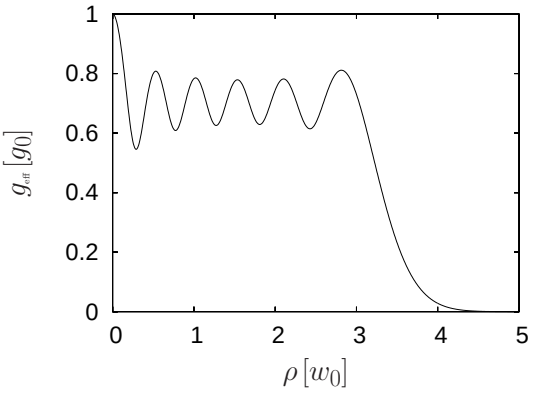

Figure 4.4: The effective coupling, g_{eff}, at an antionode of the standing wave as a function of the radial distance from the cavity axis, ρ.

it is too large. This works much better for detuned parameters, e.g. $\Delta_a/(2\pi) = -50\,\text{MHz}$ and $\Delta_c/(2\pi) = -5\,\text{MHz}$ in Fig. 4.5.

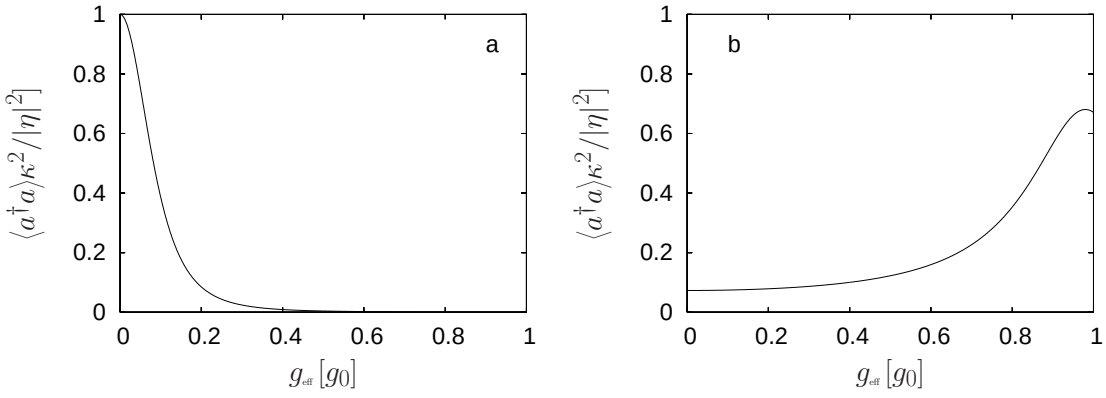

Figure 4.5: The expectation value of the photon number in the effective mode, $\left\langle a_{\text{eff}}^\dagger a_{\text{eff}}\right\rangle$, as a function of the effective coupling constant. The detunings for a) are $\Delta_a = \Delta_c = 0$, and $\Delta_a/\,(2\pi) = -50\,\text{MHz}$ and $\Delta_c/\,(2\pi) = -5\,\text{MHz}$ for b).

However, this consideration might not be important for the choice of parameters. An atom which can move freely in the cavity does usually not stay at its position forever. In the experiment described in this thesis, for example, it is not possible to observe the motion along the cavity axis in real time, as the atom moves too fast and not enough photons can be detected to overcome shot noise. Therefore, one would be content to measure the

position of the atom in the x-y-plane. For this, it is enough to know the position of the effective mode, one does not need to know the effective coupling constant. In this case, parameters where the laser is in resonance both with the cavity and the atomic transition are a good choice. However, to explain the whole procedure, $\Delta_a/(2\pi) = -50\,\mathrm{MHz}$ and $\Delta_c/(2\pi) = -5\,\mathrm{MHz}$ are chosen for the following.

Pump geometry and intensity distribution of the transmitted light

To explain the influence of the pump geometry, different pump geometries will be considered. Experimentally, it is easy to pump the cavity with a plane wave travelling parallel to the cavity axis, therefore this pump geometry is considered first. Then, some examples are shown for a more complicated pump geometry.

The pump vector is given by the overlap between the pump and the cavity mode functions. For a plane wave, the pump field does not depend on the position perpendicular to the cavity axis, thus

$$\eta_i \propto \int_{-\infty}^{\infty} \mathrm{d}x \int_{-\infty}^{\infty} \mathrm{d}y \; \psi_i \tag{4.2}$$

This yields the pump vector

$$\mathbf{I}_{\mathrm{pump}} = \eta_0 \begin{pmatrix} \sqrt{63} \\ 0 \\ \sqrt{35} \\ 0 \\ \sqrt{30} \\ 0 \\ \sqrt{30} \\ 0 \\ \sqrt{35} \\ 0 \\ \sqrt{63} \\ 0 \end{pmatrix}. \tag{4.3}$$

The last zero indicates that the atom is not pumped.

For a Fabry-Perot type cavity made of spherical mirrors, the transversal intensity pattern of the transmitted beam is the same as the transversal intensity pattern inside the cavity. This is because the transmitted light is the superposition of hermite-gaussian beams (ST91) with the same mode waist. The beams change their transversal profile in the propagation direction in the same manner, which only leads to a overall scaling of the transmitted pattern, not a change in the pattern itsself. This property is very convenient, as a camera in the far field of the cavity measures the same transversal intensity distribution pattern as exists in the cavity.

The transversal intensity distribution of the empty cavity is depicted in Fig. 4.6. Because of the symmetry of the pump, the intensity does not depend on the angle ϕ. As the

pump vector, $\mathbf{I}_{\text{pump}}$, consists only of real numbers and the mode funtions are real-valued, the relative phase between two values of the electric field of the empty cavity is either zero or 180°. At the points where the phase changes, the intensity of the light field is zero. This is the reason for the dark rings in the mode picture.

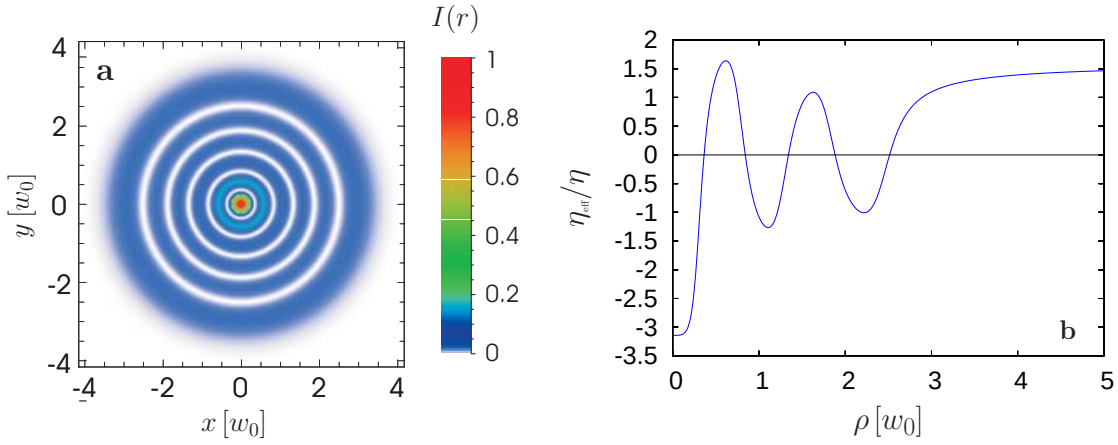

Figure 4.6: **a)** The transversal intensity distribution for an empty cavity for the modes of order 10. The cavity is pumped with a plane wave. **b)** The dependence of the effective pump, η_{eff}, from the radial distance from the cavity axis, ρ. The positions where the effective pump is zero correspond to the white rings in a).

In Fig. 4.7, the intensity distribution of the transmitted beam is drawn for some atomic positions. At the position of the atom, a bright spot appears because the atom shifts the effective mode into resonance with the laser. Thus, the transversal position of the atom can be determined without comparing the intensity distribution with calculated distributions.

A second bright spot appears at the position of the atom mirrored at the cavity axis. The reason for the mirror bright spot is the symmetry of the TEM-ij modes, as explained above. The mirror spot can not be avoided if only TEM-ij modes with $i+j = const.$ are near-resonant to the atomic transition.

To determine the axial position of the atom, the measured intensity patterns have to be compared to calculated ones. As all mode functions are proportional to $cos\,(kz_a)$ in the axial direction, see Eq. (5.2), the value of $|cos\,(kz_a)|$ can be determined with this method. The closer the atoms is to the antinode of the standing wave, the more rises the light intensity in the effective mode, see Fig. 4.5 b), and the brigher are the bright spots at the position of the atom. An example is shown in Fig. 4.7 c) and d). The pump strength and the intensity scaling is the same in all patterns.

If an atom is present a position where the light intensity is zero, it will have no influence on the light field, because it does not interact with the light field. This also clear from the effective pump as a function of ρ, Fig. 4.6. At the position of the dark rings, the effective

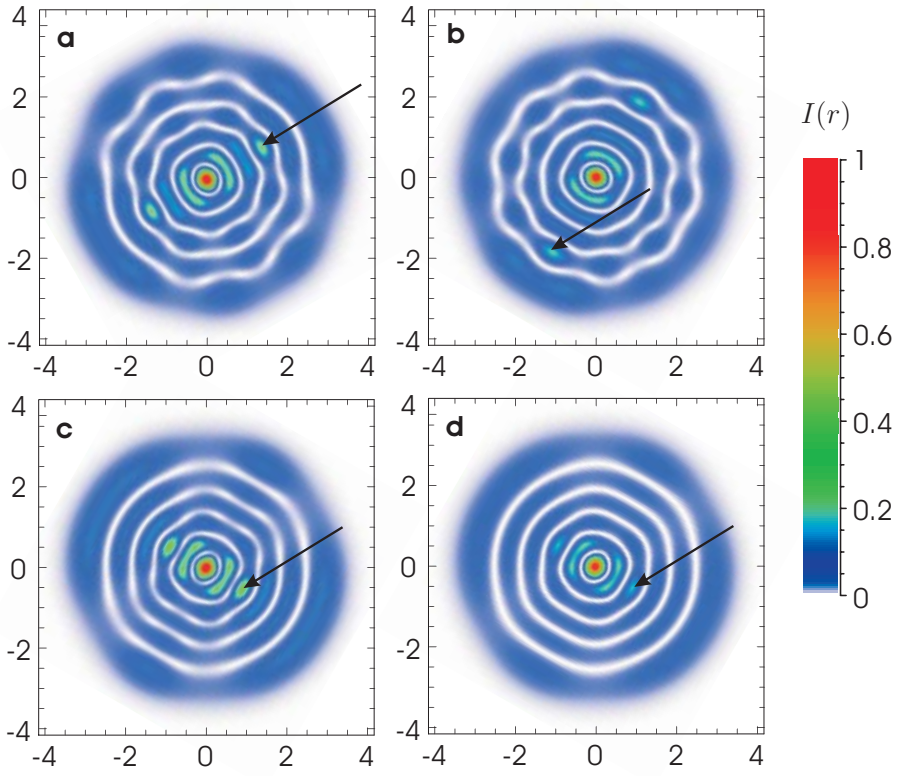

Figure 4.7: The transversal intensity distribution for the TEM-ij modes with $i + j = 10$ in a cavity with an atom inside. The position of the atom is indicated by the tip of the arrow. The cavity is pumped with a plane wave, the detunings are $\Delta_a/(2\pi) = -50\,\mathrm{MHz}$ and $\Delta_c/(2\pi) = -5\,\mathrm{MHz}$. The effective coupling constant for an atom at an antinode on the cavity axis is $g_0 = 2\pi \cdot 16\,\mathrm{MHz}$. The numbers at the axes give the x- and y-coordinates in units of w_0. For **a)-c)**, the atom is at an antinode of the standing wave in axial direction, in **d)**, the transversal position of the atom is the same as in c), but the atom is located half way between node and antinode.

pump is zero, i.e. the effective mode is not pumped. Only the non-interacting modes are pumped, thus the cavity looks as if it was empty. To avoid this, one would like to have a pump where no dark positions exist.

The dark rings disappear if more complicated patterns are used to pump the cavity. Still, some dark points appear where the atom does not interact with the pump. In the next example, the area $-2w_0 < x < 2w_0$, $-2w_0 < y < 2w_0$ has a flatter intensity

distribution than for the plane wave pump example, where a strong peak in the middle dominates the rest. The pump vector in this example is

$$\mathbf{I}_{\text{pump}} = \eta_0 \begin{pmatrix} 1 \\ 1+i \\ 0 \\ 0 \\ 0 \\ 0 \\ 0 \\ 0 \\ 0 \\ -1+i \\ i \\ 0 \end{pmatrix}. \tag{4.4}$$

Both examples for the pump vector show that no pump geometry is perfect for all positions of the atom. To circumvent this problem, one could switch between different pump geometries, depending on the measured position of the atom. For example, if initially a plane wave pump is used and the atom is seen to approach one of the dark rings, one could change the pump geometry such that it has no dark ring at this position. There will be other dark spots in the new pump geometry, too, but as long as they are not at the position of the atom, this does not matter.

4.2.3 Spatial and temporal resolution

Now, some general issues will be addressed which are important for the proposed position measurement scheme for atoms in a cavity. Certainly, the spatial and temporal resolution of the position measurement is of interest. These issues can not be addressed independent from each other: The longer the observation time is, the more photons will be detected, and the better the determination of the effective mode and the effective coupling will be. Now, a crude estimation will be made for the time needed to measure the atom's transversal position for $\Delta_a/(2\pi) = -50\,\text{MHz}$ and $\Delta_c/(2\pi) = -5\,\text{MHz}$ and the decay rates and coupling constant of the cavity used in the experiment. To determine the position of the atom, it is necessary to tell the difference between the patterns shown in Fig. 4.7. A reasonable estimate for the number of photons needed to do that is about 100. For eleven modes, this gives about 10 photons per mode. To keep the saturation of the atom below 0.1, one can use a pump strength below $\eta_{\text{eff}}^2 = 1.45\kappa^2$. This yields a maximum average photon number in the effective mode of about one. Then, for an overall photon detection efficiency of 0.1, the average time to detect 10 photons in a mode is $50\,/\kappa$, which is $5.7\,\mu\text{s}$ for the cavity in the experiment. For an atom moving freely through this cavity, this time is long enough to resolve the transversal motion of the atom, while the axial motion is too

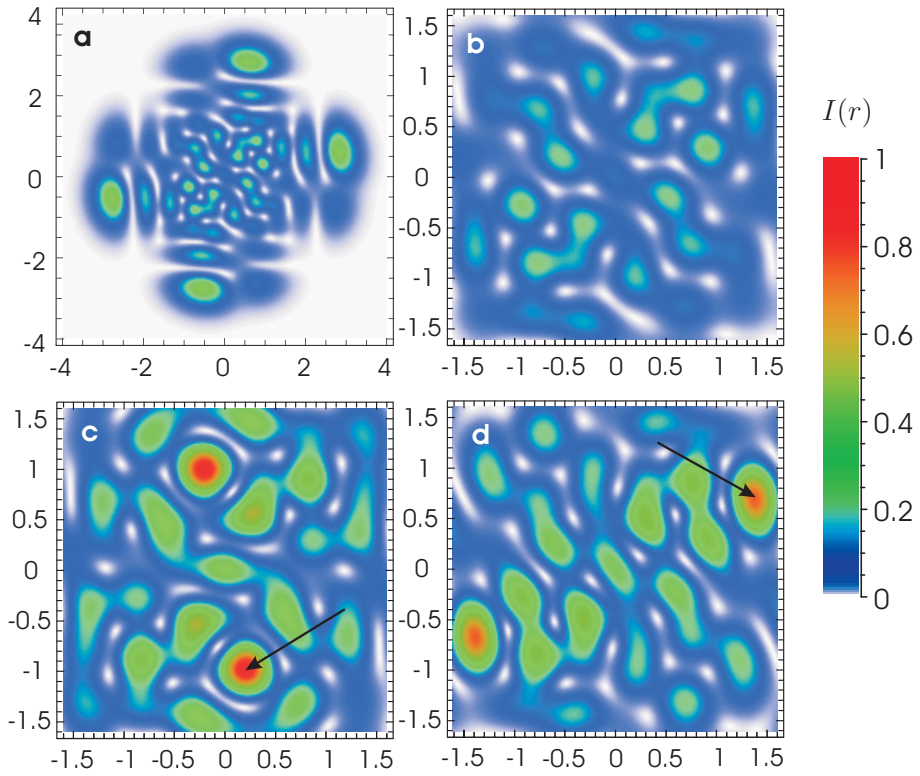

Figure 4.8: The transversal intensity distribution for the TEM-ij modes with $i+j = 10$ in a cavity. The cavity is pumped with the pump vector Eq. (4.4), the other parameters are the same as in Fig. 4.7. **a)** shows the intensity distribution of the empty cavity, **b)** is a zoom of a). In **c)** and **d)** an atom resides in the cavity, its position is given by the tip of the mirror. The pump strength and the intensity scaling is the same in all patterns. The numbers at the axes give the x- and y-coordinates in units of w_0.

fast to be resolved, see also section 6.1. The transversal resolution for this measurement time will be on the order of w_0, as this is the typical transversal length scale.

Another question that can be raised in this context is the dependence of the resolution and detectability on the mode order n. In other words, which is the best mode order n to measure the position of an atom? A few thoughts about this question are stated in the following. The full answer is beyond the scope of this thesis.

As a first step, the dependence of the effective coupling constant on the mode order will be considered. For $n = 10$, the dependence of the coupling constant on the radius ρ, Fig. 4.4, is characteristic for even n: There is a sharp peak at $\rho = 0$, where the maximum effective coupling constant is equal to the maximum coupling in the TEM-00 mode, g_0.

For increasing ρ, the coupling constant drops to a plateau where $g_{\text{eff}} \approx g_0/\sqrt{2}$, and finally, it drops to zero for large radii. The plateau reaches approximately out to $\rho = \sqrt{n}w_0$. For odd n, there is no peak in the middle but a dip which reaches down to zero. Because the coupling constant at the plateau does not change with n, the influence of the atom on the photon number in the effective mode does not depend strongly on the mode order. However, the area where an atom can be detected grows linearly with the mode order.

Still, given this result, the question whether the resolution rises or drops with increasing n remains unanswered: As the effective coupling stays constant with increasing n, but the number of modes increases, the average coupling constant per mode drops for increasing n, and the influence of the atom on the field amplitude on the mode also drops. If the pump strength of each mode is kept constant in order not to saturate the atom, the signal-to noise ratio per mode drops. However, this could be balanced by the increase of the number of modes.

Another question is whether one can get rid of the mirror image of the atom. For this, both modes with an even symmetry and modes with an odd symmetry have to be present close to the atomic transition. This could be achieved by using modes with a different number of antinodes, m, in the axial direction: In the paraxial approximation, the frequency of a TEM-ij mode in a Fabry-Perot type resonator is given by Eq. (5.3). If $1/(1 - l/r_m)$ is an odd integer, the modes where $(i + j)(1 - l/r_m) + m = const.$ are degenerate, which allows the intensity pattern to be asymmetric.

To conclude this section, the proposed scheme provides a position measurement for single atoms in a high-finesse cavity with a high spatial and temporal resolution. How the experimental challenge of building a cavity with near-degenerate higher order modes can be met, will be seen in the future. However, it does not seem impossible to achive very small frequency distances of the modes by carefully selecting the spot where the light hits the cavity mirrors.

Chapter 5

Experimental set-up

In this chapter, the key features of the experimental setup are described. To illustrate the hardware requirements, a typical measurement cycle is explained. The most sophisticated parts of the experiment are discussed in greater detail.

Some of the measurements in this thesis have been carried out at the Universität Konstanz, and some at the Max-Planck-Institut für Quantenoptik in Garching. Although the same vacuum chamber was used, the laser system, the locking and the detection scheme for the high-finesse cavity was improved after the move to Garching. Here, the new setup in Garching will be described. This chapter highlights the improvements made in the context of this thesis. Details of the old setup can be found in (MFPR99; PFM$^+$00; Mün99).

In the experiment, the interaction of single slow atoms with the light field inside a high-finesse cavity is studied. Rubidium-85 (^{85}Rb) atoms are used. They have a closed transition $5S_{1/2}\,F = 3 \leftrightarrow 5P_{3/2}\,F = 4$, which eases laser-cooling of the atoms and simplifies the interaction of the atoms with the cavity-mode. Also, at the wavelength of this transition, 780.24 nm, commercial laser-systems (Ti:Sapphire lasers, diode lasers) are readily available and relatively easy to use. A part of the level scheme of ^{85}Rb is depicted in Fig. 5.1. The decay rate of the atomic dipole moment on this transition is (MvdS99) $\gamma = 2\pi \times 2.99\,\mathrm{MHz}$.

5.1 The atomic fountain

To prepare slow atoms, a magneto-optical trap (MOT) (RPC$^+$87; MvdS99) is used to capture approximately 10^7 atoms from a Rb background vapour. Then, the atoms are cooled to temperatures of about 5 μK via polarisation gradient cooling (LWW$^+$88; DCT89). Finally, the atoms are accelerated towards the high-finesse resonator using polarisation gradient cooling which cools the atoms into a moving frame of reference, similar to the technique described in (MvdS99, section 13.4). This technique is called "moving molasses"

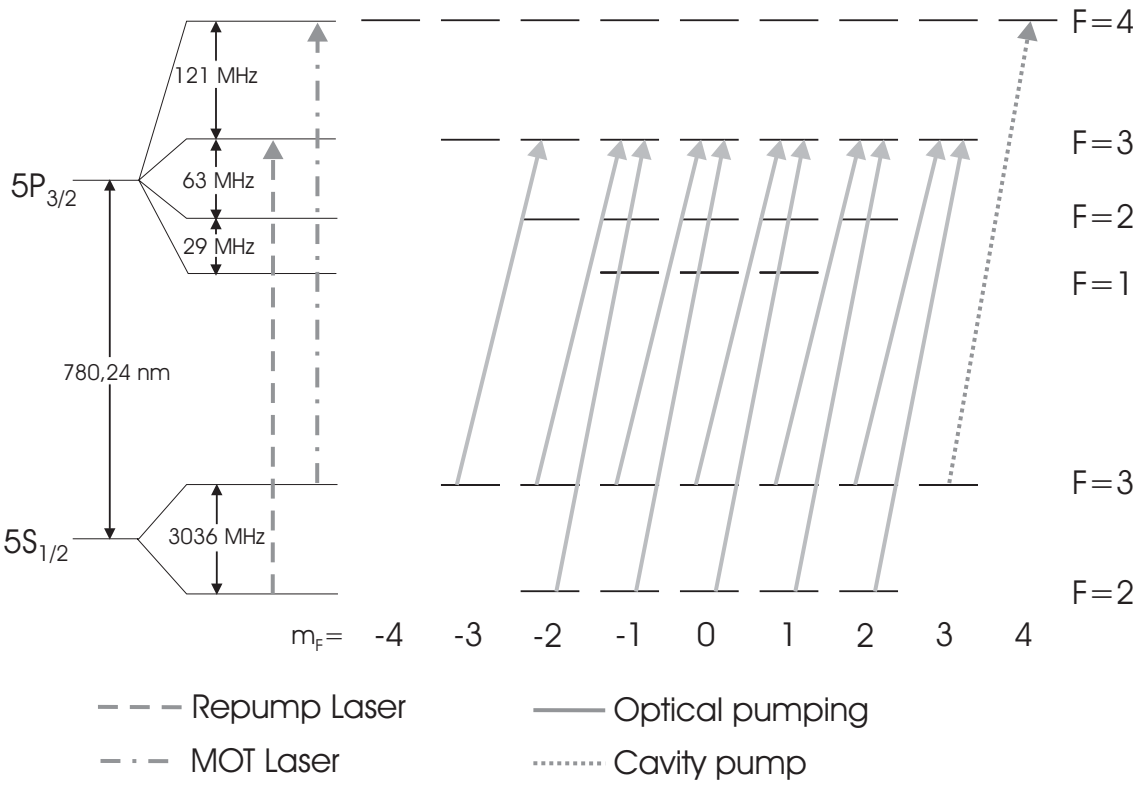

Figure 5.1: Part of the energy levels of ^{85}Rb. The transitions used in the experiment are indicated by arrows. From the $5P_{3/2}$-levels, the atom can decay with $\Delta F = 0, \pm 1$ and $\Delta m_F = 0, \pm 1$ to the $5S_{1/2}$-levels by an electric dipole transition.

here. A sketch of this setup can be seen in Fig. 5.2.

The light fields for the MOT, the polarisation-gradient cooling and the moving molassess are created by six circularly polarized laser beams near-resonant to the $5S_{1/2}\,F = 3 \leftrightarrow 5P_{3/2}\,F = 4$ transition. When the beams enter the vacuum chamber, they are oriented such that they propagate perpendicular to the faces of a cube. The vertical direction coincides with one of the (1,1,1)-directions of the cube. For MOT and polarisation gradient cooling, all six laser beams have the same frequency. For the moving molasses, the frequency of the lower three beams is slowly increased with respect to the upper beams, thus cooling the atoms into a frame which accelerates upwards. Then, the light is switched off, and the atoms are moving towards the high-finesse resonator, which is located 25.5 cm above the MOT. The final velocity of the atoms can be controlled by the final detuning between lower and upper beams.

On their way up, the atoms can pass through two horizontal light beams: In the

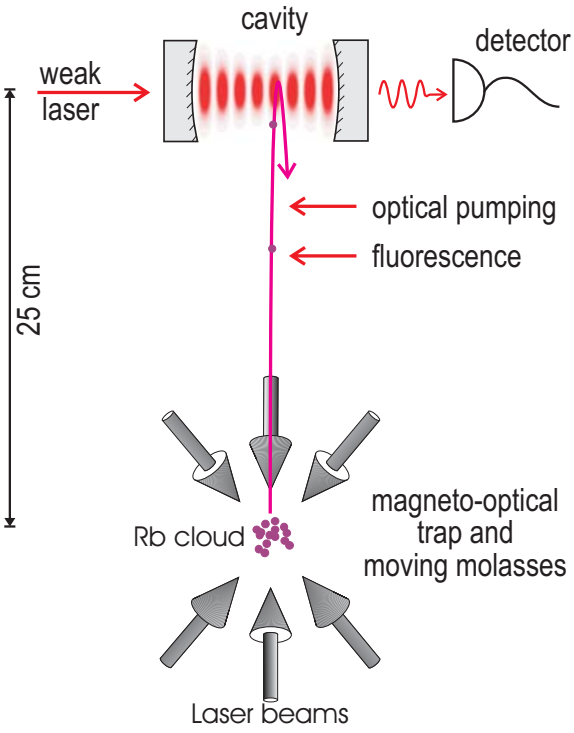

Figure 5.2: Sketch of the experimental setup.

first beam, 4 cm below the cavity, the atoms can be illuminated with resonant light to measure their number from the observed fluorescence. In the second beam, 2 cm below the cavity, the atoms are optically pumped to the desired $m_F = 3$ Zeeman sublevel of the $5S_{1/2}\,F = 3$ state. A small magnetic field of one Gauss parallel to the cavity axis defines the quantisation direction.

Assuming ballistic free flight between the MOT and the cavity, the velocity of the atoms just before entering the cavity can be calculated from the flight time and the distance between MOT and cavity, see Fig. 5.3. The mean velocity of the atoms just before entering the cavity can be adjusted in a very wide range from approximately 10 cm/s to 4 m/s. Because the atomic cloud launched from the MOT has a finite size, the atoms which arrive in the cavity at the same time do not have the same velocity: The atoms which have started lower have a larger velocity, because they have to travel a longer distance in the same time. However, the velocity spread caused by this effect is negligible. Much more important are the random recoils from the optical pumping, which lead to a velocity spread of few cm/s for atoms arriving in the cavity at the same time.

A weak laser beam near-resonant to the closed $5S_{1/2}\,F = 3\,m_F = 3 \rightarrow 5P_{3/2}\,F = 4\,m_F = 4$ transition is coupled into the high-finesse cavity. Transitions to other magnetic

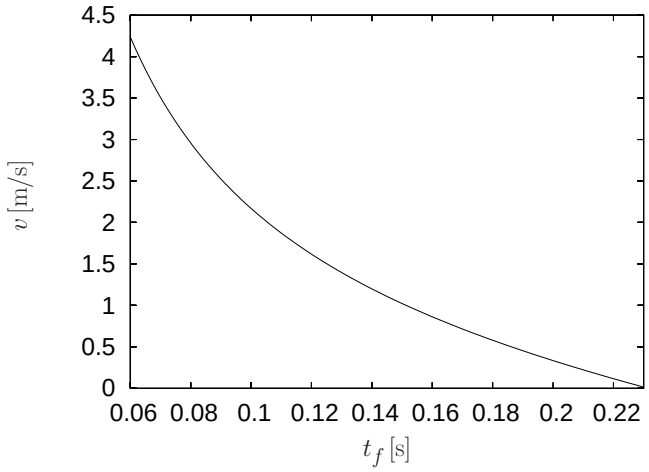

Figure 5.3: The velocity of the atoms just before entering the high-finesse-cavity, v, drawn against the flight time from the MOT to the cavity, t_f.

sublevels are suppressed because the laser beam is circularly polarized. One of the cavity modes is also near-resonant to this laser beam. To keep the detuning between the laser and the resonance frequency of this mode constant, the length of the cavity is actively stabilized. The probe light which is transmitted through the cavity is detected using single-photon counting modules. It is possible to trigger on single atoms in the cavity by comparing the cavity transmission with a pre-set value.

In the following sections, the laser system, the high finesse-cavity and the scheme for monitoring the light which is transmitted through the cavity are explained in more detail. The vacuum chamber is described in (Mus97; Fis98; Mün99).

5.2 The laser system

In the first half of this section, it is investigated which laser beams are necessary for the experiment. Afterwards, the laser setup is described, and the scheme which is used to stabilize the frequency of the lasers is explained.

5.2.1 Experimental requirements

To operate the MOT, the polarisation gradient cooling, the moving molasses, the cavity pump, and the fluorescence beam, multiple laser beams near-resonant to the $5S_{1/2}\,F = 3 \rightarrow 5P_{3/2}\,F = 4$ transitions are needed. The beams of the MOT are also used for the polarisation gradient cooling and the moving molasses. The moving molasses technique

requires that the lower three MOT beams are independent in frequency from the upper three MOT beams.

For the optical pumping, right circularly polarized laser light resonant to the $5S_{1/2}\,F = 3 \rightarrow 5P_{3/2}\,F = 3$ transition is used. The desired Zeeman state $5S_{1/2}, F = 3, m_F = 3$ is a dark state with respect to right circularly polarized light on this transition, see Fig. 5.1, thus the atoms which are already in the desired state are not heated by scattering photons of the pump beam.

Additionally, repumping light resonant to the $5S_{1/2}\,F = 2 \rightarrow 5P_{3/2}\,F = 3$ transition is needed. This is because if the atoms are illuminated with light near-resonant to the $5S_{1/2}\,F = 3 \rightarrow 5P_{3/2}\,F = 4$ transition, they can be off-resonantly excited to the $5P_{3/2}, F = 3$ state, see Fig. 5.1, from where they can decay into the $5S_{1/2}\,F = 2$ state. This state does not couple to the $F = 3 \rightarrow F = 4$ light. Atoms in this state would be lost from the MOT, or have no effect on the transmitted light in the cavity. To recover these atoms, they are repumped to the $5S_{1/2}\,F = 3$ state. This is achieved by illuminating the atoms with a laser resonant to the $5S_{1/2}\,F = 2 \rightarrow 5P_{3/2}\,F = 3$ transition. From the upper state, they decay with a large probability to the $5S_{1/2}\,F = 3$ state. The repumping light is also needed in the beam for optical pumping to address the atoms which decay to the $5S_{1/2}\,F = 2$ state.

For the stabilisation of the high-finesse cavity, laser light is used which is two free spectral ranges of the high-finesse cavity away from the $5S_{1/2}, F = 3 \rightarrow 5P_{3/2}, F = 4$ transition. This gives a wavelength of 785.24 nm if a TEM-00 mode of the cavity is used for both stabilisation of the cavity and observation of the atom. This frequency of the stabilisation laser was chosen because it is suitable for an intra-cavity dipole trap like in (YVK99), i.e. an additional conservative potential can be created to keep the atoms inside the cavity. It is not favourable to use only one spectral range as difference between the stabilisation/dipole laser and the cavity pump, because the standing waves of probe laser and dipole laser would be displaced relative to each other in the middle of the cavity. It is also experimentally not favourable to use farther detuned light, as the intensity needed to achieve a given potential height is proportional to the detuning between atomic resonance and the laser (MvdS99). For too high intra-cavity intensities (some microwatt pump power, i.e. some 100 milliwatts circulating intensity), the heating of the mirrors by the laser becomes important, which leads to unwanted changes in the length of the cavity and thus to changing cavity resonance frequencies. Also, the cross-talk between the stabilisation laser and the probe laser in the detection of the light transmitted through the cavity increases.

5.2.2 Laser setup

The laser beams described above are produced by a Ti:Sapphire laser (MBR 110 by Coherent) and and two self-built grating-stabilized diode lasers (Wol94) in a Littrow setup. The schematic laser setup is shown in Fig. 5.4

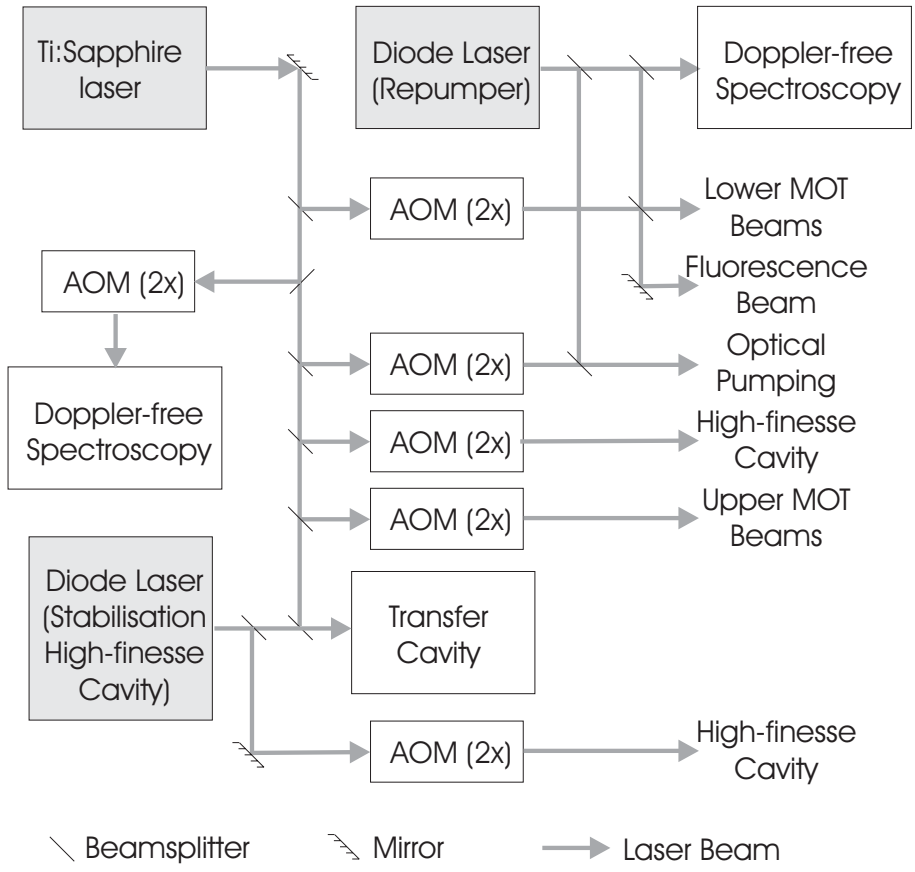

Figure 5.4: Sketch of the laser setup. The beams which pass through a beamsplitter and afterwards hit a beam stop are not shown. AOM(2x) means double-pass through an AOM.

The beams which are near-resonant to the $5S_{1/2}\,F = 3 \rightarrow 5P_{3/2}\,F = 4$ and $5S_{1/2}\,F = 3 \rightarrow 5P_{3/2}\,F = 3$ are generated by the Ti:Sapphire laser. To be able to control the frequency of each beam individually, each beam double-passes an acousto-optical modulator (AOM). In each pass, the AOM shifts the light frequency by a frequency in the range between 70 MHz to 150 MHz. The shift in light frequency by the AOM is equal to the frequency of the AC voltage the AOM is operated with, which can be easily controlled. The AOM's are also used to stabilize the light intensity in the laser beams: The intensity in the beams after the AOM is monitored by a photodiode. Its output voltage is compared to a reference voltage which is generated by the control computer. The difference is used as input for a servo. The output of the servo changes the power of the RF which is fed into the AOMs. This controls the power in the frequency-shifted part of the laser beam which leaves the AOM. The part of the laser beam which is not frequency-shifted leaves

the AOM at another angle and hits a beam stop.

The Ti:Sapphire laser was delivered from the factory with a frequency stability of 600 kHz rms. This is a considerable fraction of the cavity linewidth (HWHM) of 1.4 MHz. Therefore, the intensity transmitted through the cavity would be strongly influenced by the frequency excursions of the laser. As the transmitted intensity is the signal which is used to observe the atoms in the cavity, this was not tolerable. With some modification in its control electronics, the linewidth was reduced to 40 kHz rms. The Ti:Sapphire laser is pumped by a frequency-doubled Nd:YVO4-Laser (Verdi V10 by Coherent), which is operated at an output power of 7 W. For this pump power, the Ti:Sapphire laser has an output power of 500 mW in every-day alignment.

The laser is stabilized 260.7 MHz below the $5S_{1/2}\,F = 3 \rightarrow 5P_{3/2}\,F = 4$ transition of ^{85}Rb, or equivalently 139.7 MHz below the $5S_{1/2}\,F = 3 \rightarrow 5P_{3/2}\,F = 3$ transition, see Fig. 5.1. This is achieved by sending the light used for stabilisation of the laser twice through an AOM which shifts the light frequency upwards by 100 MHz per pass. Doppler-free saturation spectroscopy (Dem82, section 10.2.2) in a Rb vapor cell and the Pound-Drever-Hall RF modulation technique (DHK$^+$83) are employed to get an error signal for the laser frequency. The crossover line (Dem82, section 10.2.2) between the $5S_{1/2}\,F = 3 \rightarrow 5P_{3/2}\,F = 4$ transition and the $5S_{1/2}\,F = 3 \rightarrow 5P_{3/2}\,F = 3$ transition is used to stabilize the laser. This crossover line lies 60.7 MHz below the $5S_{1/2}\,F = 3 \rightarrow 5P_{3/2}\,F = 4$ transition.

The light not used for the stabilisation is split into several beams. One beam is used for the upper MOT beams, one for the lower MOT beams and the fluorescence, one for the optical pumping, and one for the probe light of the high-finesse optical cavity. Each of these beams are sent double-pass through an AOM, which allows individual control of power and frequency of each beam.

The light of the Ti:Sapphire laser is also used to stabilize the length of a Fabry-Perot type cavity, the so-called transfer cavity. Again, a Pound-Drever-Hall method is employed to produce an error signal of the light which is reflected by the transfer cavity. This cavity is $l_T = 46.8$ cm long and has a finesse of about 2000 (Ern95). Its free spectral range is $\Delta\nu_{FSR,T} = c/2l_T = 319$ MHz. That is, every 319 MHz, there is a TEM-00 mode of the cavity. Any of these modes can be used to stabilize a laser at that frequency.

One of the modes of the transfer cavity is employed to stabilize the second diode laser at a wavelength of 785.24 nm, two spectral ranges of the high-finesse cavity away from the $5S_{1/2}\,F = 3 \rightarrow 5P_{3/2}\,F = 4$ transition in ^{85}Rb. As before, a Pound-Drever-Hall method is used to get an error signal. This error signal is fed into two PID-servos which control the frequency of the diode laser, a slow one acting on the angle of the grating, and the other, faster one, on the laser diode current. With this method, a rms-linewidth of about 100 kHz is achieved. The output power of this laser is 8 mW. The light from the diode laser is itself used to stabilize the high-finesse cavity. The detuning of the TEM-00 resonance of the high-finesse cavity at 780.24 nm from the $5S_{1/2}, F = 3 \rightarrow 5P_{3/2}, F = 4$ transition of ^{85}Rb can be fine-tuned by an AOM which is double-passed by the stabilization light on

its way to the high-finesse cavity.

The repumping laser is directly stabilized onto the desired $5S_{1/2}, F = 2 \rightarrow 5P_{3/2}, F = 3$ transition of ^{85}Rb, again using Doppler-free saturation spectroscopy of Rb and a Pound-Drever-Hall RF modulation technique. As the diode current modulation is slower in the setup of this laser and the error signal is noisier, the laser has a rms-linewidth of about 500 kHz, which is more than sufficient as the linewidth of the transition is 3 MHz HWHM. The output power of the laser is about 4 mW. The light of the repumping laser is used for the MOT, for polarisation-gradient cooling, the moving molasses, the fluorescence beam, the repumping beam, and can be used to illuminate the mode volume of the high-finesse cavity from the side.

5.3 The high-finesse cavity and the detection scheme

The high-finesse cavity is the heart of the experimental setup. The requirements for the cavity design will be discussed first, then the features of the cavity used in the experiment and the detection scheme for the light transmitted through the cavity are described.

5.3.1 Experimental requirements

As was discussed in the introduction, the cavity should be built such that the regime of strong coupling is reached. For this regime, the maximum atom-field coupling constant, g_0, must be larger than both the cavity field decay rate, κ, and the decay rate of the atomic dipole moment, γ.

For the chosen $5S_{1/2}\, F = 3\, m_F = 3 \leftrightarrow 5P_{3/2}\, F = 4\, m_F = 4$ transition in ^{85}Rb at $\lambda = 780,24$ nm, the decay rate of the atomic dipole moment is $\gamma = 2\pi \times 2.99$ MHz (MvdS99). The maximum coupling constant is (see Eq. (3.2))

$$g_0 = \mu \sqrt{\frac{\omega_c}{2\hbar\epsilon_0 V}}, \tag{5.1}$$

where ω_c is the resonance angular frequency of the cavity, V is the volume of the cavity mode, and μ is the dipole matrix element of the atomic transition. The dipole matrix element can be calculated from γ and the angular frequency of the atomic transition, ω_a, using Eq. (2.27), as the transition is an electric dipole transition. The resonance frequency of the cavity has to be close to a transition frequency of the atoms for a strong interaction between cavity mode and atom. Thus, ω_c can in all practical applications be replaced by ω_a in Eq. (5.1), the angular frequency of the atomic transition used in the experiment.

Once the atomic transition is fixed, the only quantity which can be influenced experimentally is the mode volume V. For g_0 to be large, V must be small. In the optical domain, a small mode volume can be achieved easiest with Fabry-Perot type cavities, which are considered in the following. The modes of these cavities are superpositions of

Hermite-Gaussian modes (Sie86, chapter 16.4). The mode function of a TEM-ij Hermite-Gaussian mode is given by

$$\psi_{ij}(x,y,z) = \sqrt{\frac{1}{2^{i+j}\, i!\, j!}} H_i\left(\sqrt{2}\frac{x}{w_0}\right) H_j\left(\sqrt{2}\frac{y}{w_0}\right) e^{-\frac{x^2+y^2}{w_0^2}} \cos(kz), \tag{5.2}$$

where w_0 is the $1/e$ field radius of the Gaussian beam, which is also called waist of the mode, and H_i is the Hermite polynomial of order i (AS72). This formula is valid if the cavity length is short as compared to the Rayleigh length of the mode. The normalization factor is chosen such that the cross-section of all modes, see Eq. (2.24), is the same, and that the maximum value of the mode function of the TEM-00 mode is 1. The resonance frequencies of the TEM-ij modes are (Sie86, Eq. (19.3-22))

$$\omega_{c,i,j} = \frac{\pi c}{l}\left[m + \frac{i+j+1}{\pi}\arccos\left(1 - \frac{l}{r_m}\right)\right], \tag{5.3}$$

where m is an integer which gives the number of antinodes of the standing wave in the cavity, and r_m is the radius of curvature of the mirror. In this thesis, $i+j$ is called the order of the TEM-ij-mode. For fixed m, the order of the mode determines the resonance frequency of the mode.The distance between the resonance angular frequencies of two adjacent modes of the same order, $\pi c/l$, is called the free spectral range of the cavity.

Because of its simplicity, the TEM-00 mode is mainly used in experiments with atoms strongly coupled to a cavity. The mode volume of the TEM-00 mode can be calculated from Eqs. (2.22) and (5.2) as

$$V = \pi w_0^2 l/4, \tag{5.4}$$

where l is the length of the cavity. The waist is determined by the length of the cavity and the radius of curvature of the mirrors. For a symmetric cavity, i.e. when both mirrors have the same radius of curvature, the waist is given by (ST91, Eq. (9.2-16))

$$w_0^2 = \frac{\lambda l}{2\pi}\sqrt{2\frac{r_m}{l} - 1}. \tag{5.5}$$

Gathering Eqs. (2.27), (5.1) and (5.4), the coupling constant for an atom at an antinode of the standing wave of a TEM-00 cavity mode can be expressed as

$$g_0 = \frac{\sqrt{3}}{\pi}\frac{\lambda}{w_0}\sqrt{\frac{c}{l}\gamma}. \tag{5.6}$$

The cavity field decay rate, κ, is given by

$$\kappa = \frac{1}{2}\frac{c}{l}(1 - \mathcal{R}). \tag{5.7}$$

This formula is valid for a cavity with highly reflective mirrors, i.e. $\mathcal{R} \approx 1$.

As explained in the introduction, the strong coupling regime should be reached in the experiment. From Eqs. (5.6) and (5.7), the experimental requirements for the strong coupling regime can be determined: The waist of the mode, w_0, must be small for a large g_0, and highly reflective mirrors with small $1-\mathcal{R}$ should be used to achieve a small κ. The cavity length, l, must be chosen small enough in order to have $g_0 > \gamma$, but not too small to achieve $g_0 > \kappa$.

In the previous chapter, it was shown that the behaviour of the atom-cavity system depends strongly on the laser-atom and laser-cavity detuning. Experimentally, the laser-atom detuning is kept constant by stabilizing the laser frequency relaively to the atomic transition. For a constant laser-cavity detuning, also the resonance frequency of the cavity has to be stabilized. The fluctuations of the cavity resonance frequency $\delta\omega_{c,n}$ should be small as compared to the cavity line width, κ. If the length fluctuations δl are small, the ratio of $\delta\omega_{c,n}$ and κ is given by Eqs. (5.3) and (5.7) as

$$\frac{\delta\omega_{c,n}}{\kappa} = \frac{4\pi}{(1-\mathcal{R})}\frac{\delta l}{\lambda_{c,i,j}}, \tag{5.8}$$

where $\lambda_{c,i,j} = 2\pi c/\omega_{c,i,j}$ is the wavelength corresponding to the cavity resonance frequency. From this, the cavity length must be stable as compared to a small fraction of the wavelength if the mirrors are highly reflective.

The detection of the transmitted light has to meet the following requirements: For the stabilization of the cavity and for probing the transmission, two different laser beams are used. For a Fabry-Perot type cavity, the transmitted part of the two beams are colinear. The detection setup must be able to separate those beams again. Crosstalk from the stabilization light on the probe light channel should be small. Then, the detection efficiency for the probe light should be as good as possible with the noise as low as possible.

These requirements are met in the setup described in the next section.

5.3.2 Cavity and detection setup

The cavity consists of two mirrors with an intensity transmission of $\mathcal{T} = 2.2 \times 10^{-6}$ and losses of $\mathcal{L} = 5.0 \times 10^{-6}$ at $\lambda = 780\,\mathrm{nm}$. This leads to $1-\mathcal{R} = \mathcal{L}+\mathcal{T} = 7.2 \times 10^{-6}$. The finesse of the cavity, which is the free spectral range divided by the linewidth, is approximately $\mathcal{F} = \pi/(1-\mathcal{R}) = 440\,000$. The mirrors are manufactured by Research Electro-Optics. The radius of curvature of the mirrors is 20 cm. The mirrors are glued onto aluminium mounts, which are separated by a piezoelectric tube used to fine-tune the length of the cavity, see Fig. 5.5. The distance between the mirror surfaces on the cavity axis is l =122 μm. This leads to a cavity field decay rate of $\kappa = 2\pi \times 1.4\,\mathrm{MHz}$, a waist of the TEM-00 mode of the cavity of $w_0 = 29\mu\mathrm{m}$, and a maximum atom-field coupling of the TEM-00 mode of $g_0 = 2\pi \times 16\,\mathrm{MHz}$. With the aforementioned $\gamma = 2\pi \times 2.99\,\mathrm{MHz}$, the requirements of the strong coupling regime are met. The single-atom maximum

cooperativity, Eq. (2.28), is $C_0 = 30$, and the saturation photon number, Eq. (3.43), is $n_p = 0.018$.

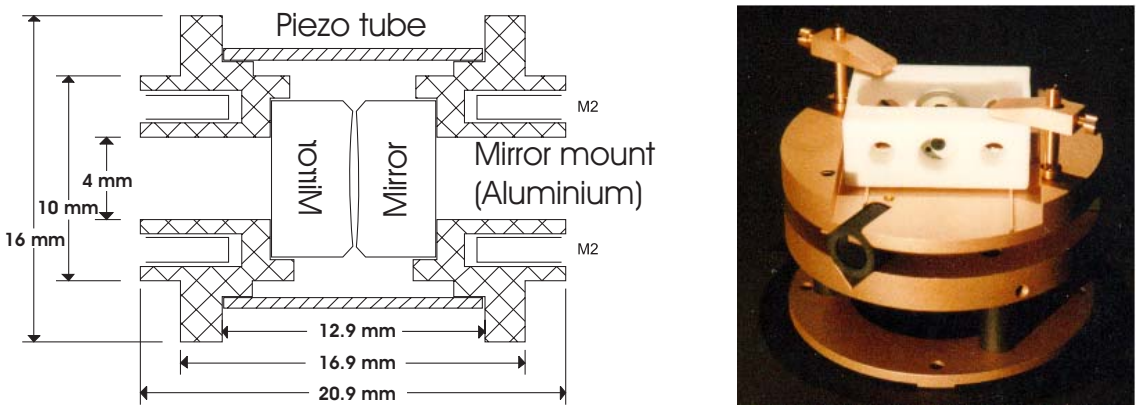

Figure 5.5: Sketch of the high-finesse cavity, and photo of the cavity and the vibration-isolation stage. In the photo, one of the mirror mounts and its front hole can be seen through the middle hole in the white Teflon block, and the piezo tube is seen through the top opening in the Teflon block. The piezo tube has 4 holes allowing access of the slow atoms and of the vacuum to the cavity modes.

Two laser beams are coupled into the cavity, namely the probe beam from the Ti:Sapphire laser and the stabilization beam from the 785 nm diode laser. Both beams can be mode-matched to the TEM-00 mode of the cavity using a telescope and two mirrors, see Fig. 5.6. By adjusting the mirrors, also a reasonable overlap between the pump beam and higher-order modes of the cavity can be achieved. The beams are circularly polarized when they impinge on the high-finesse cavity.

In the detection unit, a holographic grating with 2300 lines per mm made by American Holographics is used to separate the 785 nm stabilization light from the 780 nm probe light. The efficiency of the grating, i.e. the power of the light in the first order divided by the incident power, was measured to be 90% for a beam waist above 2 mm and a polarization of the light perpendicular to the grating lines ("horizontal polarization"). For vertically polarized light, the efficiency is much worse. In order to have the same efficiency for all polarizations, the transmitted light is split into horizontally polarized and vertically polarized light using a polarizing beam cube, see Fig. 5.7. The polarization of the vertically polarized light is turned to horizontal polarization by a half wave plate. The beams impinge on the grating, and afterwards, the polarization of the beam which was originally horizontally polarized is changed to vertical polarization with a half-wave plate. Then, the two beams are recombined with a second polarizing beam cube. The stabilization light and the probe light leave the grating with a relative angle of 0.8 degrees. Using a lens

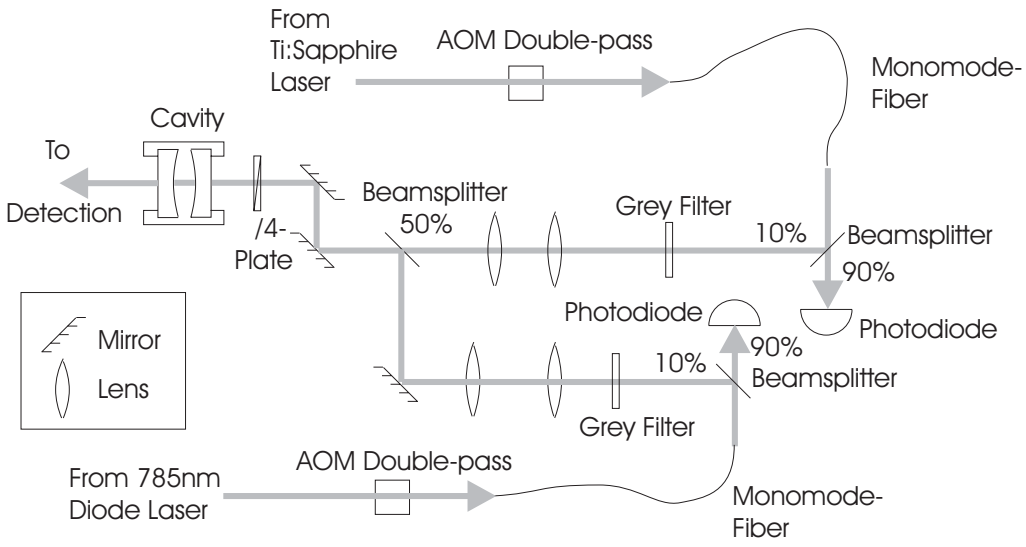

Figure 5.6: Part of the experimental setup which is used to pump the high finesse cavity.

with a focal length of 150 mm, the two beams, which have a beam waist (1/e radius of the electric field) of 3 mm, produce two foci with a waist of 190 μm and a separation of 2 mm. Placing a mirror with its edge half way between the two foci, the theoretical cross-talk of stabilization light on the probe channel should be as low as 3×10^{-7}. The measured cross-talk was 2×10^{-6}, which is good enough for the measurements in this thesis. The losses of probe light in the detection setup were measured to be 20 %, where about 10 % are due to the grating. The remaining 10 % are caused by absorption in the polarizing beam cubes and reflections from not perfectly anti-reflex-coated glass-air interfaces.

After the grating filter, the probe light is split by a polarization-independent 50% beam splitter. The two resulting beams are each focused on single-photon counting modules (SPCM-AQ-131 by PerkinElmer) with a quantum efficiency of 59 % and 49 %, respectively. The total detection efficiency, i.e. the probability of a photon to be detected if it leaves the cavity is 8.3 %. The main losses are the following: A 50 % loss factor is due to the fact that the photon can leave the cavity on either side, but only the photons on one side are detected. The photons scattered or absorbed in the coating of the high finesse cavity leads to losses of $\mathcal{L}/(\mathcal{L}+\mathcal{T}) = 70\,\%$. In a new cavity, the first loss mechanism could be diminished by using an asymmetric cavity where the incoupling mirror has a higher reflectance than the outcoupling mirror. The second loss mechanism might be mitigated by using mirrors with lower losses.

The single-photon counting modules (SPCM) produce a 8 ns wide pulse for each de-

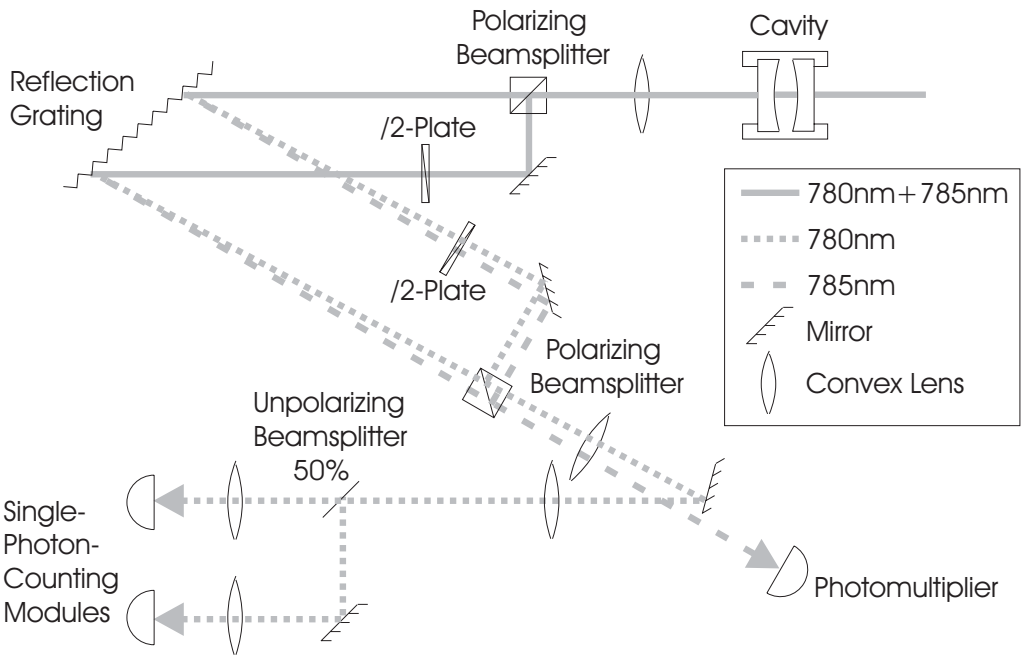

Figure 5.7: The detection setup for the light transmitted through the high-finesse cavity. The probe light is separated from the stabilizing light and is measured with two single photon-counting modules. The stabilizing light hits a photomultiplier tube.

tected photon. These pulses are elongated to 20 ns by pulse-shaping electronics. They are sent to two destinations: First, they are fed into a countrate-to-voltage converter with a variable update rate. The output of this device is used whenever the transmitted intensity is needed as an analog signal, e.g. for the feedback circuit described in section 6.3. Second, the pulses are recorded by a transient-recorder computer card. This card samples the pulses with a time resolution of 5 ns. The rising slope of each pulse is detected, the times at which they occur are stored in the computer. From these photon arrival times, the transmission of the cavity can be calculated as a function of time.

The maximum allowed count rate of the SPCM modules is about 10 MHz, typical count rates are on the order of some hundred kHz to some MHz. The dead time of the modules is on the order of 50 ns, leading to a decrease of the detection efficiency at higher count rates. For count rates of 1 MHz, the detection efficiency is reduced by about 5%. This dead time effect is corrected for when calculating the cavity transmission from the count rate of the counters.

For the stabilization of the cavity, an error signal is produced by wobbling the frequency of the stabilization laser with a peak-to-peak amplitude of 2 MHz and a frequency

of 70 kHz. The intensity of the transmitted stabilization light is detected by a photomultiplier (R3896 tube by Hamamatsu). Its output current is amplified in a self-built transimpedance amplifier. This signal is then demodulated using a lock-in amplifier (SR530 by SRS, with modified electronics to increase its bandwidth). The stabilization scheme is different from the Konstanz setup, where a RF Pound-Drever-Hall method was used which detects phase shifts in the light reflected by the cavity(Mün99).

The two methods employed in Konstanz and Garching have different merits: The RF technique uses a phase modulation with a high frequency, which was 10.7 MHz. This produces a very fast error signal; the bandwidth was about 100 kHz in Konstanz. The capture range was about 10 MHz HWHM. However, as most of the pump light is reflected off the cavity because of impedance mismatch, the signal has a high offset. This leads to a very large shot noise. Also, at low stabilization light intensities, drifting electronical offsets and background noise are a major technical problem.

The bandwidth of the lock-in error signal is limited by the modulation frequency of the stabilization laser. The bandwidth in Garching is 10 kHz, and the capture range is given by the cavity linewidth, which is 1.4 MHz HWHM. Despite of these drawbacks, the lock-in technique is much more robust, which is the reason why it is used in the Garching setup.

The cavity length stabilization loop has a bandwidth of a few 100 Hz, depending on the settings of the servo. The bandwidth is mainly limited by the piezo tube which changes the length of the cavity, in combination with the mass of the mounting of the cavity mirrors. The rms noise of the stabilized cavity resonance frequency was measured to be 250 kHz rms. This corresponds to a length stability of the cavity of 70 fm rms. Although a vibration isolation stage for the cavity was used within the vacuum chamber and noise in the lab (by ventilators etc.) was reduced to a minimum, the residual fluctuations of the cavity length are still mainly due to acoustical noise.

For some experiments, e.g. the measurement of the atomic position described in section 4.2, degenerate higher-order transversal modes are needed. From Eq. (5.3), the TEM-ij modes with the same number of antinodes n and the same mode order $i + j$ are degenerate for a cavity consisting of perfectly spherical and homogenous mirrors. In the experiment, the modes are not degenerate; the reason for this is not clear until now. However, the resonance frequencies of the observed modes are close to the frequencies predicted by Eq. (5.3). From the intensity distribution of the light leaking out of these modes, they can be described as a linear superposition of Hermite-Gaussian modes of the mode order given by their resonance frequency. As an example, see Fig. 5.8.

The splitting between the modes of the same order is small as compared to the distance between the resonance frequencies of modes belonging to different order for modes with an order below 20. For the two modes of order one, the splitting is 25 MHz, for the modes of order two, the splitting between the outermost modes is 34 MHz, see also Fig 5.8. This splitting is enough to make the experiments proposed in section 4.2 impossible with this cavity. However, it does not seem impossible that a cavity with degenerate higher-order

modes can be built in the near future.

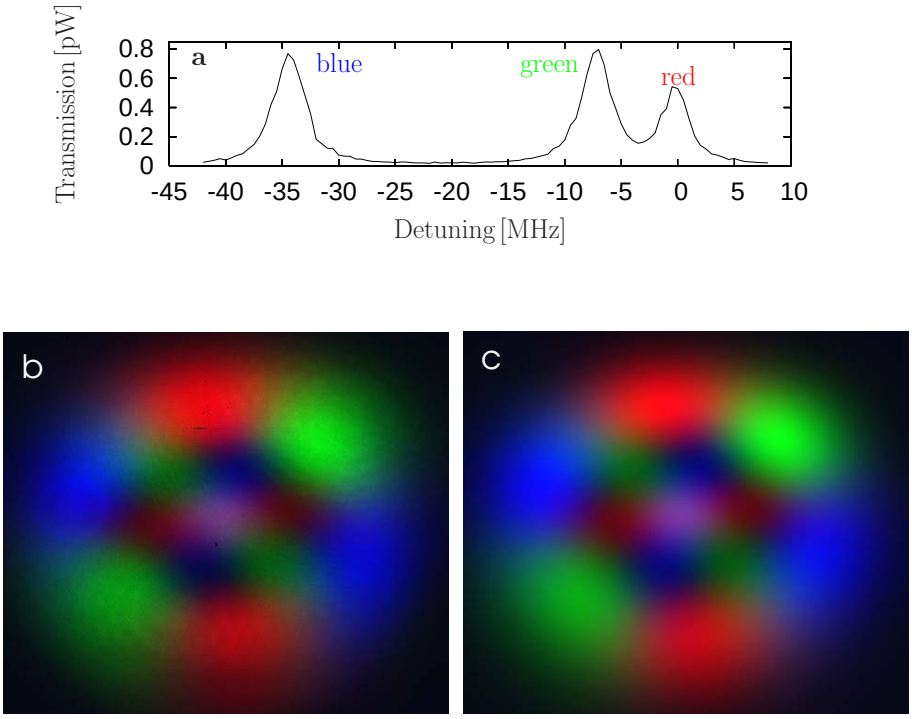

Figure 5.8: a) Measured transmission spectrum of the cavity for the modes of order 2 without an atom in the cavity. The three peaks indicate the resonance frequencies of the three modes of order 2. b) Intensity distributions of the light leaking out of these modes. The different modes are indicated by the different colors red, blue, and green. c) Fits to the transmitted intensity of the cavity. Each color represents the intensity distribution of a superposition of TEM-ij modes with $i + j = 2$. The intensity distributions are a good approximation of the measured intensity distributions in b).

Chapter 6

Control of the atomic motion

In the previous chapters of this thesis, it was explained that an atom in a high-finesse cavity can be observed with a high temporal and spatial resolution by measuring the light intensity transmitted through the cavity. It was also shown theoretically that the intra-cavity light field exerts a force on the atom. Experimentally, it was shown that this force can influence the motion of a slow atom (HCLK98), and that the light force is well described by the theory presented here (MFM$^+$99; MFM$^+$00). These forces depend on parameters like the power of the probe laser or its detuning from the atomic and cavity resonance, which can be controlled by the experimenter. An interesting question is now whether it is possible to combine those effects to control the motion of the atom in the cavity via feedback, i.e. if the information about the motion can be used to determine deviations from a desired behaviour, and change an external parameter in order to set the atom back on the right track using the light force.

In this chapter, the desired behaviour of the atom will be to stay inside the cavity as long as possible. The light force is controlled influenced by changing the pump power.

As a starting point, the motion of the atom inside the cavity will be discussed in greater detail. To compensate for the initial kinetic energy of the atoms, it is necessary to use strong light forces to be able to control the atomic motion. Thus, for the cavity used here, the intensity of the pump beam is so large that the excitation of the atom is no longer low enough to use the low-pump approximation of chapter 3. An analytic treatment of the atom-cavity system under these circumstances has, to my knowledge, not been done so far except for very special parameters (AGC92). Thus, to compare the experiment with theory, it is necessary to use the numerical methods described in chapter 3.8.

In section 6.1, the motion of the atom will be characterized and analysed theoretically for the parameters used in the experiments of this chapter. Readers who are not interested in details of the atomic motion can skip the sections 6.1.2 and 6.1.3. A first experiment towards feedback control of the atomic motion (PFMR00) is presented in section 6.2, and more sophisticated feedback methods (FMP$^+$02) in section 6.3. The perspectives of feedback methods are discussed in section 6.4.

6.1 Description of the motion of the atom

In this section, a qualitative description of the motion of an atom in a high-finesse cavity is given. For this, the magnitude of the different contributions to the light force are estimated. Then, the typical motion of an atom in a cavity is described, and quantities associated with the atomic motion will be calculated. From this analysis, the optimal parameters for trapping are identified.

The magnitude of the different parts of the light force depend on the position of the atom. The force on the atom at a given time influences the atom's position at later times and thus the force at later times. To include this in the calculation of quantities like the average heating rate, one would have to calculate sample trajectories of atoms and average the wanted quantity over them. However, to work out the connections between the different quantities and to keep calculations reasonably simple, this method will be avoided. Instead, the different contributions to the light force will be calculated numerically for different positions of an atom as described in section 3.8, and then be averaged using simple but reasonable assumptions about the distribution of the position of the atom. These averages are not as exact as the ones which one could get by calculating sample trajectories, but a reasonable accuracy can be expected.

6.1.1 Different contributions to the light force

First of all, the contributions to the light force which are most important for the motion of an atom will be identified. For this, it is instructive to consider the typical length scales in the cavity. The length scales in the different directions are very different, see Eq. (5.2): In the direction along the cavity axis, which is called 'axial direction' in the following, the light field forms a standing wave. The intensity of the light field has a periodicity of $\lambda/2$, which is $0.39\,\mu$m. For the motion of the atom in the plane perpendicular to the cavity axis, the 'transversal motion', the typical length scale is the $1/e$ radius of the mode function, w_0, which is $29\,\mu$m for the cavity used here. Therefore, the derivative of the coupling constant g_{1j} is small in the transversal direction as compared to the derivative in the axial direction. This has two consequences: First, as most parts of the light force are proportional to $\boldsymbol{\nabla}_j g_{1j}$ or $(\boldsymbol{\nabla}_j g_{1j})^2$, the motion of the atom along the cavity axis is very fast and nearly decouples from the slower transversal motion. Second, the light forces which dominate the motion of the atom are different in the two directions: The velocity-dependent force, Eq. (3.92), and momentum diffusion due to the cavity light force, Eq. (3.82), are proportional to the square of the gradient of the coupling. The dipole force, Eq. (3.39), is proportional to the gradient of the coupling, and momentum diffusion due to spontaneous emission, Eq. (3.79), does not depend on the gradient of the coupling at all. Thus, in the axial direction, where the gradient of the coupling constant is large, the dominant force is the dipole force, and momentum diffusion and velocity-dependent force add a certain degree of non-conservativity to the motion. In the

transversal direction, however, the velocity-dependent force and the momentum diffusion due to dipole fluctuations are too weak to be of any consequence. Here, the motion is dominated by the dipole force and momentum diffusion due to photon recoils.

In the following discussion, it is assumed that the TEM-00 mode of a Fabry-Perot type cavity is used. However, the results are easily transferable to any TEM mode of a Fabry-Perot type cavity.

Also, it is assumed that the light field is red-detuned from the atomic transition. In this case, three-dimensional potential wells exists for the atoms in the cavity, and they will tend to oscillate in a well. This oscillation will be investigated in the following.

6.1.2 Quantities describing the motion of the atom

The motion of an atom trapped in the cavity light field can be characterized by the depth of the trap potential, the trap frequency, the average momentum diffusion constant, the average cooling or heating rate by the velocity-dependent force, and the kinetic and potential energy of the atom. In this section, these quantities are calculated. As an example, they will be evaluated for the parameters used in the experiments described in this chapter, namely a laser-atom detuning of $\Delta_a/(2\pi) = -45\,\mathrm{MHz}$, and a laser-cavity detuning $\Delta_c/(2\pi) = -5\,\mathrm{MHz}$. The results are shown in Table 6.1.

To determine how well the atom is trapped, the trap potential induced by the light force has to be considered. The trap potential can be calculated by integrating the expectation value of the light force, Eq. (3.26), along a chosen path. The potential on the cavity axis and in the transversal direction is shown in Fig. 6.1.

The depth of the potential, V_0, is given by the integral

$$V_0 = \int_{g(\mathbf{r})=0}^{g(\mathbf{r})=g_0} \mathrm{d}\mathbf{s} \cdot \langle \mathbf{F}_{\mathrm{cav},j}(\mathbf{r}) \rangle \tag{6.1}$$

from a position where the coupling constant g is zero to a position where it is maximal. To keep the notation of chapter 3, the index j is kept here although only a single atom is considered.

The trap frequencies are more difficult to estimate, because the potential is not harmonic, see Fig. 6.1. Thus, the trap frequencies depend on the amplitude of the oscillation in the trap, which can be large. To get an estimate of the trap frequency, the potential can be approximated by a parabola which is V_0 deep and is $\lambda/2$ wide in the axial direction, and $2w_0$ wide in the transversal direction, respectively. This gives an axial trap frequency

$$\nu_a = \sqrt{32V_0/(m_{Rb}\lambda^2)}, \tag{6.2}$$

and a transversal trap frequency

$$\nu_t = \sqrt{2V_0/(m_{Rb}w_0^2)}. \tag{6.3}$$

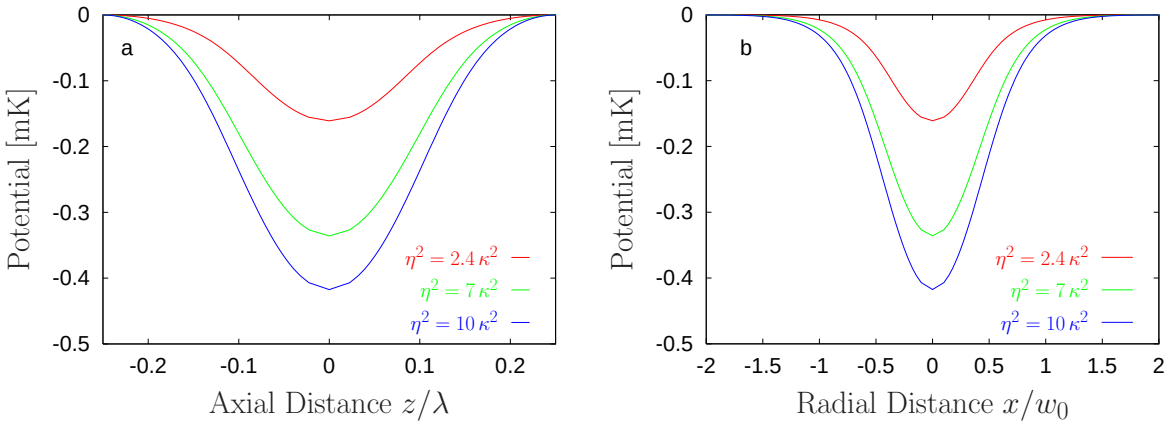

Figure 6.1: a) Axial and b) transversal trap potentials for different pump powers. In a), the catom is on the cavity axis. In b), the atom is in an antinode of the standing wave.

Next, the heating of the atom by the light force is considered. The heating rate, i.e. the rate of increase in kinetic energy of the atom, can be obtained from the definition of the momentum diffusion constant, Eq. (3.57): Momentum diffusion describes an increase in the momentum squared which is *not* due to the expectation value of the light force. For a trapped atom and averaged over an oscillation period, the dipole part of the light force does not change the atomic momentum. The velocity dependent force can influence the averaged atomic motion and will discussed later. As $E_{\mathrm{kin}} = \left|\mathbf{p}_j^2\right|/2m$, the increase of kinetic energy due to momentum diffusion is

$$\frac{\mathrm{d}\overline{E_{\mathrm{kin,a}}}}{\mathrm{d}t} = \frac{\overline{D_a}}{m_{Rb}} \tag{6.4}$$

$$\frac{\mathrm{d}\overline{E_{\mathrm{kin,t}}}}{\mathrm{d}t} = \frac{\overline{D_t}}{m_{Rb}}, \tag{6.5}$$

where $E_{\mathrm{kin,a}}$ and $E_{\mathrm{kin,r}}$ are the axial and transversal kinetic energy of the atom, respectively. Because momentum diffusion can be very different in the axial and transversal directions, the axial and transversal momentum diffusion constants are evaluated separately.

To estimate the mean momentum diffusion constants, they have to be averaged in some way, as they depend strongly on position. Here, the average of the momentum diffusion constants over over a line of length λ on the cavity axis is taken. This averages the momentum diffusion constant over the standing wave of the cavity mode. As circularly polarized light is used, the mean axial momentum diffusion, D_a, is given by the momentum diffusion due to the cavity light force, characterized by D_{cav}, plus 2/5 of the momentum

diffusion induced by spontaneous emission, which is described by D_{se}:

$$\overline{D_a} = \frac{1}{\lambda}\int_{z=0}^{\lambda} \mathrm{d}z \left[D_{dp}\left(\rho=0,z\right) + \frac{2}{5}D_{se}\left(\rho=0,z\right)\right] \tag{6.6}$$

The transversal diffusion constant is then 3/5 times the momentum diffusion constant for spontaneous emission.

$$\overline{D_r} = \frac{3}{5\lambda}\int_{z=0}^{\lambda} \mathrm{d}z\, D_{se}\left(\rho=0,z\right) \tag{6.7}$$

Next, the cooling by the velocity-dependent force has to be determined. In the experiments presented here, the atom moves slowly, therefore the friction force is linear in the velocity of the atom in a very good approximation, see the discussion in section 3.6. From Eq. (3.89), the friction force is parallel or antiparallel to the gradient of the coupling constant, g_{1j}. Only the component of the atomic velocity in direction of the gradient of the coupling constant determines the magnitude of the friction force, see Eq. (3.92). As the gradients in the axial direction are much stronger than in the transversal direction, only the axial motion is cooled, and the magnitude of the cooling only depends on the velocity component of the atom along the cavity axis. Thus, the friction force force, $\langle \mathbf{F}_{\mathrm{cav,j}} \rangle_1$, can be approximated by

$$\langle \mathbf{F}_{\mathrm{cav,j}} \rangle_1 = \mathbf{e}_{\mathrm{z}} \beta_j v_{\mathrm{z},j}, \tag{6.8}$$

where the cavity axis is parallel to the z-direction, and $\mathbf{e}_{\mathrm{z}}$ is a vector of unity length pointing in the z-direction. The momentary axial cooling rate $-r_{\mathrm{c,a},j}$, i.e. the part of the change in the axial kinetic energy which is due to the velocity-dependent force, is the velocity of the atom times the velocity-dependent force:

$$\begin{aligned} r_{\mathrm{c,a},j} &= \mathbf{v}_j \cdot \langle \mathbf{F}_{\mathrm{cav,j}} \rangle_1 \\ &= \beta_j v_{\mathrm{z},j}^2 \end{aligned} \tag{6.9}$$

Thus, the average cooling rate is $\overline{\beta_j v_{\mathrm{z},j}^2}$, or approximately $\overline{\beta_j}\ \overline{v_{\mathrm{z},j}^2}$. The average of the mean square of the axial velocity, $\overline{v_{\mathrm{z},j}^2}$, is $2/m$ times the average axial kinetic energy $E_{\mathrm{kin,a},j}$, thus

$$r_{\mathrm{c,a},j} = 2\frac{\overline{\beta_j}\ \overline{E_{\mathrm{kin,a},j}}}{m_{Rb}}. \tag{6.10}$$

The average friction coefficient, $\overline{\beta_j}$, can be estimated by averaging β_j over the standing wave in the cavity.

The motion of the atom can now be characterized using the above coefficients. Consider the dimensionless quantities

$$k_a = V_0 \nu_a m_{Rb} / \overline{D_a} \tag{6.11}$$

and

$$k_t = V_0 \nu_t m_{Rb} / \overline{D_r}. \tag{6.12}$$

They give the trap depth divided by the average energy which is deposited in the atom by momentum diffusion during one trap period. If this ratio is much larger than 1, very little energy is deposited in the atom during one oscillation. This has two effects: First, for an atom with a reasonably large oscillation amplitude in the trap, the change in atomic momentum which is induced by momentum diffusion per transversal oscillation is small as compared to the momentum the atom gets from rolling down the potential well, i.e. the motion of the atom is a conservative motion with very little disturbance. Thus, the quantities k_a and k_t can be called 'axial conservativity' and 'transversal conservativity', respectively. Second, the atom can be stored in the potential well for many oscillation periods, even if there is no cooling mechanism as in the transversal direction. If k is close to one, the atom is trapped for only few trap cycles, and the motion is highly diffusive. If k is much smaller than one, the dipole force plays only a small role, and the atom moves like a free particle under the influence of diffusion. In the experiment, the transversal conservativity is about 5, depending on the pump power, thus the transversal motion is an oscillation which is much influenced by momentum diffusion. The axial conservativity is on the order of 50, leading to regular axial motion.

If there exists a significant cooling mechanism, as in the axial direction, the equilibrium temperature, T_a, is of interest. It is given by the condition that the mean energy loss rate by the velocity dependent force, $r_{\mathrm{c,a},j} = 2\overline{\beta_j}\,\overline{E_{\mathrm{kin,a},j}}/m$, is equal to the mean energy gain rate by momentum diffusion, $\overline{D_a}/m$. For a harmonic trap potential, $\overline{E_{\mathrm{kin,a},j}} = k_B T_a/2$, thus

$$k_B T_a = -\frac{\overline{D_a}}{\overline{\beta_a}}. \tag{6.13}$$

To determine whether the cooling is large enough to trap the particle in one potential well of the standing wave, the ratio between the trap depth and the equilibrium temperature, θ, has to be calculated:

$$\theta_{\mathrm{a}} = \frac{k_B T_{\mathrm{a}}}{V_0}. \tag{6.14}$$

If θ_{a} is much smaller than one, the atom is trapped in a single potential well all the time. If θ_{a} is on the order of one in the axial direction, the atom is trapped most of the time, but sometimes, the atom's kinetic energy is larger than the potential height. Then, the atom travels over some potential wells and hills, before it is trapped again in another well. If θ_{a} is much larger than one, the atom behaves like a free particle.

The time constant for reaching the equilibrium temperature, $t_{\mathrm{eq,a}}$, can be estimated by the time which the momentum diffusion needs to increase the kinetic energy of the atom by $k_B T_{\mathrm{a}}$, thus

$$t_{\mathrm{eq,a}} = m k_B T_{\mathrm{a}}/\overline{D_a} = -m/\overline{\beta_a}. \tag{6.15}$$

If the average trap time is much longer than $t_{\mathrm{eq,a}}$, the axial motion of the atom is in thermal equilibrium. Note that the equilibrium time only depends on the average friction coefficient, $\overline{\beta_a}$, and the atomic mass, m. For this reason, a "natural" measure of the

friction coefficient is the inverse cooling time, which is obtained by dividing the friction coefficient by the atomic mass.

The last quantity which will be discussed here does not describe the atomic motion. It is a measure how well the transversal position of the atom can be determined by measuring the cavity transmission. This quantity is called the transversal observability of the atom, o_t, in the following. To define it, the signal-to-noise ratio of the cavity transmission is considered: Because of shot noise, the cavity transmission can not be determined to arbitrary accuracy. The signal-to-noise ratio is given by the square root of the number of measured photons, and thus depends on the transmission of the cavity as well as on the observation interval. If the observation interval is too long, the average over the motion of the atom will be taken, and the motion cannot be observed. A measure for the maximum possible observation interval is one period of the transversal oscillation of the atom, if the conservativity of the motion is larger than one. Thus, the expectation value of the number of observable photons is limited by $\langle n_p \rangle = \left\langle a^\dagger a \right\rangle_0 \kappa/\nu_t$. The noise is given by $\sqrt{\langle n_p \rangle}$.

The exactness of the position measurement in the cavity does not only depend on the signal-to-noise ratio for the determination of the transmission, but also on the amount the cavity transmission is changed by the atom. Two positions of the atom can be distinguished from each other if the difference in signal between the two positions is larger than the sum of noise for both positions. In the following, the position where the intracavity photon number is maximal, denoted by the subscript $_\mathrm{max}$, is compared to the position where the intracavity photon number is minimal, denoted by $_\mathrm{min}$. Thus, the transversal observability of the atom in the cavity can be defined as the difference in signal divided by the sum of the noise:

$$o_\mathrm{t} = \frac{\langle n_p \rangle_\mathrm{max} - \langle n_p \rangle_\mathrm{min}}{\sqrt{\langle n_p \rangle_\mathrm{max}} + \sqrt{\langle n_p \rangle_\mathrm{min}}} \tag{6.16}$$

$$= \sqrt{\frac{\kappa}{\nu_t}} \left| \frac{\left\langle a^\dagger a \right\rangle_{0,\mathrm{max}} - \left\langle a^\dagger a \right\rangle_{0,\mathrm{min}}}{\sqrt{\langle a^\dagger a \rangle_{0,\mathrm{max}}} + \sqrt{\langle a^\dagger a \rangle_{0,\mathrm{min}}}} \right| \tag{6.17}$$

This number must be large as compared to one in order to be able to observe the transversal motion of the atom in real time.

6.1.3 Choice of parameters

Using the results of the last section, it will be discussed here how experimental parameters should be chosen for trapping an atom in a cavity. It is assumed that the atomic and cavity parameters are fixed, i.e. γ, g_0 and κ are constants (the choice of cavity parameters will be discussed later in section 6.4). The remaining parameters which are easy to change are the laser-atom detuning, Δ_a, the laser-cavity detuning, Δ_c, and the pump strength, η. First, the requirements for trapping an atom will be discussed. Then the dependence

Pump power η^2/κ^2	2.4	7	10
potential depth V_0 [mK]	0.16	0.34	0.42
maximum excitation $\langle\sigma^+\sigma^-\rangle_{max}$	0.12	0.21	0.23
axial momentum diffusion $\overline{D_a}/(mk_B)$ [mK/ms]	3.7	5.3	6.5
transversal momentum diffusion $\overline{D_r}/(mk_B)$ [mK/ms]	0.21	0.39	0.46
axial trap frequency ν_a [MHz]	0.90	1.31	1.46
transversal trap frequency ν_t [kHz]	6.1	8.8	9.8
axial conservativity k_a	39	82	93
transversal conservativity k_t	4.6	7.6	9.0
axial friction coefficient $-\overline{\beta_a}/m$ [1/ms]	67	71	68
axial equilibrium temperature T_a [mK]	0.055	0.074	0.096
axial dimensionless temperature θ_a	0.34	0.22	0.23
axial equilibrium time $t_{eq,a}$ [ms]	0.015	0.014	0.015
transversal observability o_t	29	31	31

Table 6.1: Theoretical values for the quantities discussed in section 6.1.2 as obtained from a numerical integration of the master equation. The detunings are $\Delta_a/(2\pi) = -45\,\mathrm{MHz}$, $\Delta_c/(2\pi) = -5\,\mathrm{MHz}$, the cavity parameters are $g_0/(2\pi) = 16\,\mathrm{MHz}$, $\kappa/(2\pi) = 1.4\,\mathrm{MHz}$.

of the quantities which where presented in the previous section on the detunings and the pump power will be considered. For this, the analytical formulas for low saturation and a single atom in a single-mode cavity will be used. In the course of the discussion, it will be seen that the low saturation approximation is no good approximation anymore for optimal parameters, but as the differences are not too large, the analytical formulas can be used as a first step, and then the parameters can be fine-tuned afterwards to account for the effects of the saturation.

1) To store the atom in the cavity, a three-dimensional potential well for the atoms is needed. For this, the potential energy for an atom in the cavity must be less than the potential energy for an atom outside the cavity. Thus, **the potential energy must decrease if the coupling constant rises**.

2) Then, the potential should be strong enough to trap an atom: The depth of the potential well should be larger than the kinetic energy of the atoms just before they enter the cavity. The kinetic energy of the atoms can not be influenced by the parameters which are discussed here, therefore **the depth of the potential should be large**.

3) Also, the heating part of the cavity light force should not dominate the motion of the

atoms. In the axial direction, the effects of momentum diffusion can be controlled by the velocity-dependent part of the light force. Thus, **the velocity-dependent force should be cooling**.

4) To prevent the atom from hitting one of the mirrors, the cooling effect of the light force in this direction should be large enough to trap the particle in one antinode of the standing wave most of the time. Therefore **the dimensionless axial equilibrium temperature, θ_{a}, should be smaller than one** .

5) In the transversal direction, the velocity-dependent force does not affect the motion. Therefore, heating in the transversal direction should be as small as possible. In other words, **the transversal motion should be as conservative as possible**.

6) Then, to gain information about the position of the atom in the cavity, the atom should have a large effect on the cavity transmission. The first condition for this is that **the transversal observability, o_t, should be large**.

7) The cavity transmission can also be altered by technical noise, i.e. fluctuations in the cavity length. The changes in cavity transmission which is due to an atom in the cavity should be larger than these technical changes. Thus, **the relative change of transmission by an atom in the cavity should be large**.

These conditions will be evaluated in the following. Condition 1) is fulfilled if and only if the laser-atom detuning, Δ_a, is negative. This can be seen from Eqs. (3.30) and (3.41) in the low saturation regime, but is also true for a large saturation of the atom.

Next, it will be shown that condition 5) demands a large laser-atom detuning Δ_a. Then, the simpler formulas for a large Δ_a stated from section 3.7 can be used in the further discussion. It will be shown later that the other conditions can also be fulfilled in the limit of large Δ_a.

From condition 5), the transversal conservativity, k_t, defined in Eq. (6.12) must be large. It can be calculated from Eqs. (6.3), (6.1), (3.41), (6.7), (3.79) and (3.36) as

$$k_t = \frac{5\lambda^2}{4\pi^2 w_0}\sqrt{\frac{m_{Rb}}{2\hbar}}\frac{1}{\gamma g_0^2}\frac{\left[\arctan\left(S_{\max}\right)-\arctan\left(S_{\min}\right)\right]^{3/2}}{\sqrt{\frac{\left|g_{1j}/g_0\right|^2}{1+S^2}}}\left[|\eta|\Delta_a^{3/2}\left(\Delta_{\mathrm{c}}\gamma+\Delta_{\mathrm{a}}\kappa\right)^{1/2}\right] \quad (6.18)$$

Here, $S_{\max}$ is the dimensionless frequency distance from a normal mode peak, S, defined in Eq. (3.30), for a cavity without an atom. $S_{\min}$ is the dimensionless distance from a normal mode peak for a maximally coupled atom, i.e. $g = g_0$. The overline denotes the average over the standing wave of the cavity mode, i.e. the average over a line of length λ along the cavity axis.

Now, the dependence of k_t on the pump power and the detunings can be discussed: First, k_t is proportional to $|\eta|$, which is the square root of the pump intensity. This

indicates that a large pump power leads to a more conservative transversal motion of the atom. Remember, however, that Eq. (6.18) is only valid for low saturation.

Next, the parts of Eq. (6.18) which depend on the detunings Δ_a and Δ_c are identified. This is the factor in square brackets at the end of the equation, and the parts which involve the dimensionless distance from a normal mode peak, S. The difference $[\arctan(S_{\max}) - \arctan(S_{\min})]$ can not get larger than π, thus k_t can not be optimized to a large extent by this factor. It will be shown later that this factor is close to its maximal value in the parameter regime which is optimal for trapping. Therefore the factor $[\arctan(S_{\max}) - \arctan(S_{\min})]$ will not be considered for now. Then, using the definition of S, Eq. (3.30), the following dependence of the transversal conservativity on Δ_a and Δ_c is obtained:

$$k_t \propto \left\{ \overline{|g_{1j}/g_0|^2 / \left[\Delta_a^{3/2} \left(\Delta_c\gamma + \Delta_a\kappa\right)^{1/2} + \frac{\left(|g_{1j}|^2 - \Delta_{\mathrm{a}}\Delta_{\mathrm{c}} + \gamma\kappa\right)^2}{\left(\frac{\Delta_c}{\Delta_a}\gamma + \kappa\right)^{3/2}} \right]} \right\}^{-1} . \tag{6.19}$$

The right hand side of Eq. (6.19) can be made large only by choosing a large Δ_a and/or a large Δ_c. For $\Delta_a\kappa \gg \Delta_c\gamma$, i.e. large Δ_a, the first summand in the square brackets is proportional to Δ_a^2, and the second summand is proportional to its numerator (it will be seen later that $\Delta_a\Delta_c$ should be chosen on the order of $|g_{1j}|^2$). For $\Delta_a\kappa \ll \Delta_c\gamma$, the first summand is proportional to $\Delta_a^{3/2}\sqrt{\Delta_c}$, and the second summand is proportional to its numerator divided by $\Delta_c^{3/2}$. Therefore, a large Δ_a is much more important for a large transversal conservativity than a large Δ_c. As will be seen below, a good visibility of the atom can not be achieved if both Δ_a and Δ_c are large. Therefore it is natural to choose a large laser-atom detuning Δ_a to achieve a large transversal conservativity. This has the pleasant side effect that the formulas in section 3.7 can be used for the following.

Condition 3) can be evaluated using Eq. (3.110) and demands that S should be larger than zero. From Eq. (3.99) and for $\Delta_a < 0$, this requires that $\Delta_c < 0$. Furthermore, to ensure cooling even for a maximally coupled atom, $\Delta_a\Delta_c$ must be larger than g_0^2. These parameters imply that S and S^2 are maximal for no atom in the cavity, while for a maximally coupled atom, S and S^2 reach their smallest value.

Condition 2) is discussed using Eq. (3.106). The potential depth is given by

$$V_0 = \hbar\frac{|\eta|^2}{\kappa}\left[\arctan(S_{\max}) - \arctan\left(S_{\min}\right)\right] \tag{6.20}$$

Obviously, a large pump intensity $|\eta|^2$ creates a deep potential. However, if $|\eta|^2$ is too large, the saturation of the atom becomes significant, and Eq. (3.106) is not a good approximation anymore. For a saturated atom, the actual potential depth is smaller than predicted by Eq.(6.20).

For a deep potential well, it is also necessary that $[\arctan(S_{\max}) - \arctan(S_{\min})]$ is large. As condition 3) implies that $S_{\min} > 0$, this term can not get larger than $\pi/2$. A value close to this maximum value can be reached by choosing $S_{\min} = 0$ and $S_{\max} > 2$.

Note that if $S_{\min}$ and $S_{\max}$ are fixed, so are the detunings Δ_a and Δ_c: In the far detuned limit, $S_{\min}$ and $S_{\max}$ are given by Eq. (3.99) as

$$S_{\min} = \frac{g_0^2}{\Delta_{\mathrm{a}}\kappa} - \frac{\Delta_{\mathrm{c}}}{\kappa}, \tag{6.21}$$

and

$$S_{\max} = -\frac{\Delta_{\mathrm{c}}}{\kappa}. \tag{6.22}$$

For $S_{\min} = 0$, Δ_a and Δ_c are only determined by the choice of $S_{\max}$, and are given by

$$\Delta_a = -\frac{g_0^2}{S_{\max}\kappa}, \tag{6.23}$$

and

$$\Delta_c = -\kappa S_{\max}. \tag{6.24}$$

Now, the remaining conditions are evaluated to see if there are contradictions to the results until now, and to determine the optimal value of $S_{\max}$.

To see the implications of condition 7), the relative change in the transmission of the cavity with and without an atom, v, is calculated. It is given by Eq. (3.104) as

$$v = \frac{S_{\max}^2 + 1}{S^2 + 1} \tag{6.25}$$

As S^2 is smallest for a maximally coupled atom, v is maximal if $S = S_{\min}$. This means that a maximally coupled atom causes the largest change in the transmission as compared to the cavity without an atom. The maximum v can be made large by choosing detunings for which $S_{\min} = 0$ and $S_{\max}$ is large. For practical purposes, a maximal v larger than 5 is sufficient, leading again to $S_{\max} > 2$.

In Eq. (6.25), v does not depend on the pump strength $|\eta|$. For too large η, however, the atom becomes saturated, and v drops. This gives an upper bound for the pump strength. From numerical calculations, v drops dramatically if the atomic excitation, $\left\langle \sigma_j^+ \sigma_j^- \right\rangle_0$, is larger than 0.2. As for all the other quantities a large $|\eta|$ is advantageous, $|\eta|$ should be chosen such that the maximum saturation is $\left\langle \sigma_j^+ \sigma_j^- \right\rangle_{\max} = 0.2$.

The maximum saturation of the atom does not only depend on the pump strength, but also on the chosen detunings. In other words, to get the same $\left\langle \sigma_j^+ \sigma_j^- \right\rangle_{\max}$ for different detunings, the pump strength must be changed along with the detunings. This influences the scaling of the different quantities with Δ_a and Δ_c. In order to take this into consideration, the pump strength η should be expressed in terms of the maximum saturation. The relation between η and $\left\langle \sigma_j^+ \sigma_j^- \right\rangle_{\max}$ is the following: From Eq. (3.102), the saturation

is maximal if the atom is maximally coupled, i.e. $|g_{1j}| = g_0$, or equivalently $S = S_{\min}$ if $S_{\min} \geq 0$. From Eqs. (3.102) and (6.23),

$$|\eta| = g_0 \frac{\sqrt{1+S_{\min}^2}}{|S_{\max} - S_{\min}|} \sqrt{\left\langle \sigma_j^+ \sigma_j^- \right\rangle_{\max}}\,, \tag{6.26}$$

which is valid in the limit of large detuning and small saturation and for $S_{\min} \geq 0$.

For discussing condition 6), the observability o is calculated in the limit of large Δ_a from Eqs. (6.17), (3.104), (6.3), (6.3), and (6.26) as

$$o = \left[\frac{g_0^2 \left(1+S_{\min}^2\right) \left\langle \sigma_j^+ \sigma_j^- \right\rangle_{\max} m_{Rb}\, w_0^2}{2\hbar\kappa \left(S_{\max} - S_{\min}\right)^2 \left(\arctan S_{\max} - \arctan S_{\min}\right)} \right]^{1/4} \left| \frac{\frac{S_{\max}^2+1}{S_{\min}^2+1} - \frac{S_{\min}^2+1}{S_{\max}^2+1}}{\sqrt{S_{\min}^2+1} + \sqrt{S_{\max}^2+1}} \right|. \tag{6.27}$$

To determine the dependence on the detunings, the observability is plotted as a function of $S_{\max} - S_{\min}$ for different values of $S_{\min}$ in Fig. 6.2. There, it can be seen that for a large observability, $S_{\max} - S_{\min}$ should be large, and $S_{\min}$ should be smaller than 1. which is consistent with the constraints described so far.

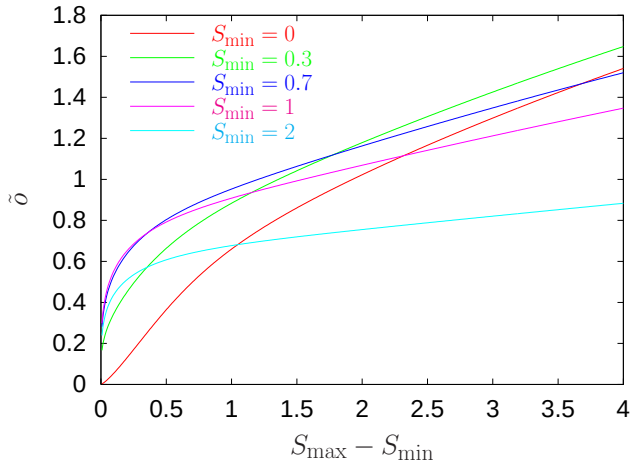

Figure 6.2: The dependence of the observability on $S_{\min}$ and $S_{\max}$. Plotted is $\tilde{o} = o \left[\frac{2\hbar\kappa}{g_0^2 \left\langle \sigma_j^+ \sigma_j^- \right\rangle_{\max} m_{Rb}\, w_0^2} \right]^{1/4}$ for different $S_{\min}$.

Condition 4) is evaluated using Eqs (6.14), (6.13), (3.107), (6.20) and (3.110) to give the ratio between equilibrium temperature and trap depth,

$$\theta_a = \frac{1}{16}\frac{\kappa^3\gamma}{|\eta|^2 g_0^2}\frac{\overline{\left(1-\frac{3}{5}\frac{|g_{1j}|^2}{g_0^2}\right)\frac{1}{S^2+1}\left(1+\frac{4g_0^2}{\kappa\gamma}\frac{|g_{1j}|^2}{g_0^2}\frac{1}{S^2+1}\right)}}{\overline{\left(1-\frac{|g_{1j}|^2}{g_0^2}\right)\frac{|g_{1j}|^2}{g_0^2}\frac{S}{(S^2+1)^3}}\left[\arctan\left(S_{\max}\right)-\arctan\left(S_{\min}\right)\right]}. \tag{6.28}$$

Here, $|\boldsymbol{\nabla} g_{1j}|^2 = k^2(g_0^2 - |g_{1j}|^2)$ was used, which stems from the sine-dependence of the coupling constant on the position along the cavity axis, see Eqs. (3.1) and (5.2).

Now, it will be discussed how the dimensionless temperature θ_a can be minimized by choosing the right $S_{\max}$ and $S_{\min}$. Disregarding the term in squared brackets at first, the denominator of Eq. (6.28) is proportional to $S/(S^2+1)^3$, which gets small for $S \ll 1$ and $S \gg 1$. The numerator stays constant for small S, and then gets significantly smaller for increasing S if S is on the order of one. For very large S, the denominator converges faster towards zero than the numerator. The maxima of both numerator and denominator have the largest influence on θ, as they are averaged separately. For a fixed S, the denominator is maximal for $S \approx 1$. Thus, $S_{\min}$ and $S_{\max}$ should be chosen such that the maximum of the denominator is included between $S_{\min}$ and $S_{\max}$. This is the case for the parameters favoured until now, namely $S_{\min} = 0$ and $S_{\max}$ larger than two.

To collect the results of the discussion in this section, the quantities used to discuss the optimal values of Δ_a, Δ_c and η are given in terms of $S_{\max}$ and $\left\langle \sigma_j^+\sigma_j^- \right\rangle_{\max}$ for $S_{\min} = 0$ in the limit of large Δ_a and small saturation:

$$v_{\max} = S_{\max}^2 + 1 \tag{6.29}$$

$$V_0 = \hbar\frac{g_0^2}{\kappa}\arctan\left(S_{\max}\right)\frac{S_{\max}^2+1}{S_{\max}^2}\left\langle \sigma_j^+\sigma_j^- \right\rangle_{\max} \tag{6.30}$$

$$o = \left[\frac{g_0^2\left\langle \sigma_j^+\sigma_j^- \right\rangle_{\max} m_{Rb}\, w_0^2}{2\hbar\kappa}\right]^{1/4}\left|\frac{S_{\max}^2+1-\frac{1}{S_{\max}^2+1}}{\sqrt{S_{\max}}\left(\sqrt{\frac{1}{S_{\max}^2+1}}+1\right)\arctan\left(S_{\max}\right)}\right|. \tag{6.31}$$

$$k_t = \frac{5\lambda^2}{4\pi^2 w_0}\sqrt{\frac{m_{Rb}}{2\hbar\kappa^3}}\frac{g_0^3}{\gamma}\frac{\left[\arctan\left(S_{\max}\right)\right]^{3/2}}{S_{\max}^3\overline{\frac{|g_{1j}/g_0|^2}{1+S^2}}}\sqrt{\left\langle \sigma_j^+\sigma_j^- \right\rangle_{\max}} \tag{6.32}$$

$$\theta_a = \frac{1}{16}\frac{\kappa^3\gamma S_{\max}^2}{g_0^4\left\langle \sigma_j^+\sigma_j^- \right\rangle_{\max}}\frac{\overline{\left(1-\frac{3}{5}\frac{|g_{1j}|^2}{g_0^2}\right)\frac{1}{S^2+1}\left(1+\frac{4g_0^2}{\kappa\gamma}\frac{|g_{1j}|^2}{g_0^2}\frac{1}{S^2+1}\right)}}{\overline{\left(1-\frac{|g_{1j}|^2}{g_0^2}\right)\frac{|g_{1j}|^2}{g_0^2}\frac{S}{(S^2+1)^3}}\arctan\left(S_{\max}\right)}, \tag{6.33}$$

To have a large relative transmission change, $v_{\max}$, a deep potential well, V_0, and a large observability, $o_{\max}$, a large value of $S_{\max}$ is favourable. However, if $S_{\max}$ gets larger than two, the axial dimensionless temperature, θ_a, gets large. Also, to get a large conservativity k_t, a small value of $S_{\max}$ is better.

In the experiment described here, the chosen detunings were $\Delta_a/(2\pi) = -45\,\mathrm{MHz}$, and $\Delta_c/(2\pi) = -5\,\mathrm{MHz}$, and the maximum pump strength was $\eta^2 = 10\kappa^2$. This corresponds to $S_{\max} = 3.6$, and $S_{\min} = -0.5$. The maximum saturation of the atom for this pump strength was calculated in a numerical simulation to be 0.23.

The value of $S_{\max}$ was found to be a good compromise to reach a good observability on the one hand, and an acceptable conservativity on the other hand. A further decrease in $S_{\max}$, which is equivalent to an increase in Δ_a, also leads to experimental problems not considered so far : First, the laser frequency gets closer to the $5S_{1/2}\,F = 3 \rightarrow 5P_{3/2}\,F = 3$ transition in ^{85}Rb, which leads to a loss of atoms into the $5S_{1/2}\,F = 2$ state because of non-perfect polarisation of the light field in the cavity, see the discussions in the sections 5.2.1 and 6.2.1. This problem can be mitigated to a certain degree, but not solved totally, by the repumping beam which illuminates the cavity from the side. The closer the frequency of the laser light is to the $5S_{1/2}\,F = 3 \rightarrow 5P_{3/2}\,F = 3$ transition, the worse the problem gets. Also, a smaller $S_{\max}$ requires a larger pump strength, see Eq (6.26). This in turn leads to a larger transmission of the cavity. Because of the dead time of the detectors, their quantum efficiency drops, leading to a lower relative transmission change and a lower observability than expected.

The negative value of $S_{\min} = -0.5$ seems to violate condition 3). However, for the maximum saturation of the order of 0.2, the equations used here have to be interpreted with caution: For large detunings, the saturation of the atom can be described in certain aspects as a decrease of the coupling constant g_{1j}, leading to a value of $S_{\min}$ which is larger than zero. An example for this can be seen in Fig. 6.6: For the pump intensity of $|\eta^2| = 0.01\,\kappa^2$, the transmission of the cavity drops if the coupling constant is increased beyond $0.92\,g_0$, which indicates that S gets negative. For larger pump intensities, this is no longer the case. This mimics the effect of a smaller coupling constant, and thus a larger $S_{\min}$.

6.2 Trapping an atom

Having discussed the motion of an atom in the cavity mode and the choice of parameters theoretically, it is now time to switch over to the experiment. In this section, an experiment where single atoms are trapped in the light field of a single-mode cavity (PFMR00) are discussed. The experimental method is described in section 6.2.1, and the results are presented in section 6.2.2.

6.2.1 Experimental method

In order to trap an atom in the high-finesse cavity, the kinetic energy of the atom should be less than the trap depth associated with the cavity light field. However, this is not enough: as transversal cooling is negligible, an atom gains as much kinetic energy by

rolling down into the potential valley as it looses while it rolls up on the other side. Therefore, the potential energy of an atom in the trap will always be larger than the trap depth: No trapping can be achieved by just creating a deep potential well.

The strategy to trap an atom in the conservative potential is as follows: From the cavity transmission, the atom-photon coupling strength $g(\mathbf{r}(t))$ can be measured, see Fig. 6.6. For a TEM-00-mode, this gives an upper limit for the distance of the atom from the cavity axis, see section 4.1. Now, slow atoms are sent through the cavity, and the cavity transmission is monitored as a function of time with a weak pump laser. Whenever the transmission rises above an appropriate threshold, a strongly coupled atom is in the cavity. At this moment, the pump intensity is increased, leading to a deeper potential well. For a large enough pump power, this potential well is deeper than the kinetic energy of the atom at the moment the potential is switched, and the atom is trapped.

The strategy of switching the pump laser intensity when an atom is detected in the cavity was implemented in the experiment in Konstanz, see also Fig. 6.3. Slow atoms were prepared in the cavity as explained in section 5.1. In the Konstanz setup, no extra stabilisation laser for the cavity existed. Instead, the cavity was stabilised on the probe laser via a Pound-Drever-Hall technique, see also section 5.3.2. For this, the laser had to be resonant to the cavity mode. As the measurement should be performed with a detuned probe laser, and because the atom changes the cavity resonance frequency, the stabilisation had to be switched off during the measurement. Thus, only the passive stability of the cavity was keeping the cavity resonance frequency from drifting, which limited the measuring interval to 5 ms. In this interval, the pump power was set to $\eta^2 = 1.5\,\kappa^2$, and the laser was detuned by $\Delta_a/(2\pi) = -45$ MHz from the $5^2\mathrm{S}_{1/2}$,F=3 $\leftrightarrow$ $5^2\mathrm{P}_{3/2}$,F=4 transition in ^{85}Rb. The laser-cavity detuning was $\Delta_c/(2\pi) = -5$ MHz. The threshold for the intensity switch was chosen such that only strongly coupled atoms activated the trigger. In the case of a trigger event, the pump intensity was switched to $\eta^2 = 12\,\kappa^2$ for 3 ms. After that time interval, the pump intensity was switched back to its former value, to check if the cavity had drifted during the measurement.

During the entire measurement, the atoms were also illuminated with repumping light resonant to the $5^2S_{1/2}\,F = 2 \leftrightarrow 5^2P_{3/2}\,F = 3$ transition from the side of the cavity. This is necessary for the following reason: Theoretically, the transition $5^2S_{1/2}\,F = 3\,m_F = 3 \leftrightarrow 5^2P_{3/2}\,F = 4\,m_F = 4$ is a closed transition, see Fig 5.1. The atoms are optically pumped to the $m_F = 3$ Zeeman substate of the $5^2S_{1/2}\,F = 3$ ground state before they enter the cavity. If the polarisation of the light field in the cavity was perfect, no other transition would be exited. However, the weak birefringence of the cavity mirrors produces a non-perfect polarisation. The misaligned part of the polarisation also drives the $m_F = 3 \leftrightarrow m_F = 3$ and $m_F = 3 \leftrightarrow m_F = 2$ transitions. These Zeeman components are also present in the $5^2S_{1/2}\,F = 3 \leftrightarrow 5^2P_{3/2}\,F = 3$ transition and are also driven by the laser. From the $5^2P_{3/2}\,F = 3$ state, the atom can decay to the $5^2S_{1/2}\,F = 2$ state, where it does not couple to the light in the cavity any more. To pump the atom from this dark state back into the cycling transition, the repumping light is needed.

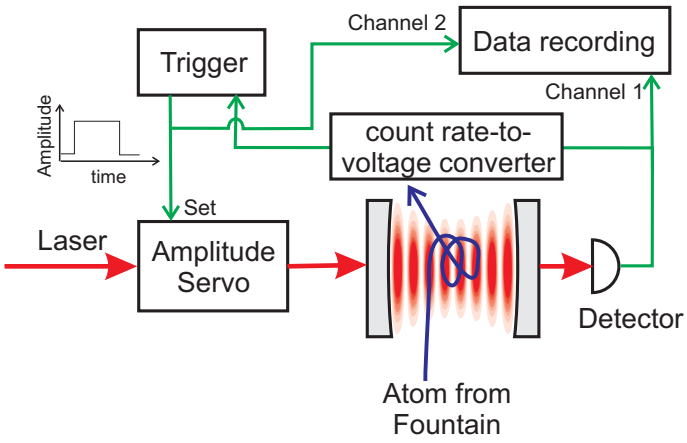

Figure 6.3: Schematic setup of the catch experiment. The clicks from the detector are converted into a voltage proportional to the detected intensity by the count rate-to-voltage converter. This signal is compared with a pre-set trigger level. Directly after the transmitted intensity has gone above the trigger level, the pump intensity is increased by a factor of eight. Both the trigger signal and the transmitted intensity are recorded for the whole measurement interval, but only traces where the trigger has reacted are saved.

6.2.2 Results

To perform the experiment, atoms were sent through the cavity as described above. Every time the trigger reacted, the trigger time and the transmission of the cavity was recorded. In Fig. 6.4, two measured trigger events are shown. In Fig. 6.4 b), the intensity was switched at the trigger time to catch the atom as explained above. As a comparison, in Fig. 6.4 a), only the trigger time was recorded, but the intensity was not changed. Whenever the transmitted intensity stays significantly above the transmission of the empty cavity, an atom is in the cavity. From this, the atom in b) leaves the cavity at $t = 1.7\,\mathrm{ms}$, and in a), it leaves at $t = 0.2\,\mathrm{ms}$. The average exit time of the atom can be determined by fitting an exponential decay to the averaged transmission, see Fig. 6.4 c) and d). This yields an average exit time of 0.31 ms for the switched intensity, and 0.08 ms if the intensity is not switched.

While the atom is in the cavity, the transmission does not stay constant, but rises and falls with a time constant of a few kHz. To investigate the origin of this, a quantum Monte-Carlo simulation of the experiment was performed, using the method of quantum trajectories described in section 3.8. In the simulation, the position of the atom is known, which facilitates the interpretation of the cavity transmission. An example of a simulated transmission is shown in Fig. 6.5. There, a similar structure can be seen in the calculated

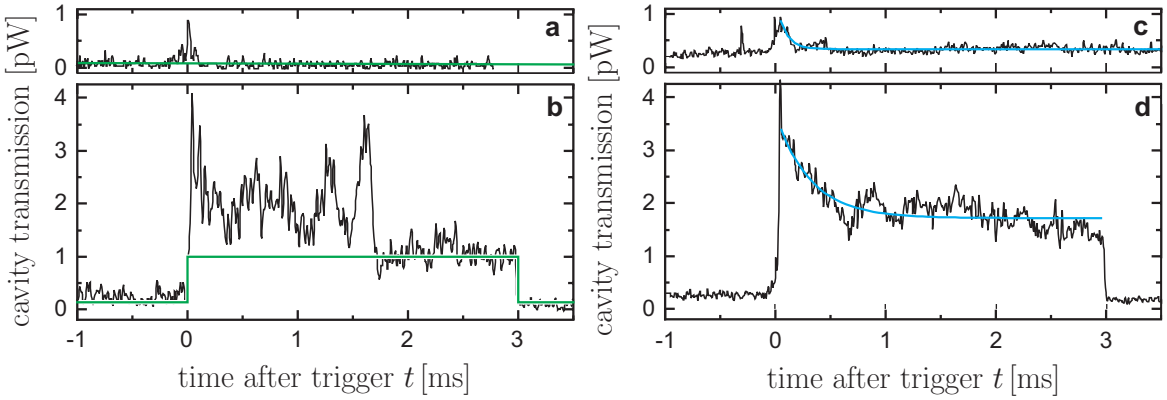

Figure 6.4: **a)** The transmitted intensity versus time for an atom traversing the cavity. The expected transmission of the empty cavity is indicated by the green line. At the trigger time, $t = 0$, the transmission is significantly higher than the expected empty cavity transmission. This is due to an atom traversing the mode. The transmitted intensity is back at the empty cavity transmission at $t = 0.2\,\mathrm{ms}$, indicating that the atom has left the cavity. The pump intensity was kept constant here, therefore the atom was not trapped. **b)** Same as in a), but with the pump intensity increased at the trigger time, $t = 0$, by a factor of eight. The measured transmitted intensity stays significantly above the expected transmitted intensity without an atom for 1.7 ms. This indicates that the atom stayed in the cavity for 1.7 ms. **c)** The transmission averaged over events as shown in a). The blue line is an exponential fit to the averaged transmission, the decay time is 0.08 ms. The decay time is a measure for the average exit time of the atom. **d)** Same as in c), but for traces where the intensity was switched as in b). The decay time of the exponential is 0.31 ms. Therefore, the atoms where the light intensity is switched stay 6 times longer in the cavity as the atoms where the intensity is not switched.

transmission. This is in most cases due to the transversal motion of the atom: Every time the atom's distance from the cavity axis is comparable to or larger than the mode waist, w_0, there is a drop in the transmission of the cavity. The experimental observation of this structure proves that there is a restoring force towards regions where the light intensity is large. Thus, the atom is trapped in the cavity light field.

In the numerical simulation, sometimes additional drops can be seen which can not be explained by the transversal motion of the atom, for example at t=0.3 ms in Fig. 6.5. The axial motion of the atom along the cavity axis, the z-axis of the coordinate system, is responsible for the drop. The z coordinate as a function of time is shown in Fig. 6.5 c). At most times, the atom stays in a single antinode of the standing wave. This is due to the

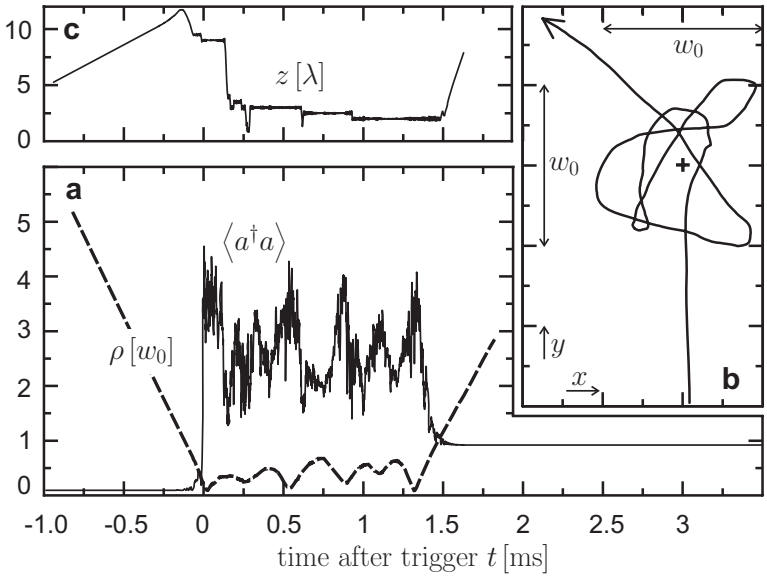

Figure 6.5: Simulation of an atom passing through the high-finesse cavity. The detunings are $\Delta_a/(2\pi) = -45\,\mathrm{MHz}$, and $\Delta_c/(2\pi) = -5\,\mathrm{MHz}$. The pump power is $\eta^2 = \kappa^2$ for $t < 0\,\mathrm{ms}$, and $\eta^2 = \kappa^2$ for $t > 0\,\mathrm{ms}$. In **a)**, the radial distance, ρ, and the cavity transmission in terms of the expectation value of the intra-cavity photon number, $\left\langle a^\dagger a \right\rangle$, is shown. An intra-cavity photon number of 1 corresponds to a transmission of 0.8 pW, see Eq. (3.20). The transmission signal closely resembles the experimental signal in Fig. 6.4. Part **b)** shows the trajectory in the plane perpendicular to the cavity axis. The atom oscillates a few times in the dipole potential; the random changes in direction are due to transversal momentum diffusion. In **c)**, the motion of the atom along the cavity axis is shown. Most of the time, the atom oscillates in a single antinode of the cavity light field, showing that the axial equilibrium temperature is less than the potential height.

balance between the velocity-dependent part of the force, which is cooling at the chosen parameters, and momentum diffusion. At some times, due to the random character of the heating, the axial kinetic energy of the atom is large enough that the atom can cross the potential hills of the standing wave. This is the case at t=0.3 ms: The atom runs over several nodes and antinodes of the field, until it is eventually cooled into another antinode of the field. As these events are rare, one can conclude that the structure which is visible in the frequency range of some kHz is mostly due to the transversal motion of the atom. The transversal motion is dominated by the conservative dipole force which keeps the atom trapped, and transversal momentum diffusion caused by spontaneous emission.

The numerical simulation can also be used to determine the mechanism which leads to the loss of the atom out of the trap. In nearly all simulated cases, the atoms are lost transversally, i.e. the distance from the cavity axis increases till the restoring forces vanish. This loss is due to transversal heating which is caused by photon recoils due to spontaneous emission. Another possible loss mechanism is that the atom hits one of the cavity mirrors. This mechanism is not significant in the experiment discussed here, as the mean distance the atoms travels along the cavity axis while being trapped is far less than the cavity length. For other cavity parameters and detunings, this is not necessarily true: In an experiment at Caltech (HLD$^+$00), hitting the mirrors is probably the main loss mechanism.

While the atom traverses several nodes and antinodes, it is expected that the light field in the cavity oscillates with a large amplitude, because the difference in expectation value of the photon number between node and antinode is large. While the atom is trapped in an antinode, the oscillation of the intra-cavity intensity has a far smaller amplitude. If this oscillation could be observed, one could distinguish between drops which are caused by running over the standing wave and drops which are caused by a transversal excursion of the atom. A direct observation of the oscillation is not possible, as the mean number of detected photons per oscillation period of the light field is on the order of only 3. But as the atom typically runs over several nodes and antinodes, it is possible to apply averaging methods, such as windowed autocorrelations (PFMR00) and windowed Fourier transforms (DLHK00). Although such methods work fine in principle, all methods yield signals which are not much larger than the shot noise in the particular experiment presented here. As the times where an atom runs over nodes of the standing wave are relatively rare, it is problematic to decide whether an observed oscillation of the light intensity is due to shot noise or to a true signal. Therefore, these methods will not be discussed here.

As a last remark on this issue, the discussion in (DLHK00), where it is argued that it is not possible to observe the z motion of the atom by windowed autocorrelations or windowed Fourier transforms, fails to address the important point. The authors argue that in their numerical simulation, the frequency of the oscillations of the light intensity changes only marginally between situations where the atom oscillates in one antinode and situations where the atom runs over several nodes and antinodes. However, also in their calculation, the amplitude of the oscillation changes between situations where the atom is trapped in a single antinode, and situation where the atom crosses several nodes and antinodes. As they do not compare the amplitude change to the shot noise, no information can be gained about this decisive point in that paper.

From Table 6.1, the axial equilibrium time is short as compared to the mean transit time of the atoms through the cavity mode. Thus, the atoms are close to thermal equilibrium in the axial direction shortly after they enter the cavity.

The long storage time of the trapped atoms is also an experimental proof for significant cooling of the atoms by the velocity-dependent force: The potential depth divided by the

average axial heating rate, $V_0 m_{Rb}/D_a$, is 65 μs for $\eta^2 = 10\,\kappa^2$. This means that without the axial cooling force, the atoms would have enough energy to cross the nodes of the standing wave on average after 65 μs. The velocity for atoms with an energy of V_0 is $v = \sqrt{2V_0/m_{Rb}} = 0.9\,\mathrm{m/s}$. Because the atoms are heated further when they can cross the nodes and antinodes and the cavity is only 122 μm long, the atoms would hit one of the mirrors on average in less than 122 μm/(0.9 m/s) = 135 μs. Because the "heating time" plus the time the atoms would need to reach the mirror, 65μs+135 μs=200 μs, is shorter than the average storage time of 0.3 ms, and the existence and the magnitude of the heating by momentum diffusion was confirmed in an independent experiment (MFM$^+$99), the heating must be cancelled by some other mechanism: the cavity-mediated cooling part of the light force first predicted in (HHG$^+$97).

6.3 Towards a longer storage time - Feedback

In the previous section, the real-time information about the atomic position was only used to switch to a deep trapping potential at the right time. However, information about the atomic position is also available during the time the atom is trapped. This information can be used to modify the light forces on the atom depending on the position or velocity of the atom in order to increase the average storage time of the atoms by feedback (FMP$^+$02). A similar feedback technique is also successfully used to cool beams in particle accelerators (vdM85).

6.3.1 Experimental method

In principle, the experimental method used for the feedback experiments is similar to the method described in section 6.2. The differences are the additional feedback circuit for the trapped atom, and some improvements in the measurement scheme which could be implemented because of the better cavity stabilisation scheme in Garching.

For the measurement, single slow atoms are prepared in the cavity as described in section 5.1. To keep the kinetic energy of the atoms as low as possible, the atoms were launched in the moving molasses with a mean velocity of 2.3 m/s. By observing the atoms with a flight time between 206 ms and 223 ms, only the slowest atoms were selected. This long observation interval was only possible because the new stabilisation laser allows active stabilisation of the cavity length during the measurement. Typical velocities just before the atoms enter the cavity can be calculated from the distance between MOT and cavity and the flight time, see Fig. 5.3: They are 0.26 m/s for the atoms with a flight time of 206 ms, and 0.09 m/s for a flight time of 223 ms.

The transmitted intensity of the stabilisation laser was 30 pW, corresponding to a maximum intra-cavity intensity of approximately 2 W/cm^2. At these intensities and a detuning from the nearest atomic resonance of 5 nm, the saturation of the atom by the

pump laser is approximately $3 \cdot 10^{-9}$, i.e. the influence of the stabilisation laser on the atoms can be neglected. The atoms in the cavity were also illuminated with repumping light through the gap between the mirrors as explained in section 6.2.

As in the experiment described in the previous section, a laser-atom detuning $\Delta_a/(2\pi)$ of -45 MHz and a laser-cavity detuning $\Delta_c/(2\pi)$ of -5 MHz was used. At these parameters, the transmission of the cavity rises if an atom enters the cavity, see Fig. 6.6. Also, a three-dimensional potential well exists for the atoms, Fig. 6.1, and the velocity-dependent force cools the axial motion of the atoms in the cavity. Some properties of the atom-cavity system for these parameters have been gathered in Table 6.1.

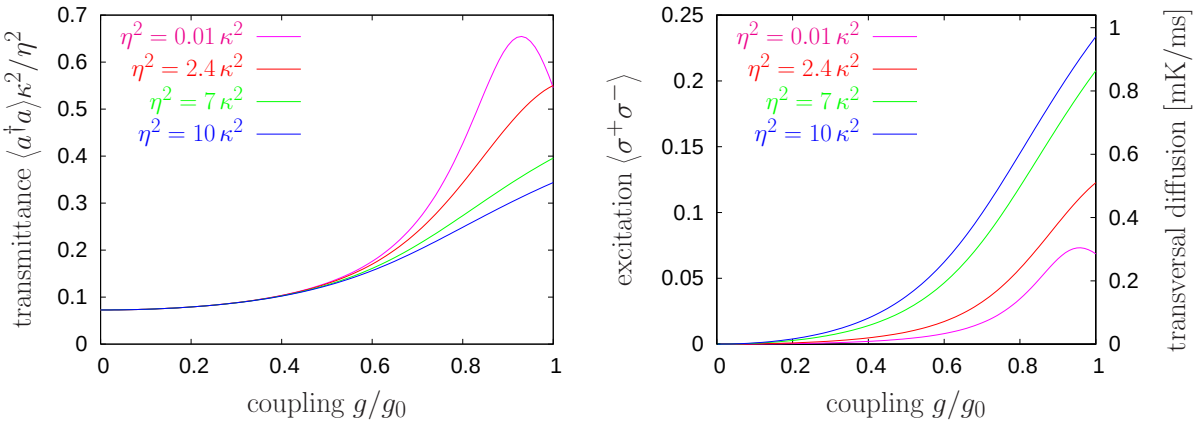

Figure 6.6: The transmittance of the atom-cavity system, the atomic excitation and the transversal momentum diffusion constant as a function of the atom-cavity coupling constant, calculated by a numerical solution of the master equation. The transmittance is normalised such that the resonant cavity without an atom inside has a transmittance of 1. The exitation and momentum diffusion constant for $\eta^2 = 0.01\,\kappa^2$ were multiplied by a factor of 100 to be visible. The detunings for both plots are $\Delta_a/(2\pi) = -45$ MHz and $\Delta_c/(2\pi) = -5$ MHz. Because of the small excitation, the agreement of the results for $\eta^2 = 0.01\,\kappa^2$ with the analytic formulas of chapter 3 is excellent.

To detect the presence of an atom in the cavity, the cavity was pumped with the 'observation power' of $\eta^2 = 2.4\,\kappa^2$, which corresponds to a transmission of the resonant cavity without an atom inside of 2 pW. This intensity was determined in an alignment measurement, which was performed before each series of measurements (A series of measurements consists typically of about 2000 launches from the MOT and lasts typically for 90 minutes). In this alignment measurement, the probe laser was scanned over the resonance of the cavity without sending any atoms into the cavity, and the transmission of the cavity was monitored. A Lorentzian was fitted to the transmission. The amplitude

of the Lorentzian gives the factor between transmission on resonance and incident pump power, which is measured by a photodiode, while its centre is used to calibrate the exact resonance frequency of the cavity.

To produce a trigger signal if an atom is strongly coupled to the cavity, the analogized signal of the two photon counters which monitor the cavity transmission is sent though a 16 kHz RC-lowpass, and then fed into the trigger input of a Delay-Gate generator. If the intensity rises above the threshold intensity of 0.8 pW, the trigger reacts. The threshold intensity is so large that the trigger never reacted if no atoms were sent through the cavity. It is also so large that only an atom which is very strongly coupled to the cavity has a chance to raise the trigger. Also, the flux of atoms was kept so low that the trigger reacted only about every 17th interval. Thus, the probability of finding two atoms simultaneously in the cavity is extremely low.

Every time the threshold is reached, the delay-gate generator produces two pulses on different outputs: The first pulse starts directly after the trigger event and lasts for 150 μs, the second pulse starts immediately after the first one and lasts for 2 ms. The time during the first pulse is called 'deceleration interval', the time during the second pulse is the 'storage interval'. During the deceleration interval, the pump power for the cavity is switched to the large deceleration power, $\eta^2 = 10\,\kappa^2$, equivalent to 8.2 pW transmitted through the resonant cavity without an atom inside. As in the previous section, this large intensity builds up a deep dipole potential, which decelerates the atom. For this intensity, the expectation value of the atomic excitation, $\langle\sigma^+\sigma^-\rangle$, is 0.23 for a maximally coupled atom. It is expected that through the dipole force, the mean velocity after the deceleration interval has decreased, whereas transversal momentum diffusion has increased the velocity spread.

During the storage interval, different strategies to trap the atom were used, which are described in the following, and are depicted in Figs. 6.9-6.11. The purpose of the different strategies is explained in section 6.3.2. For comparison purposes, experiments were performed where the pump power was not switched at all, i.e. the pump power was always equal to the observation power, even in the deceleration interval. This strategy is called 'no switch'.

The strategies differ in the way the pump power was chosen. However, in each strategy, the pump power was limited to the interval between the observation power, $\eta^2 = 2.4\,\kappa^2$ and the so-called trapping power, $\eta^2 = 7\,\kappa^2$. In this way, the pump intensity was always in a regime where the presence of an atom could be detected: It was never lower than the observation power, so that shot noise was not hiding the signal, and it was never higher than the trapping power, which is low enough to keep the saturation below 0.21, in order to not saturate the atom too much and to loose signal by bleaching the atom.

For the strategy 'hold low', the pump power in the storage interval was simply the observation power. For the strategy 'hold high', the pump power was the trapping power. The other strategies are the so-called 'ramp', where the intensity rises linearly in the first millisecond of the storage interval from the observation power to the storage power

and then stays constant, the 'proportional feedback', where the pump intensity was proportional to minus the transmittance of the atom-cavity-system plus an offset, and the 'differentiating feedback', where the pump intensity was proportional to minus the derivative of the transmittance plus an offset.

For the feedback measurements, i.e the measurements where the transmittance was influencing the pump power, the analog transmittance signal of the atom-cavity system was obtained in the following way, see also Fig. 6.7: The analogized cavity transmission was generated from the output pulses of the single-photon counting modules by a count rate-to-voltage converter, which had a update frequency of 250 kHz. The pump power was measured by a photodiode with a bandwidth of 600 kHz. Then, the output of the count rate-to-voltage converter was divided through the pump power using an analog divider to obtain the transmittance. This signal was smoothed by a 10 kHz RC-lowpass to reduce shot noise in the feedback circuit. The transmittance signal was then sent through the different feedback systems (an amplifier for the proportional feedback, and a differentiator with a bandwidth limit of 10 kHz for the differentiating feedbacks). Their output was constrained to the desired interval using a voltage clamp.

The small-signal transfer functions for the feedback schemes is depicted in Fig. 6.8. The roll-off at about 8 kHz from the lowpass in the transmittance, and the roll-off of the differentiator at high frequencies is clearly visible. As the gain of the feedback circuits was large, the voltage clamp was limiting the signal most of the time. For example, the amplitude of the small-signal transfer function for the proportional feedback was a factor of about 50 larger than the amplitude for the differentiating feedback. This had only a small effect on the output as the voltage clamp reduced the large gain to a comparator-like behaviour, see Fig. 6.11. This is also true for the differentiating feedback, only that the slopes of the pump power were not as steep as for the proportional feedback.

6.3.2 Evaluation and results

In this section, it is investigated how efficient feedback methods are in keeping an atom trapped in the cavity. To do this, it is necessary to compare the average exit time of the atoms which are subject to feedback to the average exit time of atoms trapped with other methods. Thus, a method has to be found to measure the exit time of an atom in the cavity.

The only experimentally accessible information about the position of the atom is the cavity transmission. However, if the pump power is not constant, the transmission of the cavity changes as a result of the changing pump power. To get a measure which eliminates the dependence on pump power at least for a cavity without an atom inside or with an atom inside which is not saturated, the transmission of the cavity is divided by the pump power, yielding the transmittance of the cavity. In this thesis, the transmittance is normalised such that a cavity without an atom inside which is resonant with the pump laser has a transmittance of one. Then, the transmittance can be calculated as $\left\langle a^\dagger a \right\rangle \kappa^2/\eta^2$.

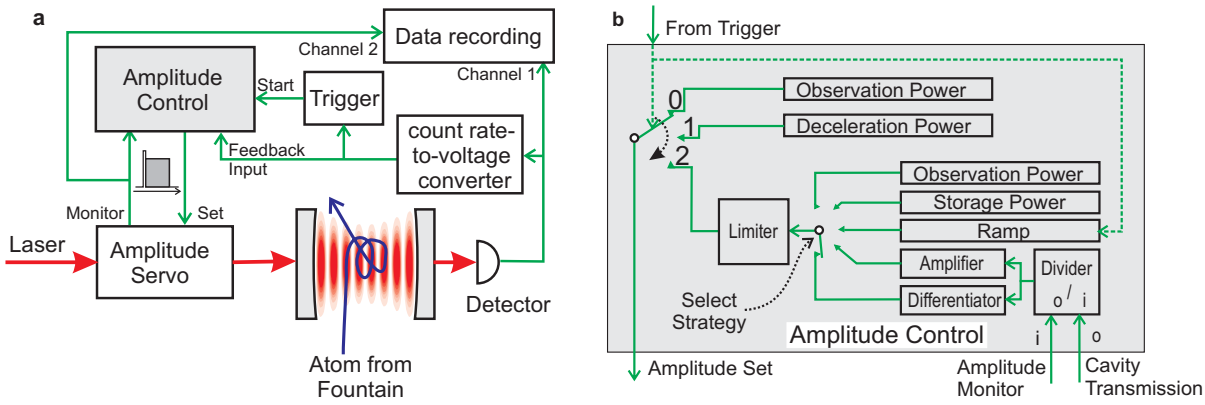

Figure 6.7: Schematic set-up for the experiments described in this section. An overview of the setup is given in a); the details of the amplitude control part of a) are shown in b). The lowpasses in the feedback part are not depicted. Also not shown is the setup for the strategy 'no switch', where the laser power is kept at observation power during the whole measurement, and the trigger time is recorded.

A plot of the transmittance as a function of the coupling constant of an atom is given in Fig. 6.6. For low saturation of the atom, the transmittance is independent of the pump power, see Eq. (3.38). For a larger pump power, the atom can be saturated, and the transmittance does depend on the pump power. However, if the transmittance lies above a properly chosen threshold, it is certain that an atom is in the cavity, independent of the pump power.

The next question is how the average exit time can be computed from the transmittance signals of the atoms. In the experiment described in section 6.2, a mean exit time was calculated by adding up the transmission signals which were synchronized to the trigger time. Then, an exponential decay was fitted to the average transmission. This is a relatively crude way to determine a exit time. In particular, the atoms which stay very long in in the cavity do not contribute much to the average exit time: At a time which is long as compared to the average exit time, most atoms have already left the cavity. Then, the noise of all transmission signals without atoms is much larger than the signal from the few events where there is an atom in the cavity.

To solve this problem, the exit time of each atom was determined individually. In order to prevent human bias, an algorithm to determine the exit time of an atom was devised, and implemented as a computer program. This algorithm is described in detail in appendix A. Basically, an atom is said to be in the cavity if the transmittance rises above a threshold for a significant time.

To investigate further when the atoms leave the cavity, the statistical distribution of

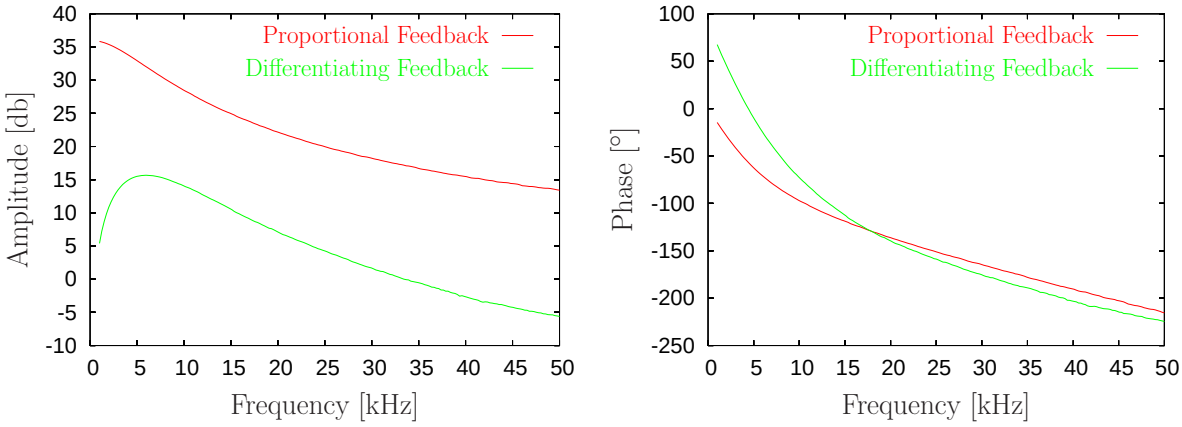

Figure 6.8: Small-signal transfer functions for the feedback experiments. A sinusoidal signal was fed into the feedback circuit instead of the output of the divider, and the voltage of the photodiode which measures the pump power was measured as response. Zero dB on the amplitude axis corresponds to an increase of the pump power η^2 of one κ^2 per transmittance increase of one. A phase of 0 degrees corresponds to a low pump power whenever the transmittance is low, and a phase of 90 degrees gives a maximal pump power for the negative slope of the transmittance. The amplitudes and offsets of the signals for measuring the transfer functions were chosen such that the voltage clamp was not active.

exit times was calculated, see Figs. 6.12 - 6.15. The exit time distributions were obtained as follows: The time axis was divided into intervals which are the same for every strategy. These intervals are indicated at the bottom of each plot, the middle of each interval gives the position on the time axis. For every trigger event, the time from the trigger to the exit time of the atom was determined, according to the exit time algorithm mentioned above. Then, all events for which the exit time was within a certain time interval were counted. This number was divided by the length of the interval and by the total number of trigger events for normalisation. This gives the relative abundance of leaving events, which is depicted as leaving probability. The bars in the vertical direction give the standard error assuming a Poissonian distribution for each interval on its own. In this case, the standard error is given by the square root of all leaving events in the interval divided by the same normalisation factor. As there are fewer atoms leaving at later times, the intervals are longer for late exit times to give a satisfactory signal-to-noise ratio.

For each strategy, two numbers have been calculated to quantify the average behaviour of the atoms, see Table 6.3.2: The first number is the average capture probability, which is defined as the number of atoms for which the time from the trigger to the atom's exit time is longer than 0.15 ms, divided by the number of all trigger events. The standard

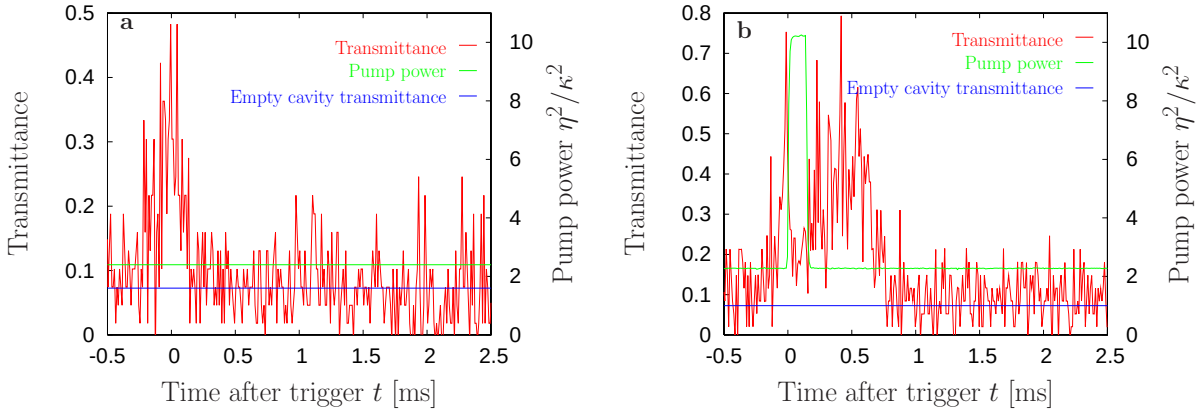

Figure 6.9: Examples of single atoms in the cavity for the strategies 'no switch' in part a) and 'hold low' in b). The time resolution for the transmittance is 10 μs. The large transmittance peak starting around $t = 0$ is caused by the atom in the cavity. The exit time for a) is $t = 0.13$ ms, and $t = 0.74$ ms for b). In b) it can be seen that the transmittance drops during the deceleration pulse because the atom is saturated. This behaviour is expected from Fig. 6.6. Also, the mean transmittance if no atom is in the cavity is very close to the expected transmittance, indicating that the stability of the cavity resonance frequency is very good.

statistical error of the average capture probability is calculated for each strategy, assuming Poissonian statistics.

The second number is the average storage time, defined as the time from trigger to the exit time of an atom averaged over all atoms where this time is longer than 0.15 ms. The constraint ensures that only the captured atoms are taken into account. The standard statistical error for the average storage time is also given in Table 6.3.2, and can be calculated by taking the standard deviation of the exit times distribution for exit times above 0.15 ms and divide this by the square root of the number of atoms which exit time was larger than 0.15 ms.

The systematical error for both numbers is believed to be smaller than the statistical error for the following reasons: Typically, every 100 trigger events, the strategy was changed in a random manner. This should eliminate long-term drifts. Also, an additional check can be made: As the pump power as a function of time before the storage interval is the same for each strategy except 'no switch', it is expected that the average capture probability is the same for these strategies. The measured capture probabilities, shown in Table 6.3.2, fulfil this condition within their statistical error.

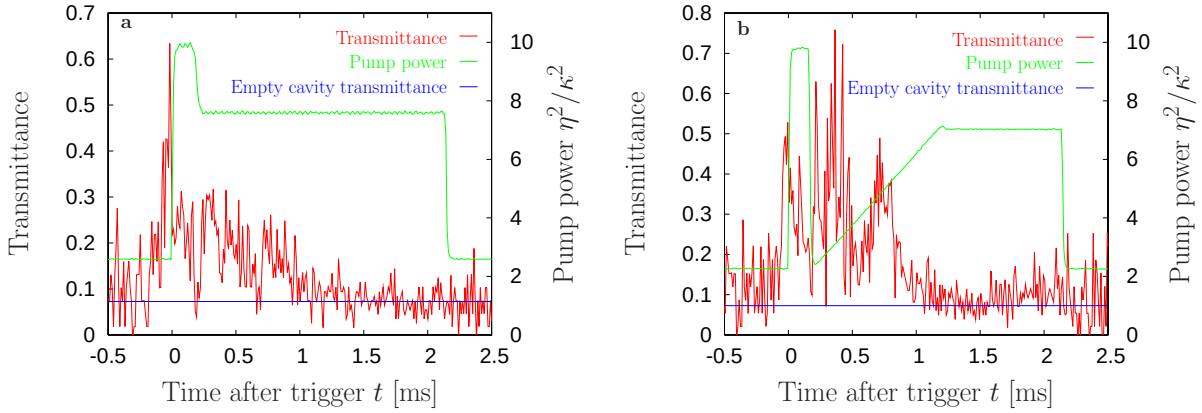

Figure 6.10: Trapped atoms in the cavity for the strategies 'hold high' in part a) and 'ramp' in part b). The exit times are 0.96 ms for a) and 0.84 ms for b).

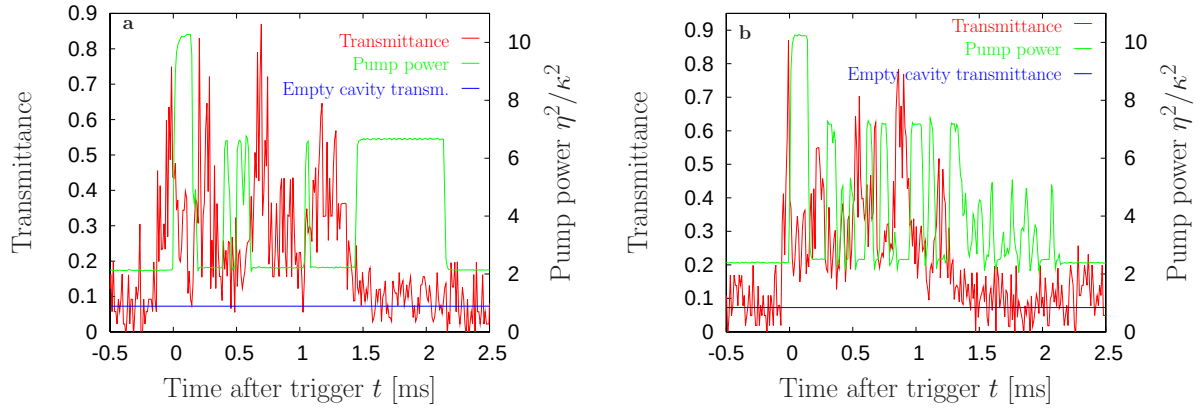

Figure 6.11: Examples for trapped atoms in the cavity for the strategies 'proportional feedback' in a) and 'differentiating feedback' in b). The exit times are 1.38 ms for a) and 1.26 ms for b).

Deceleration efficiency

First of all, it is interesting to know how efficiently the atoms are slowed down in the deceleration interval. The deceleration interval starts directly after a strongly coupled atom is detected in the cavity. At its beginning, the pump intensity is increased from the observation power, $\eta^2 = 2.4\,\kappa^2$, to the deceleration power, $\eta = 10\,\kappa^2$. This increases the potential depth by a factor of 2.5, see Table 6.1 and Fig. 6.1. The stronger light forces decelerate the atom while it is leaving the cavity. If the potential is deep enough, the atom turns around and moves again to the centre of the cavity: it is trapped. During

Strategy	Sum of trigger events	Average capture probability	average storage time [ms]
'No Switch'	1098	0.217 ± 0.012	$0.15 + 0.259 \pm 0.019$
'Hold low'	871	0.339 ± 0.016	$0.15 + 0.298 \pm 0.018$
'Hold high'	1113	0.371 ± 0.015	$0.15 + 0.328 \pm 0.016$
'Ramp'	724	0.327 ± 0.017	$0.15 + 0.364 \pm 0.033$
'Proportional Feedback'	590	0.368 ± 0.020	$0.15 + 0.395 \pm 0.023$
'Differentiating Feedback'	2246	0.340 ± 0.010	$0.15 + 0.401 \pm 0.015$

Table 6.2: The average capture probabilities and the average storage times of the different storage strategies.

the deceleration interval, the atom is heated by momentum diffusion. This heating can prevent trapping of the atom. Also, if the trigger does not fire at the optimal time, the atom may escape trapping.

After the atom has turned around, it is slow enough to be trapped also in a weaker trap. Therefore, the light power may be decreased after a certain time. In the optimal case, this would be after a quarter of an oscillation of the atom in the trap. Then, the deceleration interval is over, and the storage interval begins.

To check the efficiency of the deceleration pulse, the pump power was switched back to the observation power during the storage interval (strategy 'hold low'), and compared to an experiment where the pump power was not switched during the deceleration interval and the storage interval (strategy 'no switch'). Some single trigger events are shown in Fig. 6.11.

To visualize the average behaviour of the atoms, the distribution of exit times is shown in Fig. 6.12. After a peak at an exit time of about 0.1 ms, the number of atoms which are leaving drops for larger exit times. However, for the strategy 'hold low', more atoms leave at larger exit times than for 'no switch'. This means that some atoms are kept from leaving the cavity by the deceleration pulse.

The efficiency of the deceleration pulse can be quantified by the average capture probability. For the strategy 'no switch'. the average capture probability is 0.217 ± 0.012, and for 'hold low', it is 0.339 ± 0.016. Thus, the number of captured atoms is significantly increased by the deceleration pulse.

The relatively large number of atoms which are captured even without switching the light intensity is due to momentum diffusion: By chance, some atoms get decelerated by the random kicks due to photon recoils, and are subsequently trapped in the cavity light field. It was checked in a numerical simulation that the increase in the number of catched atoms by a factor of 1.5 for the strategy 'hold low' can not be explained by the effects of

momentum diffusion; it is due to the conservative part of the light force.

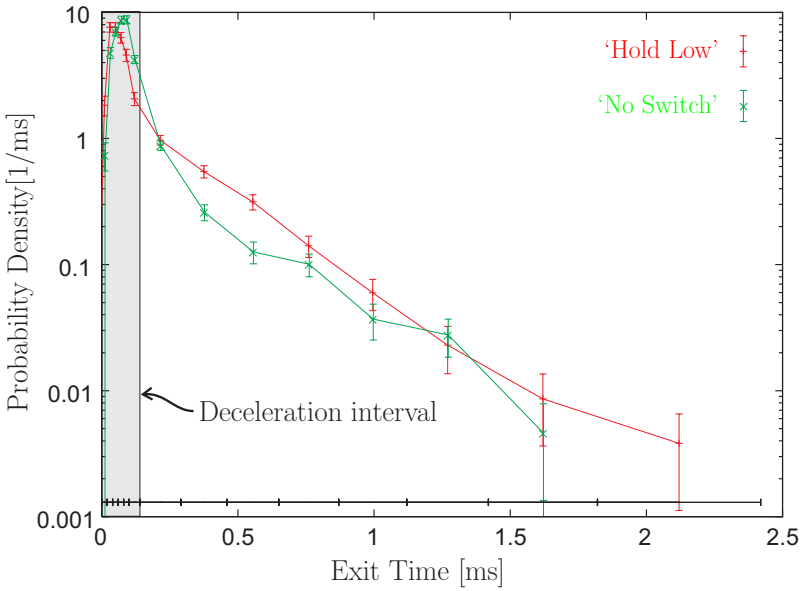

Figure 6.12: The distribution of exit times, i.e. the probability for an atom to leave the cavity in a certain time interval drawn against the exit time, for the strategies 'no switch' and 'hold low'. The intervals over which the probability was averaged are drawn above the time axis. The bars in y direction give the standard error of the probability assuming a Poissonian distribution for each time interval. For the strategy 'no switch', less atoms leave the cavity after $t = 0.2\,\mathrm{ms}$ than for the strategy 'hold low'. This indicates that the deceleration pulse present in strategy 'hold low' successfully slows down the atoms.

With this preparation, about a third of the atoms which have produced a trigger can be used to compare the different strategies to store an atom in the cavity.

'Hold low' and 'hold high'

To discuss the interplay between the dipole force, which tends to keep the atoms in the cavity, and momentum diffusion, which boils them out, the strategies 'hold low' and 'hold high' are compared. Some single events are shown in Figs. 6.9 b) and 6.10 a).

In the distribution of exit times, Fig. 6.13, the probability distributions for the two strategies differ only slightly. This is reproduced by the average storage times, which differ by less than two standard errors. For 'hold low', the mean storage time is $0.15 + 0.298 \pm 0.018\,\mathrm{ms}$, and for 'hold high', the mean exit time is $0.15 + 0.328 \pm 0.016\,\mathrm{ms}$, see Table 6.3.2.

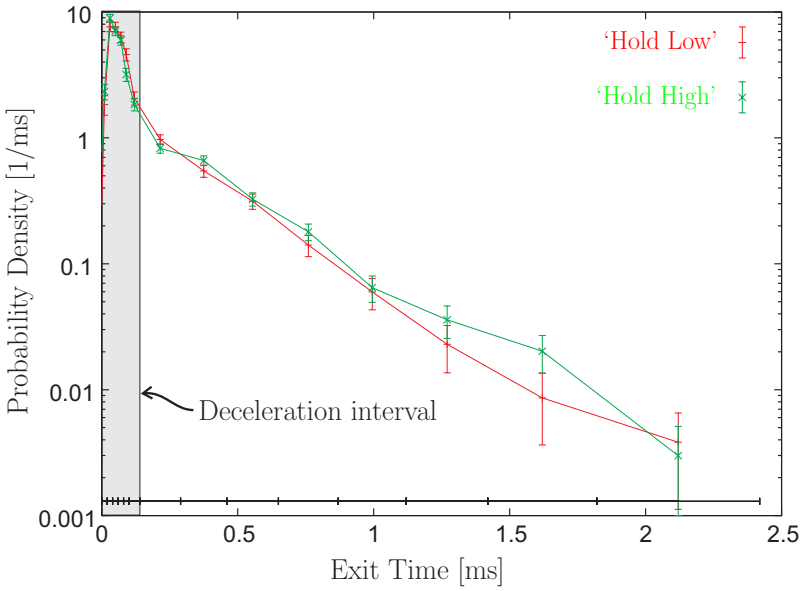

Figure 6.13: The distribution of exit times for the strategies 'hold high' and 'hold low'. The distribution of exit times is nearly the same in the two cases. The reason for this is discussed in the text.

At first thought, it is surprising that the exit time is nearly the same for both strategies, as the higher potential walls during the storage interval for 'hold high' should make it more difficult for the atoms to leave the cavity. However, for 'hold high', transversal momentum diffusion is also larger in the storage interval because of the higher light intensity. Thus the atoms gain more energy per time interval, and can climb the higher potential wells nearly as fast as the atoms which are subject to the strategy 'hold low'.

In order to leave the cavity, the atom needs an energy which is equal to or larger than the trap depth. The energy of the atom consists of the kinetic energy and the potential energy in the light field at the beginning of the storage interval, and the energy which is gained through momentum diffusion. The average kinetic energy at the beginning of the storage interval is the same for both methods, as it only depends on the atomic fountain and the pump power before the storage interval. The potential energy of the atom at the beginning of the storage interval depends on the depth of the potential during the storage interval, and the position of the atom at the beginning of the storage interval. For 'hold high', the walls of the potential well are higher, leading to a larger potential energy of the atom, if the bottom of the trap is taken as zero for the potential energy. The position distribution of the atoms directly after the deceleration pulse is the same for both strategies. The energy gain by momentum diffusion per time interval is also larger for the strategy 'hold high'.

For the loss of the atoms out of the trap, the ratios between the discussed energies and the trap depth are important: The kinetic energy is the same for both strategies, thus the kinetic energy divided by the trap depth is larger for 'hold low' than for 'hold high'. The potential energy at the beginning of the storage interval, divided by the trap depth, is approximately the same for both strategies. The heating rate by transversal momentum diffusion divided by the trap depth is also slightly smaller for the strategy 'hold high', see Table 6.1. Thus, both the kinetic energy and transversal momentum diffusion can lead to a slightly longer storage time for the strategy 'hold high' as compared to 'hold low'.

'Ramp'

From the results for the previous strategies, it can be seen that the storage time can be increased if the dipole potential is large and transversal momentum diffusion is small. However, an increase in potential is typically accompanied by an increase of momentum diffusion. For example, both grow linearly with the pump power for low saturation and constant detunings. One method to diminish the effects of momentum diffusion relies on the fact that the depth of the potential well is only important at the moment when the atom tries to leave the cavity, whereas the effects of momentum diffusion are proportional to its integral over time. In order to increase the ratio between momentary potential height and the integral over momentum diffusion, the strategy 'ramp' was implemented. There, the pump power starts at observation power after the deceleration pulse, increases linearly with time in one millisecond, and then stays constant, see also Fig. 6.10. The strategy 'ramp' has the additional advantage that the potential is low at the beginning of the storage interval where the atoms are suspected to be rather at the edge of the mode, because they are near their turning point. A low pump power at this point leads to a low potential energy of the atoms in the beginning.

The mean exit time for this strategy is $0.15 + 0.364 \pm 0.033\,\mathrm{ms}$, which is one standard error above the exit time for trapping power during the storage interval.

Feedback

In the strategies discussed up to now, the real-time information about the position of the atom while it is trapped in the cavity light field was only used to determine the exit time of the atom. In the experiments described in this section, a feedback loop was implemented which was active in the storage interval: The position information gained by the observation of the cavity transmission influenced the pump power and thus the light force on the atom.

In one feedback strategy, called 'proportional feedback', the pump power was high whenever the transmittance of the cavity was low, i.e. when the atom was at the edge of the cavity mode. With this strategy, the dipole force towards the cavity axis was increased whenever the atom was near the edge of the mode and thus was in danger to

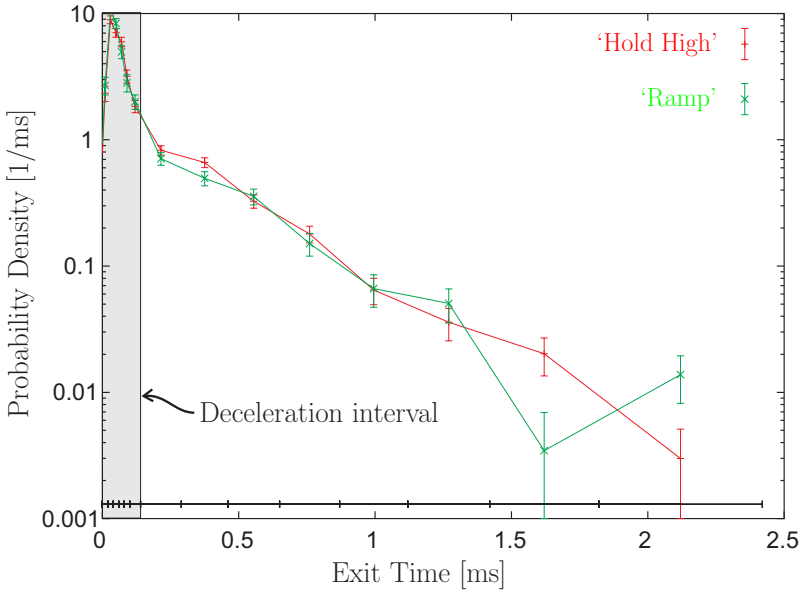

Figure 6.14: Comparison of the distribution of exit times for the strategies 'ramp' and 'hold high'. The slight difference between the distributions amounts to a mean storage time which is one standard error larger for the strategy 'ramp', see Table 6.3.2. The unregularities for exit times larger than 1.5 ms are probably due to statistical fluctuations.

leave the cavity, whereas the pump power was low when the atom was in the middle of the cavity to decrease momentum diffusion. The exit time for this method was measured to be $0.15 + 0.395 \pm 0.023$ ms, which is 2.9 standard errors above the exit time for the strategy 'hold high'. This increase in exit time was possible even for a potential which was on average lower than the one for trapping power during the storage interval. Note that for ideal proportional feedback, the atom is neither heated nor cooled on average by the dipole part of the light force. As the feedback loop used here is severely bandwidth-limited, this is not the case in the experiment: Consider the example of an atom which moves to the edge of the mode and then turns round and moves to the cavity axis again. For an ideal proportional feedback, the pump power and thus the force on the atom does not depend on whether the atom is moving outward or inward. Therefore, the atom does not loose or gain energy via the dipole force. If the feedback has a finite reaction time, the pump power increases 'too late' on the atom's way outward, and decreases 'too late' on its way in again. This leads to a weaker dipole force if the atom moves outward, and a stronger force on its way in again. As the dipole force points towards the cavity axis, the force difference between the delayed feedback and the ideal, conservative case always points into the direction of the velocity of the atom. In other words, the integral $\int \mathbf{F} \cdot \mathrm{d}\mathbf{s}$

is positive, which leads to an increase in the energy of the atom, i.e. to heating. Still, the larger storage time as compared to the 'hold high' strategy shows that the effects of avoiding momentum diffusion are larger than the heating by delayed feedback.

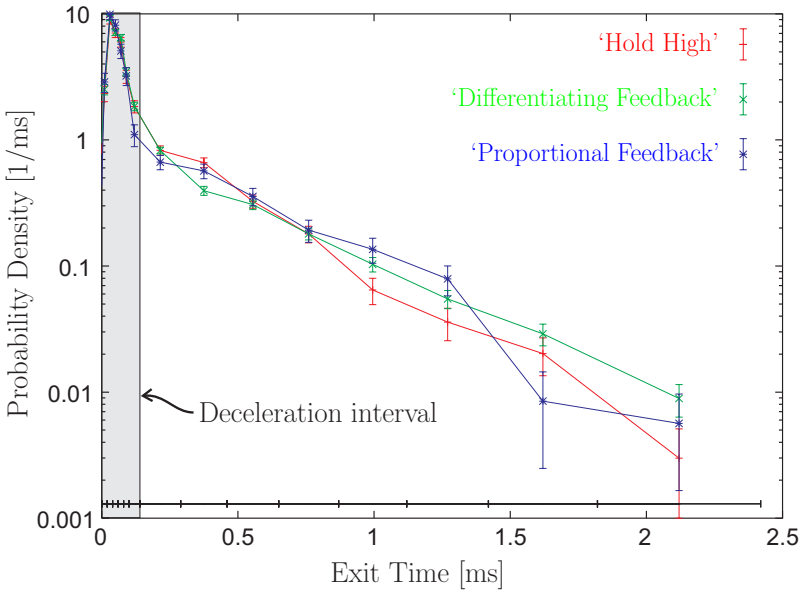

Figure 6.15: The exit time distributions for the strategies 'hold high', 'proportional feedback' and 'differentiating feedback'. Comparing the two feedback distributions to the one for 'hold high', it is clearly visible that the atoms are kept longer in the cavity by the two feedback strategies than by the strategy 'hold high'.

The other feedback strategy, 'differentiating feedback', was designed to cool the transversal motion. For this purpose, the pump power and thus the restoring force was increased whenever the cavity transmittance was decreasing, i.e. when the atom was moving away from the cavity axis. When the transmittance was increasing, i.e. when the atom was moving inwards, the pump power was made low. The aim was to make the integral $\int \mathbf{F} \cdot \mathrm{d}\mathbf{s}$ negative, thus cooling the atom.

The average storage time for this strategy is $0.15 + 0.401 \pm 0.015\,\mathrm{ms}$. This is not significantly larger than the average storage time for proportional feedback. However, due to better statistics, this result is 4.5 standard errors above the result for constant storage power during the storage interval.

The small difference in average exit times for the differentiating and the proportional feedback is an indication that the cooling expected for the differentiating feedback is no dominant effect. This does not mean that there is no cooling at all, but only that the effect is not large enough to be observed with the current method. There are several reasons for this: The first is the diffusive motion of the trapped atom, i.e. the atom gets

kicks in random directions which increase its kinetic energy. The atom moves back and forth in the potential well only a few times before it escapes, i.e. the average energy gain per 'hit of the wall' is large. Because of the randomness of diffusion, the atoms even can gain enough energy to leave the potential well in one hit of the wall, and leave the cavity instantly. The larger the energy gain per hit of the wall is, the more probable are such events. In these cases, the atom would leave the cavity even for a 'perfect feedback', in the sense that the determination of the position of the atom works perfectly: The feedback mechanism would raise the potential well to its maximum height if the atom moves outward. If the atom manages to gain enough energy to cross the wall on its way out, it escapes from the trap.

A second reason for non-observation of the cooling effect is that for the most measured atomic transits, including the one shown in Fig 6.11, many changes in the transmittance happen fast on the timescale where the feedback reacts: If there is a drop in the transmittance, as e.g. at $t = 0.3\,\mathrm{ms}$ or $t = 0.9\,\mathrm{ms}$ in Fig 6.11 a), there is a substantial increase in the pump power approximately $10\,\mu\mathrm{s}$ afterwards. At that time, the decrease of the transmittance has stopped, it is relatively constant at a small value. Thus, the effect is nearly the same as for proportional feedback, where the pump power is also increased whenever the transmittance is low.

The obvious solution for this problem seems to be to increase the bandwidth of the transmittance circuit, ν_f. However, increasing ν_f yields an increase of the shot noise in the derivative of the transmittance which is proportional to $\nu_f^{3/2}$, because the amplitude of the shot noise in the transmittance itself rises proportional to $\nu_f^{1/2}$, and the timescale in which the transmittance changes is proportional to $1/\nu_f$. Thus, a larger bandwidth would lead to a dramatic increase in noise in the feedback circuit, which would not be tolerable.

A third reason for non-observable cooling is the symmetry of the TEM-00 mode: Consider the motion of the atom in a cylindrical coordinate system with coordinates ρ, ϕ and z, where the z-axis is the cavity axis. For the TEM-00 mode which was used for trapping, the coupling is independent of ϕ. Because the dipole force and the velocity-dependent force point in the direction of $\boldsymbol{\nabla} g$, the angular momentum associated with the ϕ motion is not affected by those forces. Therefore, this degree of freedom can not be cooled by feedback. Instead, the average angular momentum squared increases with time, as the momentum diffusion due to spontaneous emission also acts in the ϕ direction. Then, the centrifugal forces will eventually lead to a loss of the atom, no matter how well the feedback works.

To solve this problem, higher-order cavity modes could be used to break the axial symmetry, for example the TEM-10 or TEM-01 modes. If only one of these modes is pumped, the potential is not axially symmetric any more, and the ϕ-motion can also be cooled. If the TEM-01 and TEM-10 modes are near-degenerate, one could even change the pump geometry depending on the position of the atom to increase the cooling of

the ϕ-motion. The reason why these modes were not used in the experiment discussed here is that the transmission signals from atomic transits through these modes are more difficult to interpret, because there exists more than one intensity maximum in the plane perpendicular to the cavity axis, and there is more than one cavity mode near-resonant to the atomic transition.

Despite all of these intrinsic problems and experimental difficulties, a significant increase in exit time was observed when a feedback mechanism was used. It also needs to be stressed that large improvements can be made by designing a cavity more suitable for feedback experiments. The choice of cavity parameters for improved feedback is discussed in the next section.

6.4 Perspectives

In this section, it will be investigated how the present limitations in storage time for feedback can be overcome. From the discussions above, the limiting factor for feedback is transversal momentum diffusion. To investigate how transversal momentum diffusion can be decreased, i.e. how the transversal motion of the atom can be made more conservative, the analytical formulas for the limit of large laser-atom detuning will be used, adopted for the situation where only a single atom stays in the cavity. They are only valid if the saturation of the atoms is small, which is not the case for the current parameters. However, it can be expected that the analytical formulas show the right directions.

The constraints on the parameters were already investigated in section 6.1.3. Equations (6.29)-(6.32) will now be used to discuss the optimum cavity design parameters. For the TEM-00 mode of a Fabry-Perot type cavity, the accessible design parametes are

- The length of the cavity, l,
- The waist of the cavity mode, w_0,
- The mirror reflectance, $\mathcal{R}$.

They influence the maximum coupling strength of a single atom, g_0, and the field decay time of the cavity, κ. From Eqs. (5.6) and (5.7),

$$\kappa \propto \frac{1-\mathcal{R}}{l}, \tag{6.34}$$

$$g_0 \propto \frac{1}{w_0\sqrt{l}}. \tag{6.35}$$

To determine the detunings and the pump power, it is assumed that the system is on a normal mode peak if the atom is maximally coupled, i.e. $S_{\min} = 0$. The distance from a normal mode peak for no atom in the cavity, $S_{\max}$, is kept constant for different cavity designs, and also the maximum saturation of the atom, $\left\langle \sigma_j^+ \sigma_j^- \right\rangle_{\max}$, is kept constant. For

a discussion of these choices, see section 6.1.3. Also, it is assumed that the averages where $|g_{1j}|^2/g_0^2$ appear remain constant, as $|g_{1j}|^2/g_0^2$ equals the mode function squared at the position of the atom, and it is assumed that the atom moves through the same parts of the wave function.

Under these circumstances, the relative change in the transmission between an maximally coupled atom in the cavity and a cavity without an atom, $v_{\max}$, the potential depth, V_0, the maximum observability, $o_{\max}$, the transversal conservativity, k_t, and the dimensionless axial temperature, θ_a, given in the Eqs. (6.29)-(6.32) have the following dependence on l, w_0, and $\mathcal{R}$:

$$v_{\max} = const. \tag{6.36}$$

$$V_0 \propto \frac{1}{w_0^2\,(1-\mathcal{R})} \tag{6.37}$$

$$o_{\max} \propto \frac{1}{(1-\mathcal{R})^{1/4}} \tag{6.38}$$

$$k_t \propto \frac{1}{w_0^4\,(1-\mathcal{R})^{3/2}} \tag{6.39}$$

$$\theta_a \propto \frac{(1-\mathcal{R})^3\,w_0^4}{l} \tag{6.40}$$

It can be seen that to achieve good conditions to trap an atom in the cavity, a small cavity waist and a large reflectance are very important. The cavity length has no effect on the most parameters, except on the dimensionless axial temperature for which a long cavity is better.

Of further experimental interest is the transversal trap frequency, ν_t, and the maximum transmission, $P_{\text{trans,max}}$. From Eqs (6.3), (6.30), (3.20), (3.104), and (6.26)

$$\nu_t \propto \frac{1}{w_0^2\sqrt{1-\mathcal{R}}} \tag{6.41}$$

$$P_{\text{trans,max}} \propto \frac{\mathcal{T}}{w_0^2\,(1-\mathcal{R})^2} \tag{6.42}$$

Thus, for a cavity with a smaller waist, both the radial trap frequency and the transmitted intensity increases if $S_{\min} = 0$ and both $S_{\max}$ and $\left\langle \sigma_j^+ \sigma_j^- \right\rangle_{\max}$ are kept constant. This poses some experimental challenges: First, to implement feedback, the control electronics has to be fast enough to react on the radial motion of the atom, which gets more difficult as the radial trap frequency increases. Then, for higher transmitted power, the quantum efficiency of the SPCM-Modules, which are used to detect the transmitted intensity, decreases because of their dead time. However, both problems seem to be manageable, and do not balance the tremendous increase in radial conservativity which can be gained by a smaller waist.

Another experimental problem mentioned in section 6.1.3, the additional hyperfine transitions in ^{85}Rb at $\Delta_a/(2\pi) = -121\,\mathrm{MHz}$ and $\Delta_a/(2\pi) = -184\,\mathrm{MHz}$, can be overcome by choosing w_0 small enough. From Eqs. (6.23), (6.34) and (6.35), the scaling of Δ_a is

$$\Delta_a \propto -\frac{1}{S_{\max} w_0^2 \sqrt{1-\mathcal{R}}}, \tag{6.43}$$

where the dependence on $S_{\max}$ was also kept. If a cavity was built using mirrors with a radius of curvature of 1.3 cm and the same mirror reflectance and transmittance as now, the TEM-00 mode would have a waist of $w_0 = 15\,\mu\mathrm{m}$ for the same cavity length as now. For a $S_{\max}$ of 2, Δ_a could be increased by a factor of over six, leading to a $\Delta_a/(2\pi)$ of -320 MHz, which is far beyond the frequencies of the other hyperfine transitions. By using the formulas in section 6.1.3 to include the dependence on $S_{\max}$, the transversal trap frequency would be a factor 4 larger than it is now, which should be easily manageable. The cavity transmission would be a factor 7 larger, which would decrease the detection efficiency due to the deadtime of the single photon counters by a factor on the order of 0.7. Also, the observability would drop slightly by a factor of 0.6. Both factors are moderate and should not be a large problem. The potential depth would increase by a factor on the order of 4, the transversal conservativity by a factor on the order of 25, and the dimensionless axial equilibrium temperature would be a factor on the order of 70 lower. With such cavity parameters, a tremendous increase in trapping time by feedback should be possible.

Chapter 7

Conclusion and outlook

In this thesis, the interaction between slow atoms and a cavity light field was investigated. Special emphasis was laid on observing and controlling the motion of a single atom in the cavity. It was shown that the transmission properties of the cavity can be understood intuitively if the cavity light field is considered as a classical light field. To calculate the light force acting on the atom, a quantum description of the light field is needed. For this, a theory was developed which can describe the interaction of several atoms in the cavity with several quantized modes of the light field. Within the framework of this model, a novel method for measuring the position of a single atom in the cavity was proposed, which uses several degenerate cavity modes.

In the experiment described in this thesis, single atoms were trapped in the cavity light field. The motion of the atoms was observed in real-time by measuring the cavity transmission. The average storage time of the trapped atoms was a factor of four larger as compared to atoms not influenced by the light force. The theoretical analysis of the light force revealed a complicated motion of the atoms in the cavity. The main reason for the loss of atoms out of the trap was identified to be due to heating by random photon recoils.

In a second experiment, feedback strategies were applied to control the motion of the trapped atoms. Feedback uses the real-time information gained about the atomic position to change the light force acting on the atoms. By diminishing photon recoils, the average storage time of the atoms was increased significantly by feedback. It was shown that with a changed cavity geometry, even cooling by feedback should be possible. This technique should increase the storage time of atoms in the cavity dramatically, thus making experiments feasible which depend on a long storage time of an atom in the cavity, such as the production of single photons on demand (KHBR99; HLKR00).

As further perspectives, it may be possible to improve feedback cooling such that the quantum nature of atomic motion becomes important (VK97; DPTW98), and to cool the atom to its vibrational ground state. In these cases, the feedback would be an example of a quantum feedback circuit, like it is discussed in (MVT00). Also, several atoms might

be trapped in a cavity to investigate long-range light forces between strongly coupled atoms (MFM$^+$00) further. It might also be possible to build a cavity where some higher-order transversal modes are degenerate to demonstrate a two-dimensional measurement of the atomic position as proposed in section 4 experimentally, or to develop this method as a new method of microscopy for phase objects in biology like cells or parts of a cell.

Appendix A

Algorithm to determine the exit time of an atom

In section 6.3, the exit times of the individual atoms traversing the cavity was used to determine the mean storage time of the atoms. The algorithm used there to determine the exit time of an atom is described here in detail. The following steps are taken:

1. The intensity transmitted through the cavity versus time is calculated by dividing the time axis into 10 μs intervals. For each of those intervals, the number of detected photons is counted. This number is corrected for the detector dead time. Then, adjacent averaging of three neighboring bins is performed, giving a time resolution of 33 kHz. The same procedure is done for the pump power. Finally, the transmitted intensity is divided through the pump power, to give the transmittance of the cavity. For an empty cavity, the mean value of the transmittance is independent of the pump power, but depends on the detuning from the cavity resonance. The transmittance is scaled such that the empty cavity on resonance has transmittance of one. For a detuned cavity, the response is smaller. For an atom inside the cavity at a fixed position, the response depends on the pump power in the following way: For very low pump powers, equation (3.38) for the expectation value of photons inside the cavity is valid, and the response is independent of the pump power. For higher intensities, the saturation of the atom increases, and the response drops. Fig. 6.6 shows the transmittance as a function of intensity and coupling strength of an atom.

2. The transmittance of the empty cavity is calculated by drawing a histogram of transmittances for the whole 20 ms-long observation interval, only the time intervals when the pump intensity was not equal to the observation were discarded for this procedure. The mean value of this probability distribution gives the transmittance of the empty cavity, plus a contribution from the times when there was an atom in the cavity. As the probability of finding an atom in the cavity is small, the mean value is in good approximation the transmittance of the empty cavity.

3. For each trigger event, a time interval is considered which starts 0.7 ms before the trigger and ends 3 ms after the rising of the trigger. The transmittance for such a time interval is depicted in Fig. A.1.

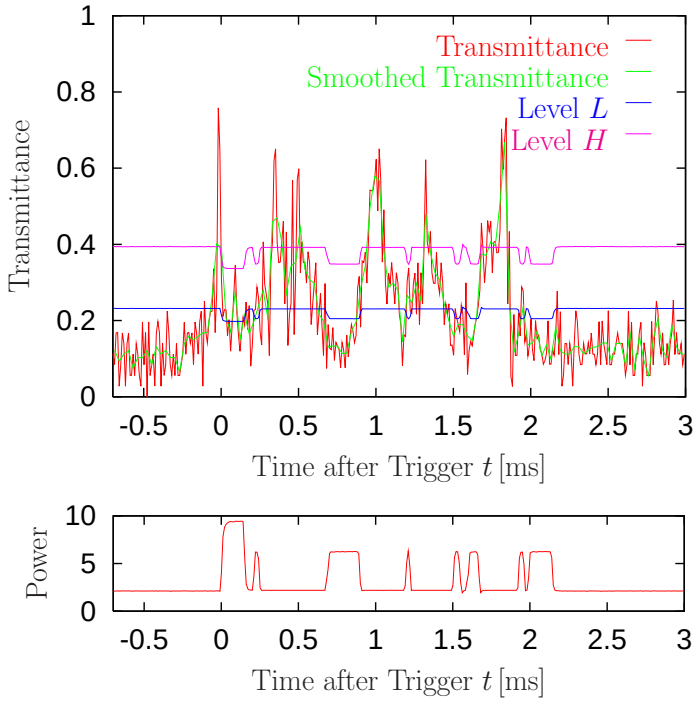

Figure A.1: An experimental signal of a single atom trapped in the cavity. The red line gives the transmittance of the cavity with a time resution of 10 μs, the green line has a time resolution of 30 μs. At $t = 0.7$ ms and $t = 1.4$ ms, the smoothed transmittance drops below level L for longer than 0.1 ms. As the smoothed transmittance rises again above level L within 0.5 ms and stays there for longer than 0.1 ms, both events are regarded as long excursions of one atom to the edge of the mode. The exit time algorithm yields an entrance time of $t = -0.06$ ms, and an exit time of $t = 1.96$ ms. The drops in the levels L and H are due to a larger pump power at these times.

4. In this time interval, a time-dependent comparison level, L, is calculated for the transmittance: The transmittance of the empty cavity, as calculated in 2., is multiplied by a factor of 1.2, which allows for cavity drifts. To this number, an allowance for shot noise is added, which is three times the standard deviation of the empty cavity transmittance with a 30 μs time resolution, to give the level L. Another comparison level, H, is the level L times 1.7. For a larger pump power, the shot noise in the transmittance is smaller, thus

the levels L and H are lower for smaller shot noise.

5. If the transmittance stays above the level L for longer than 0.1 ms, it is decided that an atom has entered the cavity. The entrance time of this atom is the time where the transmittance has first risen above level L. If the transmittance rises above level H, it is also defined that an atom has entered the cavity at the point where the transmittance has risen above level L, even if the transmittance does not stay as long as 0.1 ms above level L. If, on the other hand, the cavity response drops below level L before the 0.1 ms are completed and it did not rise above level H, one can not be sure whether an atom was in the cavity or whether the increased response was due to shot noise, therefore it is defined that no atom entered in the cavity at this point.

6. The preliminary exit time of the atom is defined as follows: If the cavity transmittance drops below level L and stays below level L for 0.1 ms, the preliminary exit time of the atom is set to the point where the transmittance dropped below level L. If the transmittance drops below level L but rises again above level L within 0.1 ms, it is defined that the atom has stayed in the cavity. Then, this procedure is repeated for the next drop of the transmittance below level L.

7. From numerical simulations of atomic trajectories, one can see that sometimes an atom almost leaves the cavity, and then returns to the middle of the cavity. In such a case, the transmittance drops to almost the empty cavity level for longer than 0.1 ms, and then rises again. In the experiment, an alternative explanation for such a signal would be that a second atom has passed the cavity. In order not to miss the first possibility and yet not to include too many two-atom events, it is defined that two peaks of the transmittance which are due to an atom as described in 5. belong to the same atom if they are not further apart than 0.5 ms. In other words, if the transmission rises above the comparison potential again in less than 0.5 ms after it has fallen below the comparison potential, and both peaks qualify as being due to an atom in the cavity, it is defined that both peaks are caused by the same atom, and the exit time of the atom is the preliminary exit time for the second peak as calculated in 6. Otherwise, the peaks belong to different atoms, and the exit time of the first atom is the preliminary exit time of the first peak. The second atom is discarded in cases where it overlapped with the trigger interval of the first atom.

To evaluate the experimental signal according to this procedure, a computer program was written. In about 95% of the trigger events, the program sets the exit time exactly as one would have done by hand. Most of the cases where one would have decided differently by hand are events where the transmittance was close to level L for some time, but did not manage to stay above level L for 0.1 ms. In these cases, one can argue that the algorithm described above only reacts on really strongly-coupled atoms. Also, it is better to follow a well-defined algorithm which is the same for every trigger event than to decide by hand, which is very liable to be biased by the desired result of the experiment.

Bibliography

[ACDF94] Kyungwon An, J.L. Childs, R.R. Dasari, and M.S. Feld. Microlaser: A Laser with One Atom in an Optical Resonator. *Phys. Rev. Lett.*, 73:3375, 1994.

[AGC92] P. Alsing, D.S. Guo, and H.J. Carmichael. Dynamic Stark effect of the Jaynes-Cummings system. *Phys. Rev. A*, 45:5135, 1992.

[AS72] M. Abramowitz and I.A. Stegun. *Handbook of Mathematical Functions*. National Bureau of Standards, 10th edition, 1972.

[BCH+81] R.J. Ballagh, J. Cooper, M.W. Hamilton, W.J. Sandle, and D.M. Warrington. Optical Bistability in a Gaussian Cavity Mode. *Appl. Optics*, 37(2):143, 1981.

[Bet47] H. Bethe. The Electromagnetic shift of Energy Levels. *Phys. Rev.*, 72:339, 1947.

[BEZ00] Dirk Bouwmeester, Artur Ekert, and Anton Zeilinger, editors. *The Physics of Quantum Information: Quantum Cryptography, Quantum Teleportation, Quantum Computation*. Springer Verlag, 2000.

[BNB+92] F. Bernardot, P. Nussenzveig, M. Brune, J.-M. Raimond, and S. Haroche. Vacuum Rabi Splitting Observed on a Microscopic Atomic Sample in a Microwave Cavity. *Europhys. Lett.*, 17(1):33–38, 1992.

[BVW01a] S. Brattke, B.T.H. Varcoe, and H. Walther. Generation of Photon Number States on Demand via Cavity Quantum Electrodynamics. *Phys. Rev. Lett.*, 86(16):3534–3537, 2001.

[BVW01b] S. Brattke, B.T.H. Varcoe, and H. Walther. Preparing Fock states in the micromaser. *Opt. Expr.*, 8(2):131–144, 2001.

[Car93] H. Carmichael. *An Open Systems Approach to Quantum Optics*. Springer, 1993.

[CCBFO00] H.J. Carmichael, H.M. Castro-Beltran, G.T. Foster, and L.A. Orozco. Giant Violations of Classical Inequalities through Conditional Homodyne Detection of the Quadrature Amplitudes of Light. *Phys. Rev. Lett.*, 85(9):1855–1858, 2000.

[DCT89] J. Dalibard and C. Cohen-Tannoudji. Laser cooling below the Doppler limit by polarization gradients: simple theoretical models. *J. Opt. Soc. Am. B*, 6(11):2023–2045, 1989.

[Dem82] W. Demtröder. *Laser Spectroscopy*. Springer-Verlag, 1982.

[DHK+83] R.W.P Drever, J.L. Hall, F.V. Kowalski, J. Hough, G.M. Ford, A.J. Munley, and H. Ward. Laser phase and frequency stabilization using an optical resonator. *Appl. Phys. B*, 31:97, 1983.

[Dir27] P.A.M. Dirac. The Quantum Theory of the Emission and Absorption of Radiation. *Proc. Roy. Soc. A*, 114:243, 1927.

[DLHK00] A.C. Doherty, T.W. Lynn, C.J. Hood, and H.J. Kimble. Trapping of single atoms with single photons in cavity QED. *Phys. Rev. A*, 63:013401, 2000.

[DPTW98] A.C. Doherty, A.S. Parkins, S.M. Tan, and D.F. Walls. Motional states of atoms in cavity QED. *Phys. Rev. A*, 57(6):4804–4817, 1998.

[Ern95] U. Ernst. Stabilisierung der Differenz zweier Laserfrequenzen mit Hilfe eines optischen Resonators. Diplomarbeit, Universität Konstanz, 1995.

[ESBS91] B.-G. Englert, J. Schwinger, A.O. Barut, and M.O. Scully. Reflecting slow atoms from a micromaser field. *Europhys. Lett.*, 14(1):25–31, 1991.

[Fis98] T. Fischer. Dynamik einzelner Atome in einem optischen Resonator hoher Finesse. Diplomarbeit, Universität Konstanz, 1998.

[FMP+01] T. Fischer, P. Maunz, T. Puppe, P.W.H. Pinkse, and G. Rempe. Collective light forces on atoms in a high-finesse cavity. *New Journal of Physics*, 3:11.1–11.20, 2001.

[FMP+02] T. Fischer, P. Maunz, P.W.H. Pinkse, T. Puppe, and G. Rempe. Feedback on the motion of a single atom in an optical cavity. *Phys. Rev. Lett.*, 88:163002, 2002.

[GKH+01] G.R. Guthöhrlein, M. Keller, K. Hayasaka, W. Lange, and H. Walther. A single ion as a nanoscopic probe of an optical field. *Nature*, 414:49–51, 2001.

[GR99] Markus Gangl and Helmut Ritsch. Collective dynamical cooling of neutral particles in a high-Q optical cavity. *Phys. Rev. A*, 61:011402R, 1999.

[GZ00] C.W. Gardiner and P. Zoller. *Quantum Noise*. Springer, 2nd edition, 2000.

[HBR91] S. Haroche, M. Brune, and J.-M. Raimond. Trapping atoms by the vacuum field in a cavity. *Europhys. Lett.*, 14(1):19–24, 1991.

[HBT56] R. Hanbury-Brown and R.Q. Twiss. Correlation Between Photons in Two Coherent Beams of Light. *Nature*, 127:27, 1956.

[HCLK98] C.J. Hood, M.S. Chapman, T.W. Lynn, and H.J. Kimble. Real-time cavity QED with single atoms. *Phys. Rev. Lett.*, 80(19):4157–4160, 1998.

[HGHR98] G. Hechenblaikner, M. Gangl, P. Horak, and H. Ritsch. Cooling an atom in a weakly driven high-Q cavity. *Phys. Rev. A*, 58(4):3030–3042, 1998.

[HHG+97] P. Horak, G. Hechenblaikner, K.M. Gheri, H. Stecher, and H. Ritsch. Cavity-induced atom cooling in the strong coupling regime. *Phys. Rev. Lett.*, 79(25):4974–4977, 1997.

[HLD+00] C.J. Hood, T.W. Lynn, A.C. Doherty, A.S. Parkins, and H.J. Kimble. The Atom-Cavity Microscope: Single Atoms Bound in Orbit by Single Photons. *Science*, 287:1447–1453, 2000.

[HLKR00] M. Hennrich, T. Legero, A. Kuhn, and G. Rempe. Vacuum-Stimulated Raman Scattering Based on Adiabatic Passage in a High-Finesse Optical Cavity. *Phys. Rev. Lett.*, 85(23):4872–4875, 2000.

[HRF+02] P. Horak, H. Ritsch, T. Fischer, P. Maunz, T. Puppe, P.W.H. Pinkse, and G. Rempe. Optical kaleidoscope using a single atom. *Phys. Rev. Lett.*, 88(4):043601, 2002.

[Jac75] J.J. Jackson. *Classical electrodynamics*. J. Wiley and Sons, 2. ed. edition, 1975.

[KHBR99] A. Kuhn, M. Hennrich, T. Bondo, and G. Rempe. Controlled generation of single photons from a strongly coupled atom-cavity system. *Appl. Phys. B*, 69(3):373–377, 1999.

[Lan72] S. Lang. *Linear Algebra*. Addison-Wesley, second edition, 1972.

[Lug84] L.A. Lugiato. Theory of optical bistability. In E. Wolf, editor, *Progress in optics*, volume XXI, pages 71–216. Elsevier Science Publishers B.V., 1984.

[LWW+88] P. Lett, R. Watts, C. Westbrook, W. Phillips, P. Gould, and H. Metcalf. Observation of Atoms Laser Cooled Below the Doppler Limit. *Phys. Rev. Lett.*, 61(2):169, 1988.

[Mau] Peter Maunz. Dissertation, Technische Universität München.

[Mau99] P. Maunz. Photoneninduzierte Bewegung einzelner Atome in einem optischen Resonator. Diplomarbeit, Universität Konstanz, 1999.

[MCD93] K. Mølmer, Y. Castin, and J. Dalibard. Monte Carlo wave-function method in quantum optics. *J. Opt. Soc. Am. B*, 10(3):524–538, 1993.

[MFM+99] P. Münstermann, T. Fischer, P. Maunz, P.W.H. Pinkse, and G. Rempe. Dynamics of single-atom motion observed in a high-finesse cavity. *Phys. Rev. Lett.*, 82(19):3791–3794, 1999.

[MFM+00] P. Münstermann, T. Fischer, P. Maunz, P.W.H. Pinkse, and G. Rempe. Observation of Cavity-Mediated Long-Range Light Forces between Strongly Coupled Atoms. *Phys. Rev. Lett.*, 84:4068–4071, 2000.

[MFPR99] P. Münstermann, T. Fischer, P.W.H. Pinkse, and G. Rempe. Single slow atoms from an atomic fountain observed in a high-finesse optical cavity. *Opt. Comm.*, 159:63–67, 1999.

[Mün99] Peter Münstermann. *Dynamik einzelner Atome in einem optischen Resonator höchster Finesse*. Dissertation, Universität Konstanz, 1999.

[MS99] Pierre Meystre and Murray Sargent, III. *Elements of Quantum Optics*. Springer-Verlag, Berlin, third edition, 1999.

[MTCK96] H. Mabuchi, Q.A. Turchette, M.S. Chapman, and H.J. Kimble. Real-time detection of individual atoms falling through a high-finesse optical cavity. *Opt. Lett.*, 21(17):1393–1395, 1996.

[Mus97] R. Muscheler. Realisation einer Fontäne optisch gekühlter Atome. Diplomarbeit, Universität Konstanz, 1997.

[MvdS99] Harold J. Metcalf and Peter van der Straten. *Laser Cooling and Trapping*. Springer-Verlag, New York, 1999.

[MVT00] S. Mancini, D. Vitali, and P. Tombesi. stochastic phase-space localisation for a single trapped particle. *Phys. Rev. A*, 61:053404, 2000.

[MWM85] D. Meschede, H. Walther, and G. Müller. One-Atom Maser. *Phys. Rev. Lett.*, 54(6):551–554, 1985.

[PFM+00] P.W.H. Pinkse, T. Fischer, P. Maunz, T. Puppe, and G. Rempe. How to catch an atom with single photons. *Journal of Modern Optics*, 47:2769–2787, 2000.

[PFMR00] P.W.H. Pinkse, T. Fischer, P. Maunz, and G. Rempe. Trapping an atom with single photons. *Nature*, 404:365–368, 2000.

[Pur46] E.M. Purcell. Spontaneous emission probabilities at radio frequencies. *Phys. Rev.*, 69:681, 1946.

[Rev48] Physical Review. On Quantum-electrodynamics and the Magnetic Moment of the Electron. *Phys. Rev.*, 73:416, 1948.

[RGO+99] A. Rauschenbeutel, G.Nogues, S. Osnaghi, P. Bertet, M. Brune, J.M. Raimond, and S. Haroche. Coherent Operation of a Tunable Quantum Phase Gate in Cavity QED. *Phys. Rev. Lett.*, 83(24):5166–5169, 1999.

[RGO+00] A. Rauschenbeutel, G.Nogues, S. Osnaghi, P. Bertet, M. Brune, J.M. Raimond, and S. Haroche. Step-by-Step Engineered Multiparticle Entanglement. *Science*, 288:2024–2028, 2000.

[RPC+87] E.L. Raab, M. Prentiss, A. Cable, S. Chu, and D.E. Pritchard. Trapping of neutral sodium atoms with radiation pressure. *Phys. Rev. Lett.*, 59(23):2631, 1987.

[RTB+91] G. Rempe, R.J. Thompson, R.J. Brecha, W.D. Lee, and H.J. Kimble. Optical bistability and photon statistics in cavity quantum electrodynamics. *Phys. Rev. Lett.*, 67:1727–1730, 1991.

[RWK87] G. Rempe, H. Walther, and N. Klein. Observation of quantum collapse and revival in a one-atom maser. *Phys. Rev. Lett.*, 58(4):353–356, 1987.

[SC88] C.M. Savage and H.J. Carmichael. Single-Atom Optical Bistability. *IEEE J. Quant. Electron.*, 24(8):1495–1498, 1988.

[Sie86] A.E. Siegman. *Lasers*. University science books, 1986.

[ST91] B.E.A. Saleh and M.C. Teich. *Fundamentals of Photonics*. Wiley-Interscience, 1991.

[VC00] V. Vuletić and S. Chu. Laser cooling of atoms, ions, or molecules by coherent scattering. *Phys. Rev. Lett.*, 84(17):3787–3790, 2000.

[vdLvEvDW01] A.M. van der Lee, M.P. van Exter, N.J. van Druten, and J.P. Woerdman. A physical explanation of excess quantum noise due to non-orthogonal modes. *New Journal of Physics*, 3:2.1–2.15, 2001.

[vdM85] S. van der Meer. Stochastic cooling and the accumulation of antiprotons. *Rev. Mod. Phys.*, 57(3):689–700, 1985.

[VK97] D.W. Vernooy and H.J. Kimble. Well-dressed states for wave-packet dynamics in cavity QED. *Phys. Rev. A*, 56(5):4287–4295, 1997.

[Wal91] W. Walter. *Analysis 2*. Springer, 3rd edition, 1991.

[Wol94] S. Wolf. Entwicklung und Charakterisierung eines frequenzstabilen Diodenlasers. Diplomarbeit, Universität Konstanz, 1994.

[YVK99] J. Ye, D.W. Vernooy, and H.J. Kimble. Trapping of Single Atoms in Cavity QED. *Phys. Rev. Lett.*, 83(24):4987–4990, 1999.

Publications

P. Münstermann, T. Fischer, P.W.H. Pinkse, and G. Rempe. Single slow atoms from an atomic fountain observed in a high-finesse optical cavity. *Optics Communications,* **159**:63-67, 1999.

P. Münstermann, T. Fischer, P. Maunz, P.W.H. Pinkse, and G. Rempe. Dynamics of single-atom motion observed in a high-finesse cavity. *Physical Review Letters* **82**:3791-3794, 1999.

G. Rempe, T. Fischer, P. Maunz, and P. Münstermann. Single slow atoms observed one by one in a high-finesse optical cavity *"Laser Spectroscopy IX". R. Blatt, J. Eschner, D. Leibfried, F. Schmidt-Kaler (Eds.), World Scientific, Singapore, 150-159*, 1999.

P. Münstermann, T. Fischer, P. Maunz, P.W.H. Pinkse, and G. Rempe. Observation of Cavity-Mediated Long-Range Light Forces between Strongly Coupled Atoms. *Physical Review Letters* **84**:4068-4071, 2000.

P.W.H. Pinkse, T. Fischer, P. Maunz, and G. Rempe. Trapping an atom with single photons. *Nature* **404**:365-368, 2000.

P.W.H. Pinkse, T. Fischer, P. Maunz, T. Puppe, and G. Rempe. How to catch an atom with single photons. *Journal of Modern Optics* **47**:2769-2787, 2000.

T. Fischer, P. Maunz, T. Puppe, P.W.H. Pinkse, and G. Rempe. Collective light forces on atoms in a high-finesse cavity. *New Journal of Physics* **3**:11.1-11.20, 2001.

P. Horak, H. Ritsch, T. Fischer, P. Maunz, T. Puppe, P.W.H. Pinkse, and G. Rempe. Optical Kaleidoscope Using a Single Atom. *Physical Review Letters* **88**:043601, 2002.

T. Fischer, P. Maunz, P.W.H. Pinkse, T. Puppe, and G. Rempe. Feedback on the motion of a single atom in an optical cavity *Physical Review Letters* **88**:163002, 2002.

Danksagung

Mein Dank gilt zuallererst meinen Mitstreitern Peter Maunz, Thomas Puppe und Pepijn Pinkse, mit denen ich extrem offen und und konstruktiv zusammenarbeiten konnte. Peter Maunz hat mich ausserdem mit den Tiefen und Untiefen der Programmierung in C++ vertraut gemacht, Thomas Puppe hatte den Humor, mehrere Jahre mit mir zusammen in einem Büro zu verbringen, und Pepijn Pinkse hat sich sowohl beim Schreiben einiger Artikel als auch bei der Bezwingung von Alpengipfeln grosse Verdienste erworben.

Auch meinen Eltern, die mir mein Studium ermöglichten und mir auch später stets zur Seite standen, möchte ich ganz herzlich danken.

Professor Gerhard Rempe danke ich dafür, daß er mir die Mitarbeit an einem so interessanten Projekt ermöglichte, und daß er uns sehr freie Hand beim Experimentieren und Neuaufbau des Experiments liess.

Meinem Vorgänger Peter Münstermann danke ich für die Einführung in die Kniffe der Experimentalphysik, die Unterstützung bei der Fehlersuche, für die Aufbauarbeit am Experiment und dabei vor allem für die Mutter aller Cavities, die heute noch im Einsatz ist.

Allen Mitgliedern der Arbeitsgruppe danke ich für die positive Arbeitsatmosphäre, die gemeinsamen Skitage und sonstige Freizeitaktivitäten, und das fleissige Mitdiskutieren bei den Gruppensitzungen.

Helmut Ritsch, Peter Horak, Peter Domokos und Markus Gangl danke ich für interessante Diskussionen und für die gute Zusammenarbeit bei den Überlegungen zur Positionsmessung einzelner Atome.

Ausserdem möchte ich den Technikern Josef Bayerl, Franz Denk, Peter Sachsenmaier und Helmut Stehbeck danken, die mit bislang unübertroffener Präzision konstruieren, Metall bearbeiten und löten können und denen z.B. die Mutation von Deckengestellen zu Bodengestellen so wunderbar gelungen ist.

Allen, die am Aufbau des Experiments beteiligt waren, insbesondere frühere Mitarbeiter und Hiwis, möchte ich für ihren Beitrag beim Gelingen der Experimente danken.

Nicht zuletzt möchte ich auch meinen Freunden und meiner Schwester danken, die das Leben ausserhalb des Instituts so interessant machten und mich auch während der steinigeren Strecken der Dissertation moralisch unterstützten.